

For New Technology Network

**NTN**®

# TECHNICAL REVIEW

No.  
**80**

**Special Issue;**  
**Environment and Energy**  
October 2012



*The newly established renewable energy management demonstration area promotes efficient, effective energy usage*

Our Advanced Technology R&D Center in Kuwana City, Mie Prefecture, is not only working towards advancing and developing cutting edge technologies, but is also improving and integrating core **NTN** technologies such as tribology, raw materials, surface modification, composite materials, and simulation technology. The slogan “Advanced Technology = Global No. 1, Global First” promotes the creation of innovative technologies that lead to state-of-the-art solutions and global environmental conservation, such as next-generation tribo-materials, highly functional new materials, a sustainable energy utilization system, and an advanced computing scientific simulation.

Additionally, in December of last year, a “Natural Energy Management Demonstration Area” was established to start assessing energy-related systems. In this facility, new added tracking-type solar panels and an experimental greenhouse-type solar panels have been installed. These come as an addition to existing solar and wind power generation facilities to form a micro smart grid, which includes an electric vehicle charging station. A micro hydropower generation unit was also installed in an adjacent park to conduct power generation experiments.

We will promote effective utilization of natural energy including development of various energy-related systems around “technologies that support rotation,” which **NTN** has been fostering thus far, through cultivation of plants using natural energy.

▼ Advanced Technology R&D Center and Wind Turbines



▼ Renewable Energy Management Demonstration Area



Demonstration under way with a linear module installed (p.19)



▲ Micro-hydropower generator installed in the nearby park (usually covered for safety as shown in the picture. p.6)



# TECHNICAL REVIEW

**No.80**

**Special Issue:**  
**Environment and Energy**

# NTN TECHNICAL REVIEW No.80

## CONTENTS

<b>Preface</b>	Yoshinobu YASUDA	1
<b>Contribution</b>	<b>Sustainable Society Powered by Renewable Energy</b> - An Approach from Millennium Sustainability Studies - Masao TAKANO Associate Professor, Nagoya University Graduate School of Environmental Studies	2
<b>● Special Issue for Environment and Energy Engineering</b>		
	<b>Market of Wind Power Generation Industry, Technology Trends and Bearing Technology of NTN</b> Michio HORI, Yusuke YAMADA and Masahiko KATAOKA	8
	<b>Application of Condition Monitoring System for Wind Turbines</b> Akitoshi TAKEUCHI, Takashi HASEBA and Hiroshi IKEDA	15
	<b>Motorized Linear Module for Tracking System of Solar Light / Solar Heat Power Generation</b> Tomoyuki OWADA and Masaki KAGAMI	19
	<b>Development of Induction Through-hardening and Induction Tempering Methods with Temperature Control and Microstructural Control in Bearing Steel</b> Takumi FUJITA and Nobuyuki SUZUKI	23
	<b>Rolling Bearing for Environments of Ultrahigh Temperatures</b> Miki ARIHANA and Takayuki KAWAMURA	31
<b>● Special Issue for Manufacturing Technology "NTN supports the "Mono-Zukuri" manufacturing through the advanced technology"</b>		
	<b>Machine Tool Main Spindle Bearings with "Air Cooling Spacer"</b> Yuushi ONDA, Mamoru MIZUTANI and Masatsugu MORI	38
	<b>Parallel Link High Speed Angle Control Equipment (PHACE)</b> Hiroshi ISOBE and Yukihiro NISHIO	42
	<b>Development of the Lubricating Oil Supply Unit with Self-generatig Power Supply</b> Kaoru OMOTO and Hiroyoshi ITO	48
	<b>NTN Linear Modules Series</b> Ulrich GIMPEL, Michael WILLE, Tomoyuki OWADA and Masaki KAGAMI	52
<b>● Technical Papers Technical Articles New Products</b>		
	<b>Evaluation of Local Mechanical Properties of High Strength Steels by Indentation Method</b> Takeshi OGAWA, Noriaki SAKANAKA and Yukio Matsubara	58
	<b>TMR : A New Frontier for Magnetic Sensing</b> Christophe DURET and Shintarou UENO	64
	<b>Long Life Technology of Grease for Journal Bearing</b> Takamasa TANAKA and Hidenobu MIKAMI	72
	<b>Market Trend and High-Functionality of Wheel Bearings for Off-Highway Truck</b> Kenichiro NAITO, Naota YAMAMOTO and Katsunori SONE	78
	<b>Multi Layer BEARPHITE</b> Yosuke SUGAI and Toshihiko MOURI	83
	<b>Introduction of Magnetic Material Products</b> Takuji HARANO, Shinji MIYAZAKI and Hajime KATSUURA	87
<b>● Our Line of Award Winning Products</b>		
	<b>"The Japanese Society of Tribologists 2011" Technology Award</b> <b>Advancement of Cage Stress Analysis of Rolling Bearings</b> Tomoya SAKAGUCHI, Kazuyoshi HARADA and Sadatsune KAZAMA	92
	<b>"2011 'CHO' MONODZUKURI Innovate Components Awards" Machinery Component Award</b> <b>Desktop Type Microscopic Coating Applicator</b> Motohiro UCHIYAMA	93
<b>New Products Information</b>		94

## *A message for the special Environment and Energy issue*



**Yoshinobu YASUDA**  
Managing Director

It has been one and a half years since the Great East Japan Earthquake, and there is a lot of talk regarding Japan's energy future. Forms of renewable energy such as solar, wind, tidal, and geothermal are currently under review worldwide, and there is no question that they will bring safe, clean power, and help to prevent global warming. However, renewable energy has its own share of challenges like cost and consistency; thus, improving the efficiency and reliability of power generation systems is imperative.

Under these circumstances, NTN actively participated in offshore wind power generation projects, smart community initiatives, and demonstrations of experimental projects in several regions. NTN also established the "Renewable Energy Management Demonstration Experiment Area" within the Advanced Technology R&D Center. The purpose of this area is to develop relevant system technologies through activities such as cultivating plants with renewable energy.

A special "Environment and Energy" issue was published for the 26th Japan International Machine Tool Fair (JIMTOF2012), which takes place from November 1st to 6th and focuses on "Mono-Zukuri" innovation. This issue featured NTN's products and technologies that relate to reducing the environmental load. Also in this issue, we introduce you to "Sustainable Society Powered by Renewable Energy—An Approach from Millennium Sustainability Studies" by Associate Professor Masao Takano of Nagoya University Graduate School of Environmental Studies, who is recognized as one of the leading experts in creating systems for the globe and society. In the following "Environment and Energy" issue, technologies and products related to renewable energy and the environment are introduced, with a focus on wind and solar power generation. Further, the "Manufacturing Technology" issue introduces next-generation technologies and new products that were exhibited in JIMTOF2012, which support manufacturing capabilities.

NTN will celebrate its centennial in 2017. We strive to contribute to the sustainable development of the society under our corporate philosophy, "For New Technology Network: We shall contribute to international society through creating new technologies and developing new products."

# For New Technology Network

# Sustainable Society Powered by Renewable Energy

## - An Approach from Millennium Sustainability Studies -



**Masao TAKANO**

**Nagoya University Graduate School of Environmental Studies**

Future style of energy usage in Japan is at great concern after the accident of Fukushima Daiichi nuclear plant. From the viewpoint of Millennium sustainability, the society should be powered by not fossil fuels nor nuclear power but by renewable energy. Principal automobiles may be electric vehicles shared in communities and charged by small hydropower station in rural area.

### 1. Introduction

The Great East Japan Earthquake on March 11, 2011, and the resulting accident at Fukushima Daiichi Nuclear Power Plant were both shocking incidents. An increased interest toward a sustainable society and the concept of “energy shift” emerged. However, there is some confusion regarding this concept. This article will provide an introduction to the basic concept of millennium sustainability and discuss its specific applications, mainly on the energy sector.

### 2. Basic concept of millennium sustainability

#### 2.1 Learning from “Limits to Growth”

The concept of “millennium sustainability” was first created in the year 2000 at the Science and Technology Forum, which was held every year by the Science and Technology Agency. This forum allowed free discussion among scholars of several disciplines for 3 days, with the intent of developing ideas for future policies in science and technology.

One notable breakout session led by Mr. Manabu Akaike, an expert in science and technology, and Dr. Shin-ichi Kawakami, of Gifu University Faculty of Education, discussed “Security, science and technology of the 21st century from the perspective of Earth Science.”

A range of findings were reviewed from the “Limits to Growth”<sup>1)</sup>, which stemmed from the Earth System theory in this breakout session. “Limits to Growth” is a

product of the research commissioned to D. H. Meadows, of the Massachusetts Institute of Technology, by the think tank “Club of Rome”, a group of prominent scholars, at the United Nations Conference on the Human Environment held in Stockholm in 1972.

Dr. Meadows and his colleagues used computer modeling to simulate how factors such as world population, food production, industrial production, availability of resources, and pollution would change. At this time, computer simulation was not widely available as it is today. This made the idea of using it to foresee the future a bold effort.

In this case, the growth means factors increase exponentially or quadratically. For example, if the population doubles in 50 years, it doubles in the next 50 years, which is 4 times the original population. The world in the 20th century was, indeed, an era of the growth.

The program called “World3”, written by Meadows and his colleagues, adjusted a number of parameters to simulate the sharp increase in the population, food production, and industrial production of the 20th century, i.e., the growth. These factors were used to predict the behavior of 100 years of the 21st century.

The picture of the 21st century shown in the result was quite disastrous. The industrial production would peak in around 2020 and then start a sharp decline. This would result in a drop of agricultural production, as it depends on industrial products such as chemical fertilizers, pesticides, agricultural machines, and others. The drop in agricultural production would lead

to the rapid decrease in food production followed by a steep reduction of population with little delay, as the food cannot support the peak population.

The simulation results showed that the food production per capita would peak in the 1980s and decrease in the 21st century. The average life expectancy in the world, which was drastically extended in the 20th century, would begin rapidly shortening starting in the middle of the 21st century. Due to the increased mortality rate of children.

The reason for the sharp decline of industrial production in the program is the drastic decrease of available resources (underground reserve of oil, etc., is assumed) as a result of the rapid increase of the industrial production in the 20th century. That would require increased investment for extraction of more difficult and more costly resources. The capital for the industrial production itself would then start experiencing shortage, triggering a downward spiral of reduced reproduction.

The release of this paper caused a big debate in the world involving many both in favor and against the theory. Meadows and his co-authors published revisions recalculating the assumptions in 1985 and again in 2002, concluding that the original estimates in the 1970s were largely correct, even with the inclusion of the subsequently accumulated data.

## 2.2 Millennium sustainability/unsustainability

**Fig. 1** is a graphical representation of unsustainability in our current society, based on the concept of "Limits to Growth." Underground resources are kept in the earth. They are removed to produce goods. When the goods are consumed, waste is produced. The waste is stored somewhere in the earth as "polluted material."

For example, oil is extracted to produce gasoline at a refinery. We fill up our cars at gas stations and drive them, consuming gasoline. The material changes its form in this process and is discharged from the exhaust pipe as carbon dioxide. However, the material did not come from nothing and never disappears, following the law of conservation of mass. At a glance, gasoline looks like it has disappeared from the tank, but in reality, it is stored in the atmosphere as carbon dioxide.

Society depending on this material flow will sooner or later face a dead end. The resources in the earth will be depleted and the pollution will continue to accumulate. The use of gasoline faces these two dead ends with the depletion of oil and the global warming issue. Nuclear power faces the same issue with the depletion of the natural uranium and proper radioactive waste disposal.

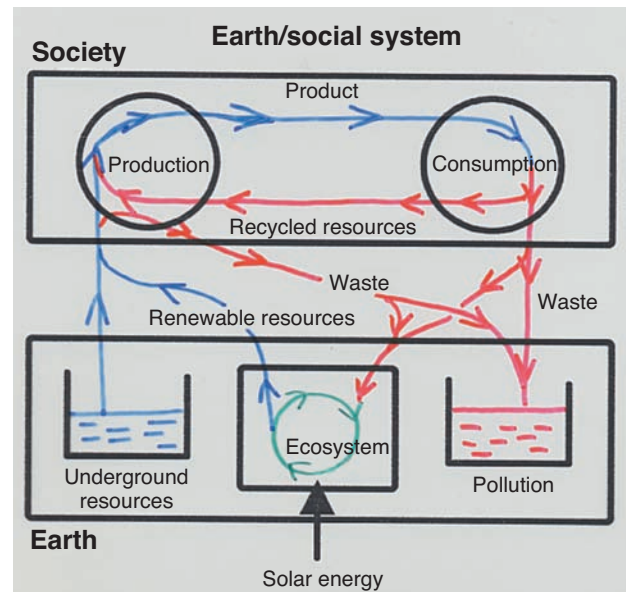


**Fig.1** Schematic figure of material flow in 20th century type society

Meanwhile, we adopt resources from the ecosystem as well, such as wood and food. As these resources are renewed, if the ecosystem is properly maintained, the resources obtainable from the ecosystem are called renewable resources. The produced waste can also be returned to the ecosystem, after it is properly processed.

In about 1,000 years, the earth's resources will most likely be depleted. The graphical representation of the material flow will be as shown in **Fig. 2**. There are no longer any underground resources, therefore, there is no pollution which makes us free from the waste issues. We obtain resources from the ecosystem and return the waste to the ecosystem. In other words, humanity will also live as a part of the ecosystem.

The society in this manner, which is also sustainable 1,000 years ahead, is called millennium sustainability. The basic idea of the millennium sustainability studies is to start the first step now, aiming for that type of society in the future.

However, that does not mean we should go back to the Stone Age. The metal that used to be underground before is now stored in society. We can use it carefully through recycling. The resources in the ecosystem can be used in such a manner that enriches the ecosystem by the use of advanced science and technology rather than destroys it. This is the concept of millennium sustainability science and technology<sup>2)</sup>.

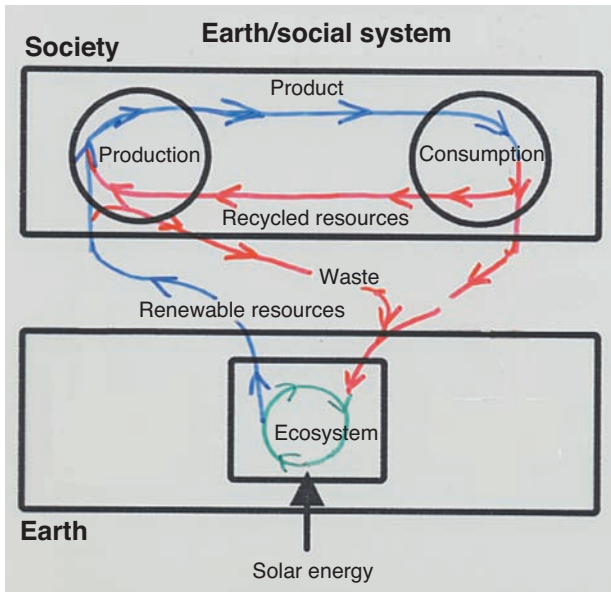


**Fig.2** Schematic figure of material flow in future sustainable society

### 3. Three-step energy shift

#### 3.1 Phase-out of nuclear power

Now, let me discuss the future use of energy from the point of view of millennium sustainability. The feed-in tariff program for renewable energy began in July this year. This program ensures the purchase of renewable power by power companies at a fixed price when renewable power plants are constructed. Therefore, the investment can be recovered with certainty, making the renewable power plants profitable. This is an epoch-making event in the history of the Japanese energy industry. The construction of megawatt solar plants is in progress in many regions, and micro-hydropower plants are also planned in different regions.

Under these circumstances, the concept of “energy shift,” which will promote nuclear phase-out by shifting the energy to renewable power, is gaining the support of many. However, this concept also means that the “Nuclear plants must be operated until renewable energy can effectively replace them.” If so, nuclear plants must be running for quite some time, as the renewable energy cannot produce the amount of power that nuclear power plants have been producing soon enough.

Instead, the nuclear power plants can be stopped immediately. The energy shift should be planned in three phases. The first phase is to immediately stop the nuclear power plants and restart the thermal power plants that have been halted. It will become

clear that every power company has the capacity to produce enough power to meet the maximum demand with the existing thermal and hydropower plants even without the nuclear power generation. In fact, a significant amount of thermal and hydropower capacity has been suspended because the preference of power generation was given to nuclear power plants.

As we have witnessed, although the summer of 2012 was the third-hottest summer after WWII, there was no need for planned outages as none of the nuclear power plants were running except Ooi Power Plant of the Kansai Electric Power Company. It was proven that the power supply is sufficient even without nuclear power plants, except for the Kansai Electric Power Company. Even for Kansai Electric Power Company, it has become clear that there was no need to run the Ooi Power Plant.

In the second step, cities can be provided with cogeneration (combined supply of heat and power) fueled by natural gas (metro gas). Small form-factor fuel cells fueled by metro gas will gain popularity in homes and offices. Heat produced together with electricity is effectively used for supplying hot water and air. The buildings will be equipped with photovoltaic panels on the rooftop. A picture of smart grid cities, where numerous individual power facilities are connected by ICT, will be a reality.

Alternatively, in the rural area, every village can aim for energy independence. It is expected that there will be numerous villages that can become energy independent, if they take full advantage of abundant renewable energy resources readily available in the rural areas.

And in the third step, the cities can also shift to renewable energy, aiming for the entire society to be fueled by the renewable energy 100%. This is the “millennium sustainable” society independent from soon-to-be-depleted resources, that is, the society that can function even 1,000 years ahead.

#### 3.2 Challenges of oil phase-out

Currently, about half of the ultimate oil reserve is used, approaching the peak production. It is not depleted immediately; however, decreased production causes price increase, as the supply cannot meet the entire demand. In fact, since 2000, the crude oil price entered an unstable period where the price repeats sudden jumps and drops.

The problem does not stop at the price. Since the “bottom of the tank” is now visible, the question of who controls the remaining oil has affected two wars fought in recent history, the Gulf War and the Iraq War. These wars were fought by two presidents Bush and

the president Hussein of Iraq. Iraq boasts the second largest oil reserve in the world. The control of the Iraq oil went from the Iraq government to the U.N. after the Gulf War and then transferred from the U.N. to the hands of American and British government after the Iraq War.

Therefore, it is imperative to phase out from the society dependent on oil. The energy shift is not only for nuclear phase-out. Oil phase-out is also a critical issue.

Natural gas is still abundant; therefore, it can be used as an interim solution. However, the bottom of the resources may be observed in the latter half of the 21st century causing conflict over its interest.

Its procurement has already become tight. There is tension between Japan and China over the development of a natural gas field in the East China Sea and also the use of a large gas field developed in Sakhalin, Russia. The original plan of laying pipeline to Japan is stagnant, as another plan of laying pipeline to China emerged later. There are similar tensions over natural gas resources around the world.

Therefore, the Japanese society should aim for 100% renewable energy by 2050, phasing out all natural gas dependency, as well. This can be Japan's most effective contribution to world peace. Japan's conversion to a society of millennium sustainable energy utilization is not only important for protecting the domestic lives, but also essential for creating world peace.

#### 4. Toward the society of millennium sustainable energy utilization

##### 4.1 Renewable energy in urban areas

In the third step of the energy shift, urban areas also need to replace natural gas with renewable energy, such as biomass, toward 2050.

However, that is not possible with the current energy consumption. Fig. 3 shows an idea for the future energy utilization. The amount for 2050 shows the estimate of total available renewable energy in Japan. It is only 1/3 of the current energy supply.

In order to realize a society of 100% renewable energy, it assumes that drastic energy conservation is necessary. The level of conservation is about 1/3 for the entire society, in some cases, 1/10. The Japanese population is decreasing. It is estimated that the population in 2050 will become about 80% of that in 2010, which means the reduction of energy per capita is not as drastic as the above. Still, significant energy conservation is required.

Technological evolution is an important factor; however, that is not sufficient. The energy

consumption of an air conditioner has reduced to about 1/3 in 20 years. However, we are installing at least three of such air conditioners in our homes, so the power consumption in our homes continues to increase even when the overall power consumption of society decreases. Automobile fuel consumption has drastically improved, however, larger cars with more weight have lower gas mileage and most tend to buy larger cars with improved fuel consumption when purchasing new vehicles.

These problems cannot be solved solely by individual efforts. To start, we must create a society where individual air conditioners are not required for each room and cars are not required to be driven around town.

To achieve this, towns must be compact. The decreased population and resulting change in urban structure may provide the necessary condition. The town structure needs to create a shorter distance between work and home which does not require commuting by car. A different lifestyle may also be required. In addition, forests and farmland need to be placed around the urban area to avoid the heat island phenomenon for more comfortable summers. Cogeneration by biomass and area heating/cooling can possibly be accomplished if society evolves from natural gas cogeneration and smart grid.

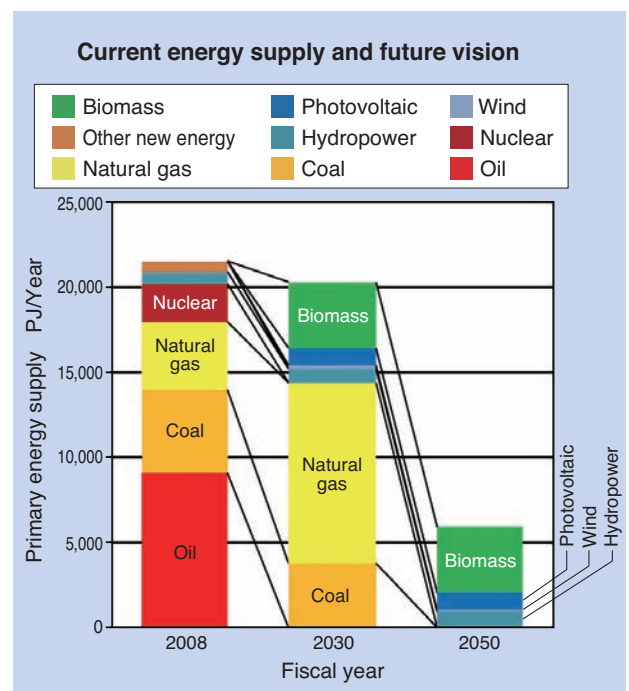


Fig.3 Primary energy supply; Present situation and the future vision

#### 4. 2 Possibilities for the small-scale hydropower

Hydropower plants are a promising renewable resource in Japan. Not large-scale hydropower plants that require construction of dams, but small-scale plants of the 1 MW range or micro- hydropower of a few to tens of kW and even smaller pico- hydropower.

Under the feed-in tariff program, hydropower of tens of kW and larger can become profitable by selling power to power companies. Due to the staged fixed-price structure, hydropower of 1MW is particularly advantageous. Many of these small-scale hydropower plants were in fact constructed about 100 years ago. **Fig. 4** shows the diagram of those power plants, in which the water drawn upstream from the intake gate runs down the high-pressure steel pipe and operates the turbine. **Fig. 5** is a picture of Hirose power plant in Sakauchi, Ibigawa, Gifu Prefecture, with 3.2 MW of output, which was constructed in 1925. It is still up to date and working properly. The construction of this type of plant slowed down after WWII, however, with the feed-in tariff program, it is expected to see a renewed construction boom.

Further, several manufacturers are developing water mills in the area of micro- and pico-hydropower plants, which are not profitable under the feed-in tariff program. **Fig. 6** is a power generation system using axial-type turbines developed in my laboratory.

It can be set in an agricultural waterway and produces 30 W of output. It generates power in a small drop of water and withstands frequent dust such as leaves in those waterways. It is expected to be used for self-support, typically in the mountains where no power lines are provided, or as an emergency power source during power outages as a result of natural causes. In the developing countries, there are many regions without power. It is expected that the residents in those regions can invest in and maintain these types of power generation systems on their own,.

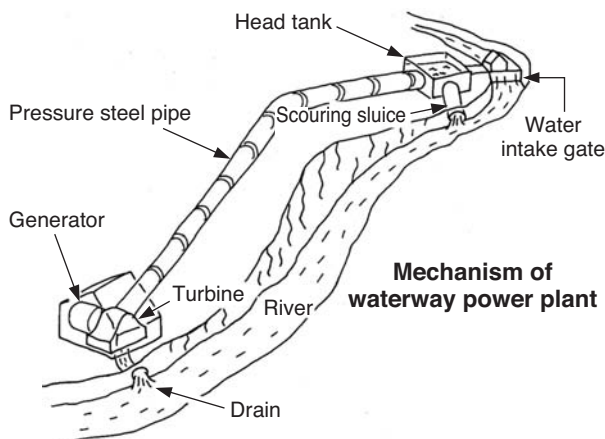


**Fig.4** Schematic figure of small hydro power station

#### 4. 3 Sustainable automobile utilization in the future

How about transportation in rural areas? Rural areas pose the biggest problem because cars are more necessary. The mainstream cars in the millennium sustainable society in 2050 should be electric cars, with the power source in that case being hydropower generation. The power management to match the unstable photovoltaic and wind power generation with the similarly fluctuating electricity demand is a tough task. Instead, it stable hydropower generation would be most suitable, and in particular, micro-hydropower.



**Fig.5** An example of small hydro power station



**Fig.6** Power generation system using axial type turbine set in a small irrigation canal

For example, let us consider a micro-hydropower plant of 1 MW of output. Usually, water can be taken stably during the day and night. If the power demand during the night is 30% of the rated output, the remaining 70%, which is 0.7 MW, can be used to charge electric cars. This is enough to charge 200 Mitsubishi i-MiEV electric vehicles at the same time. A charging station can be installed within a village which can be used for car sharing.

## 5. Conclusion

The utilization of energy in the future should be determined through thorough discussions and agreements, particularly, by the younger generation. The major issue is that there has not been such a framework thus far. It is important, from now on, to continue discussions on how to drive the future energy utilization to bring forward different thoughts, ideas, and concepts. I hope this paper will serve as a reference for those discussions.

## Reference

- 1) D. Meadows, et al. "Limits to Growth," Diamond, Inc., 2005
- 2) Edited by Shigen-Kyokai, "Millennium sustainability – creation of coexisting/recycling civilized society," Japan Institute for Community Affairs, 2003
- 3) Masao Takano, "Big power of small hydropower," Quarterly magazine "Chiiki (region)" No. 9, 2012

### <Author biography>

#### Masao Takano

Associate Professor, Nagoya University Graduate School of Environmental Studies

- 1962 Born in Yamaguchi Prefecture
- 1981 Enrolled in Nagoya University Faculty of Science. Received Doctorate of Science in Earth Science
- 1993 Nagoya University Faculty of Science supporting staff  
Participated in the research project "Decoding the Earth's Evolution" to examine the Earth history and learned the approach of using the concept of "Coexistence of lives and Earth" to tackle the Earth history.  
Realized that the era of humans is very distinctive in the 4.6 billion years of Earth history.
- 1996 Associate Professor, Faculty of Science
- 2001 Participated in the establishment of Nagoya University Graduate School of Environmental Studies, Associate Professor  
Engaged in research and education toward creation of "Millennium Sustainability," which aims for Earth and societal system that can function 1,000 years ahead when the underground resources are depleted, working together with many experts of different disciplines.  
Also, participates in activities for realizing "Millennium Sustainable society" working together as a citizen with government and NPOs.

# Market of Wind Power Generation Industry, Technology Trends and Bearing Technology of NTN

Michio HORI\*  
 Yusuke YAMADA\*  
 Masahiko KATAOKA\*



Recently large-sized wind turbine generators and off-shore wind turbine generators have been promoted globally in the field of wind turbine generators. It is not merely growth, but also accompanying innovations towards higher reliability, longer lives, and higher efficiency. In this paper, the industry trends will be introduced, along with bearing technologies, which contribute the movement of the industry.

## 1. Introduction

Wind power generation has evolved into clean energy with the least impact on the environment, without any CO<sub>2</sub> emission.

Fig. 1 shows the trend of the total capacity of wind turbines. Although the progress slowed slightly due to the recent economic situation, the total capacity in the world reached about 240 GW<sup>1)</sup>, which is equivalent to 60 nuclear power plants\* and it is expected that the growth will continue in an accelerated fashion.

\* Nuclear power plant: 1 million kW/station; facility availability 80%  
 Wind power generation facility: facility availability 20% assumed

Fig. 2 shows the average capacity per unit of newly

installed wind turbines<sup>1)</sup> for each year. The average capacity grew from 1.30 MW/unit in 2005 to 1.66 MW/unit in 2010. However, it is converging at 1.68 MW/unit in 2011.

The reason behind it may be that, since the majority (98.5%) of the wind turbines installed in 2011 were on-shore models, they could have been restricted by not only the cost of the wind turbine itself, but also by other conditions such as road transportation and construction, with reasonable maximum capacity.

Fig. 3 shows the relation between the number of installed wind turbines last year and their capacity. Most of the wind turbines were between 1.5 MW and 2.5 MW<sup>1)</sup>; therefore, it is considered the mainstream for the time being.

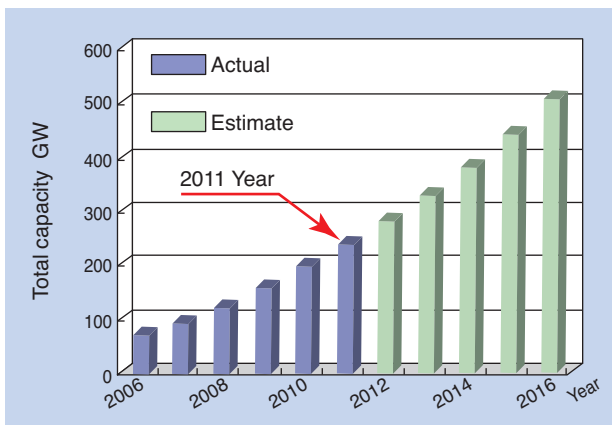


Fig. 1 Transition of total capacity of wind turbines

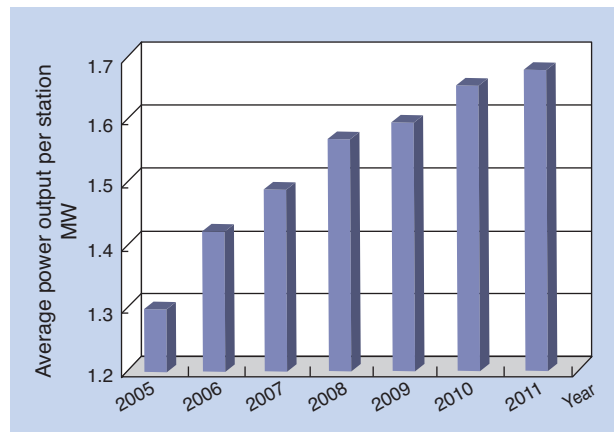
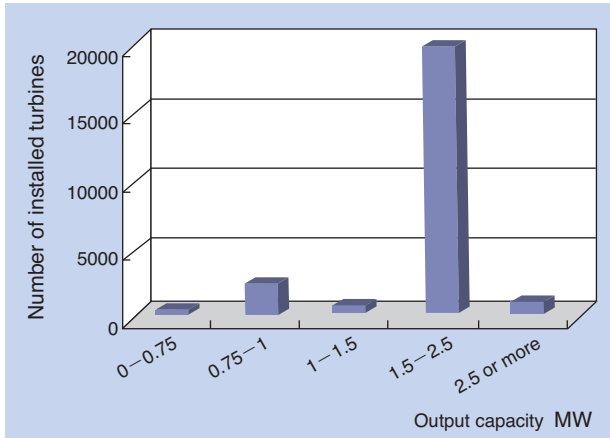
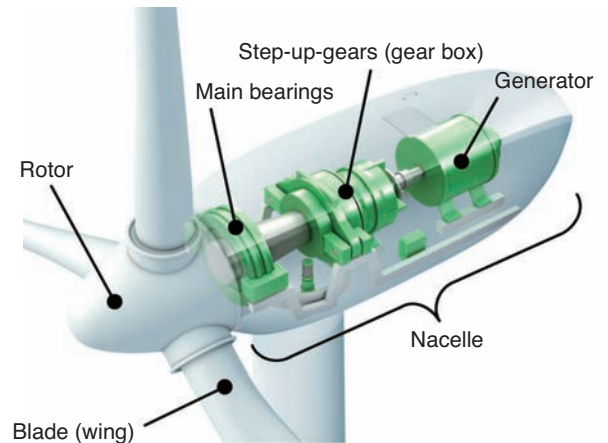


Fig. 2 Average capacity per one unit of newly installed wind turbines<sup>1)</sup>

\* Industrial Machinery Division New Energy Engineering Department



**Fig. 3** The number of installed wind turbines in 2011 and their capacities <sup>1)</sup>



**Fig. 4** Structure of wind turbine

## 2. Offshore

Because of the shortage of adequate sites for on-shore installation and for power efficiency/facility runtime improvement, wind turbine manufacturers are developing larger turbines targeting offshore applications on a full scale.

Today, more than 70% of the cases under consideration by NTN are for offshore applications, and therefore it is expected that the average capacity will increase again within 5 to 6 years.

## 3. Technology trend of bearings for offshore wind turbines

Wind turbines come in many types, such as horizontal axis and vertical axis. We will introduce you to the representative three-blade (wing), horizontal-axis-type large wind turbines. Fig. 4 shows the nacelle portion of the induction generator, which is the mainstream design today. The wind is received by the blades, which rotates the rotor and the power is converted to electric energy by the generator.

Offshore wind turbines are not easily accessible; therefore, ease of maintenance and reliability are emphasized and several mechanisms have been developed in addition to the components in the nacelle (main shaft – step-up gear – generator).

- 1) Main shaft - generator (direct drive)
- 2) Main shaft - multiple generator (friction drive)
- 3) Main shaft - step-up gear/generator unit
- 4) Main shaft - hydraulic step-up gear - generator

Each type has advantages and disadvantages. The optimum configuration may change depending on the economic conditions such as material cost; therefore, every manufacturer is diligently conducting development.

NTN has been developing and supplying bearings that meet the required characteristics for the applications of main shafts, step-up gears, generators, etc., for on-shore wind turbines, as well as the bearings for the above-mentioned offshore wind turbines.

Recently, we have also been developing a Condition Monitoring System (CMS) to address offshore applications. We introduce you to their technological trend in the following section.

## 4. Main bearings

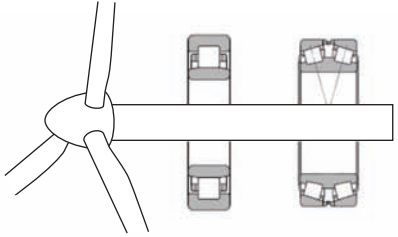
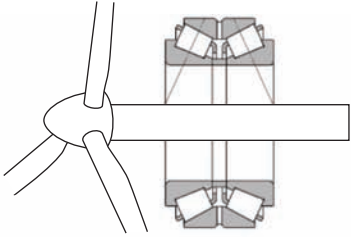
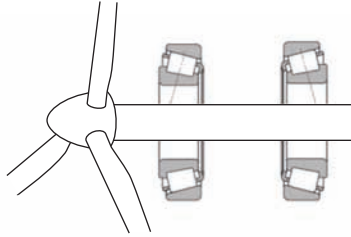
Main bearings that support rotors are becoming larger, however offshore wind turbines use bearings of extremely large size that are not used in regular industrial machines.

The mainstream specification of the bearing configuration for the main shaft uses two self-aligning roller bearings, which have high allowance for installation errors when they are mounted in the turbines. However, for purposes of floating bearings and due to the light-weight requirements for larger offshore applications, various configurations are emerging, as shown in Table 1.

When the main bearings are failed and need to be replaced, the rotor and the main shaft that the main bearings support need to be removed from the nacelle at a huge expense. The replacement cost becomes even larger for offshore wind turbines; therefore, very high reliability is required for the main bearings.

Evaluation of main shaft bearings using bench test machines is made extremely difficult due to the variations in load conditions and the necessary evaluation time. It is therefore important to ensure reliability using component tests and analytical technologies.

**Table 1** Bearing layout of offshore wind turbine

Structure	A		B	C	
Layout					
Bearing type	Rotor side	Generator side		Rotor side	Generator side
					
	Cylindrical roller bearing	Double row tapered roller bearing with vertex of contact angles inside of bearing	Double row tapered roller bearing with steep vertex of contact angles outside of bearing	Single row tapered roller bearing	Single row tapered roller bearing

**4.1 Optimization of the internal design of bearings**

In larger main bearings, rigidity that affects the deformation resistance of the entire cage is an important factor, in addition to the cage strength. As a result, the impact of the rolling elements and the cage weight on the rotational performance is evaluated through analysis. Fig. 5 shows an example of the motion analysis of a single-row tapered roller bearing.

In this analysis, operating conditions are simulated to confirm the cage strength by calculating the load and stress applied to the supports of the cage. With such dynamic and static analyses, the specifications of rolling elements and the cage can be optimized, and a high-load capacity design in the predetermined size can be achieved.

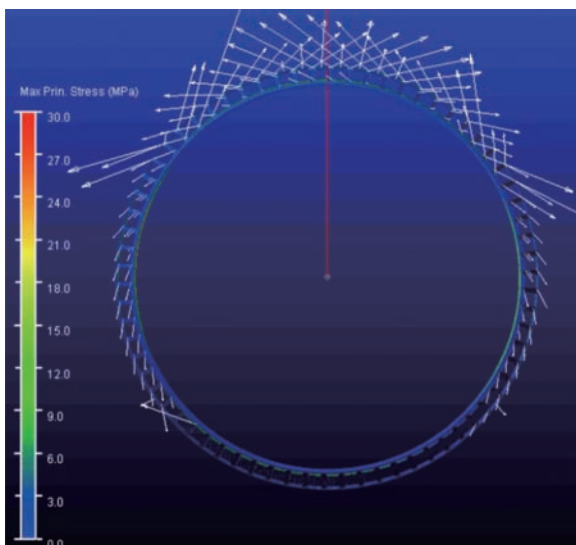


**Fig. 5** Movement analysis example of single row tapered roller bearing

**4.2 Optimization of the peripheral design of bearings**

The life of the bearings and the contact stress between the rolling elements and raceways are evaluated based on the calculation of weight of each rolling element, drawn from the structural analysis considering the peripheral structure. This is done because the life of the bearings is largely affected by the peripheral structure such as the housing, and its impact increases as the size increases.

Fig. 6 shows the housing for self-aligning roller bearings used for inner ring rotation. When self-aligning roller bearings are used, the housing is connected to the frame (nacelle) at the two ends. Therefore, the load of the rolling element increases compared with the calculation result of the rigid element at the 8-o'clock region in Fig. 7. This is because the connections with the frame have somewhat higher rigidity and resistance to deformation, the load is applied to local points. Therefore, when used for inner ring rotation, the shape of the housing and the location of the connection points that fit the operating conditions are particularly important.

Fig. 8 shows an example of analytical result of double row tapered roller bearings used in outer ring rotation. In the case of outer ring rotation, the housing does not have connecting surfaces and since the thickness (rigidity) on the circumference is uniform, the load is evenly distributed, so the load on the rolling elements can be minimized.

As shown, the structure around the bearings has a significant impact on the life of the bearings.



Fig. 6 Analytical model of housing for spherical roller bearing

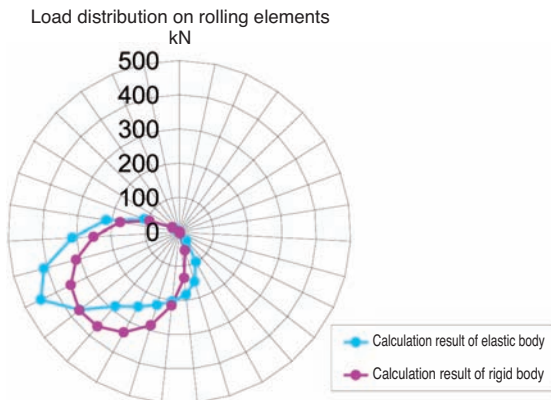


Fig. 7 Analytical result of spherical roller bearing

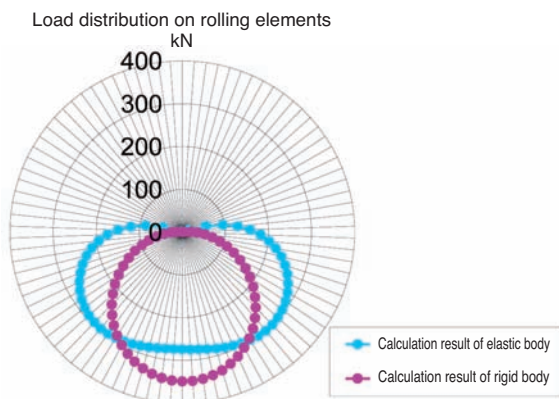


Fig. 8 Analytical result of double row tapered roller bearing

Therefore, NTN provides the most appropriate bearings not only through the bearing internal design, but also after analysis that includes the peripheral structure.

#### 4.3 Best layout of bearings

As mentioned above, in order to prolong the life of the bearings, it is necessary to either make the rigidity of the housing circumference uniform or make the distribution of rigidity as even as possible.

In general, the load on the main bearings is determined by the radial load on the rotor center in the  $F_z$  direction, axial load in the  $F_x$  direction, and the moment load in the  $M_y$  direction in the coordinates

shown in Fig. 9. Therefore, moment load is reduced by the positioning of the bearings inside the rotor, resulting in the reduction of the bearing load.

As explained above, positioning of the bearings inside the rotor and using them in outer ring rotation contribute the most to the longevity of the bearings, light weight of the nacelle and compact bearing size, which is the best design.

#### 4.4 For higher reliability

NTN has a variety of test machines to meet the requirements of its customers. We use them to confirm the reliability of the analytical results and collect the basic data of lubrication for the optimum maintenance.

Also, we are planning to commission a large test device that can be used to evaluate bearings of 4 m of outer diameter, which is the actual size used for offshore wind turbines (Fig. 10). This test device is able to control not only temperature and humidity, but also severe environmental conditions such as dust. We will be proving high reliability by building up verification of functionality and basic data using these machines.

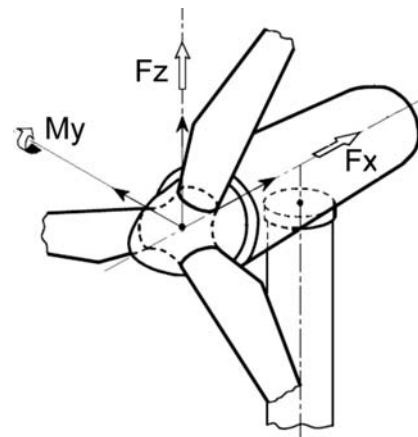


Fig. 9 Coordinate system of main bearing

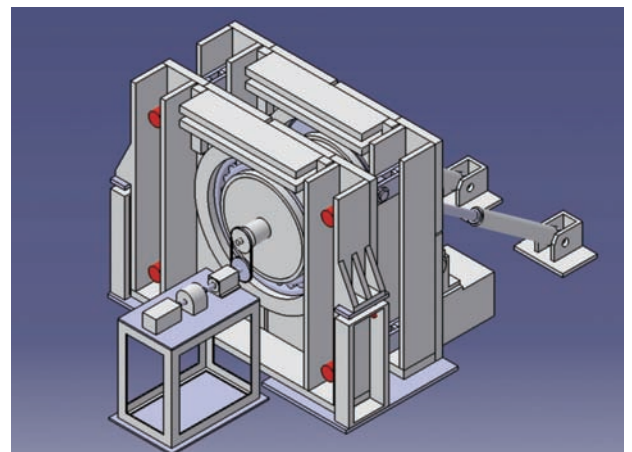


Fig. 10 Bearing testing machine for offshore wind turbine

## 5. Bearings for step-up gears

While the size of wind turbine generators is increasing, there are requirements for lighter and more compact step-up gears (Fig. 11) despite increased input torque.

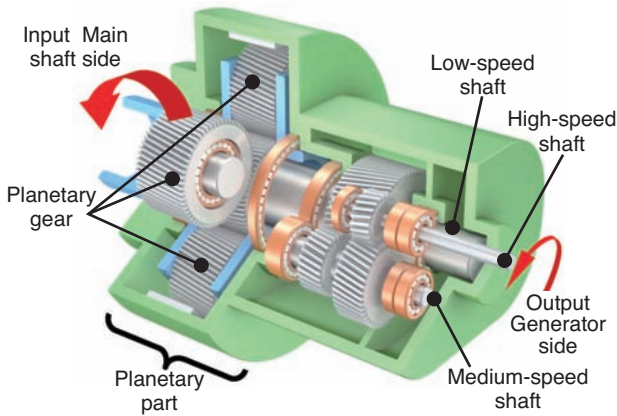


Fig. 11 Structure of general gearbox

### 5.1 Optimization of the internal design of bearings

For lightweight and compact step-up gears, the radial size of the planetary portion is important. Therefore, step-up gear manufacturers consider thinning the housing walls and reducing planetary gear sizes and bearings, in order to reduce the radial size as much as possible. We determine and propose specifications for bearings by analyzing the deformation of and load distribution on different parts, including the bearing peripheral structure, in addition to the operating conditions such as the load and spindle speed (Fig. 12).

Additionally, torque and spindle speed of a step-up gear can vary depending on the wind conditions. Since long-life and high reliability are needed even when the input condition changes, NTN applies specifications dedicated to step-up gears.

We optimize the crowning shape that mitigates harmful edge stress applied to the roller, which is the rolling element, when high load is applied to the bearings. Fig. 13 shows the comparison of distribution of contact stress between standard crowning and special crowning when high load is applied. It can be seen that the edge stress is reduced by applying special crowning to the rollers.

Also, bearings for medium/high-speed shafts support relatively low loads. We have developed a special surface treatment for inner/outer rings and rollers for preventing surface damage by sliding, such as smearing. (Fig. 14)

The special surface treatment raises the oil film formation capability to prevent surface damage caused by smearing due to metal contact. Fig. 15 shows the test results comparing standard and special surface treated products against smearing. More than twice the resistance to smearing was attained.

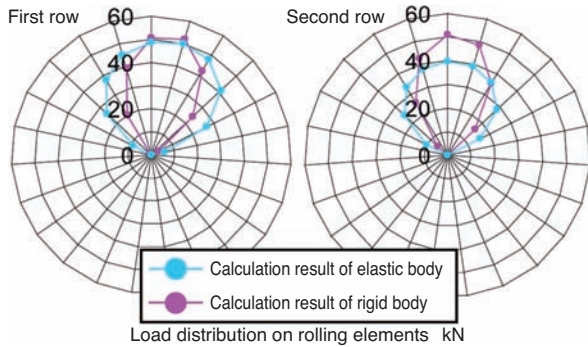


Fig. 12 Analytical result of planet bearing including structure in surrounding

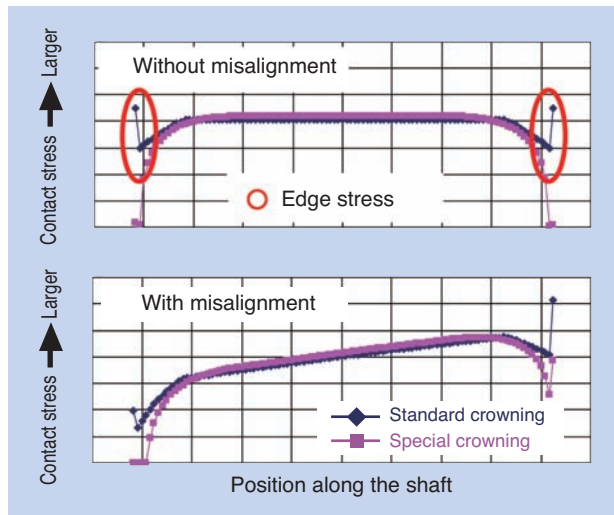


Fig. 13 Comparison of contact stresses of rolling element



Fig.14 Special surface treatment bearing

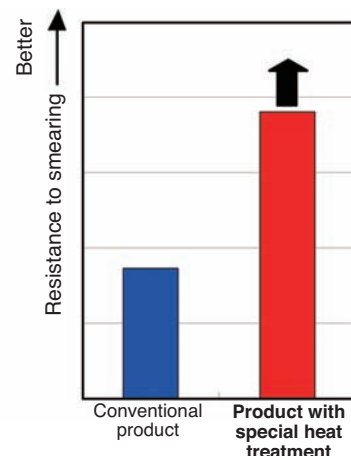


Fig.15 Examination result of smearing

### 5.2 Addressing changing step-up-gears

Along with larger and offshore applications, step-up gears are also changing.

**Table 2** shows different configurations of step-up gears. Conventionally, the input rotation from the main shaft is increased 100 times by mechanical step-up gears, and then the power is relayed to the generator; however, due to the requirements of higher reliability and compact size, different types of step-up-gears are being proposed.

#### (1) Multiple generator configuration

To enhance reliability, this type replaces the complex mechanical step-up gears with a simpler friction-drive speed-up mechanism to drive multiple generators. When NTN constant velocity type joints (**Fig. 16**) are used for torque transmission between

**Table 2** Speed increasing system

Mechanical type (conventional configuration)	
(1) Multiple-generator configuration	
(2) Unitization of step-up gears and generator	
(3) Hydraulic type	

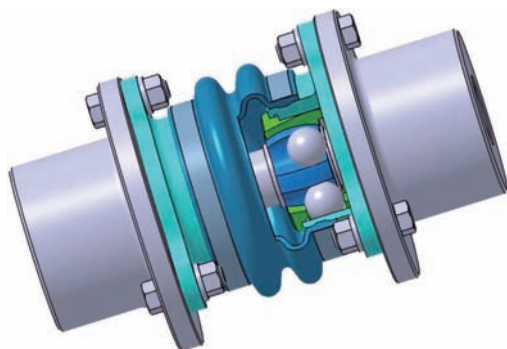


**Fig. 16** Constant velocity joint

the step-up mechanism and generator, the reliability can be further improved.

#### (2) Unitization of step-up gears and generator

By combining step-up gears with a generator into a unit, the size can be reduced. Compared to conventional power train, the rotation speed is relatively slow, making the speed-up ratio 10–20 times to simplify the structure for improved reliability.

#### (3) Mechanism to replace step-up gears

Speed is increased by a hydraulic pump/motor instead of step-up gears. Since rotation speed can be controlled by controlling the pump/motor, in addition to reliability improvement, the number of components can be reduced.

Step-up mechanism is facing a significant period of transition as the wind turbines are applied offshore. The requirements for bearings significantly vary depending on each of these mechanisms. NTN is diligently developing bearings suitable for each of these requirements.

## 6. Bearings for generators

Generally, deep groove ball bearings are used for generators supporting both sides of the rotor. The shaft diameter for a 1.5-MW-class turbine is about 150 mm.

NTN markets the “MEGAOHM™” series of bearings for generators.

This product has a special ceramic applied to the outside cylindrical surface to the sides of the bearing outer ring by thermal spraying (**Fig. 17**) and is used not only for wind turbines but also for a wide range of applications such as main motors for rail cars, general purpose motors, etc.

Also, for achieving even higher reliability for offshore application, we have a line-up of bearings using ceramic balls as shown in **Fig. 18** instead of steel balls. Because of reduced temperature rise due to ceramic balls, lubricant life can be increased.

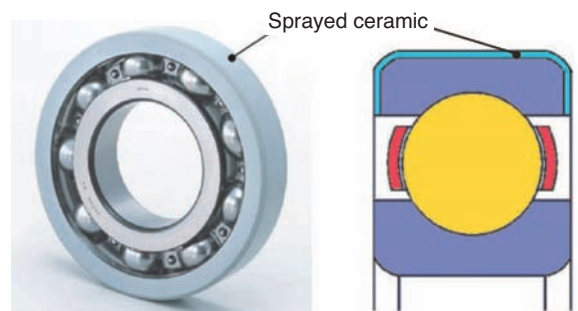


**Fig. 17** Ceramic insulated bearing



Fig. 18 Ceramic balls

## 7. Condition monitoring system

Windmills are often installed in remote locations away from cities, in the mountains, along the coast, etc.. If any failure occurs in offshore windmills, in particular, the repair cost can become huge.

To reduce this cost, the condition monitoring system (CMS) for wind turbine generators is attracting attention.

By using CMS, conditions of wind turbine generators can be remotely monitored for early detection of anomalies to prevent secondary damage, which leads to improvement of availability. This system will be separately discussed in detail.

## 8. Conclusion

Wind power is a new energy expected to grow further and the requirements for the operating environment, economy, and reliability are increasing.

NTN is moving forward with development and analysis, so that we can contribute to the development of wind power generation, in response of those requirements.

## Reference

- 1) BTM Consult : Word Market Update 2011

Photo of authors



Michio HORI  
New Energy Engineering  
Department  
Industrial Machinery Division

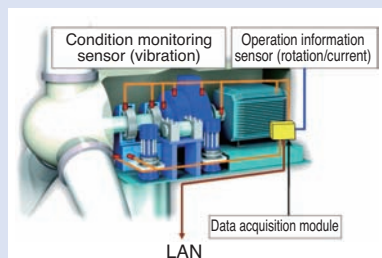


Yusuke YAMADA  
New Energy Engineering  
Department  
Industrial Machinery Division



Masahiko KATAOKA  
New Energy Engineering  
Department  
Industrial Machinery Division

# Application of Condition Monitoring System for Wind Turbines



Akitoshi TAKEUCHI\*

Takashi HASEBA\*

Hiroshi IKEDA\*

NTN has developed a Condition Monitoring System for wind turbines. CMS can detect the failure of main bearings, gearboxes, generators, and many mechanical components of wind turbines in their early stages. One feature of CMS is that users can monitor from a remote location. This system includes a data acquisition module, data management software and monitoring and analysis software for a client PC and was the first in Japan to acquire GL certification. In this paper, the structure and the diagnostic method of NTN's CMS will be introduced.

## 1. Introduction

Japan is 13th<sup>1)</sup> in the world, with wind power generation capacity of 2.5 GW in 2011. It is expected that it will significantly increase with the import tariff program that started in July this year. On the other hand, as the fixed price will be reviewed annually, further efforts are required, including reduction of the maintenance cost and improvement of capacity usage.

The main components of windmills such as blades, main bearings, step-up gears, and generators are located at the top of the tower. Therefore, repair and/or replacement of the equipment requires a supersized crane. In addition, since most of the windmills are located in the mountainous areas where access is challenging, maintenance cost is high. Further, the shutdown period may be prolonged, resulting in low availability if replacement components are not secured before the shutdown caused by failure.

Condition monitoring systems (CMS) for wind power generators target early detection of component deterioration from symptoms such as vibration and temperature, preventing proliferation of damage and enabling earlier ordering of replacement components for increased uptime. In addition, maintenance costs can be saved since the windmills are monitored remotely, reducing the need for site visits.

Since adequate sites for wind power generation are becoming scarce on-shore, it is expected that offshore

installations will increase<sup>2)</sup>. Access to these locations is even more difficult than on-shore installation for transporting replacement components, which will cause longer shut down when major failures are encountered. Therefore, Germanischer Lloyd (GL) recommends the use of GL approved CMS for offshore wind turbines.

In order to contribute to the advancement of maintenance, NTN has developed CMS based on its own vibration diagnostics technology. The system was the first in Japan to acquire GL-type approval.

## 2. System configuration

NTN's CMS consists of (1) a data acquisition module and measurement sensors, (2) data management software, (3) monitor/analysis software, as shown in Fig. 1. "(1) Data acquisition module" measures vibration, etc., with the sensors installed on the wind turbine and sends the data to the server through the Internet for storage. "(2) Data management software" performs a primary diagnosis of the data and issues an alarm if the data exceeds the threshold.

In addition, when "(3) Monitor/analysis software" is installed on a PC connected to the Internet, alarms and data can be monitored at a remote location from the wind turbine. This software also has an analysis function, enabling detailed diagnostics.

\*New Energy Engineering Department Industrial Machinery Division

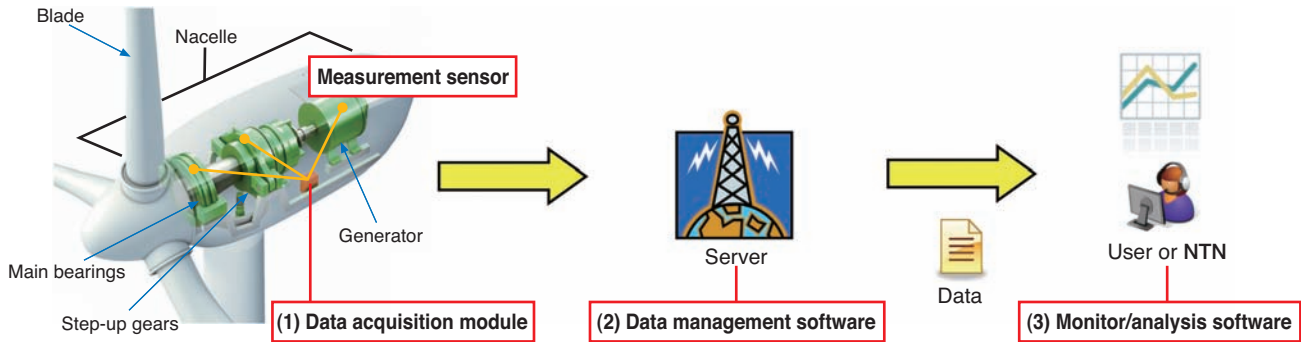


Fig. 1 Structure of NTN's CMS

### 3. Data acquisition module

Table 1 shows the specifications for “(1) Data acquisition module” and Fig. 2 shows its external view. The module is the world’s smallest, for easier installation into the nacelle, even on existing wind turbines. Since it has high dustproof/waterproof capabilities and a wider operating temperature range, it can be used in a wide variety of environments, including offshore applications.

Different sensors for vibration, rotation, current, temperature, etc., can be used and changing of the number of channels can also be accomplished easily.

Table 1 Specification of data acquisition module

Item	Specification	
Measured signals	Vibration (built-in acceleration sensor in the amplifier)	max16ch
	Temperature (thermocouple)	max 6ch
	Voltage (AC, DC, current sensor)	max 4ch
	Rotational speed (proximity sensor)	1ch
Power supply	AC90 ~ 260V (50/60Hz)	
Case dimension	250 × 290 × 108 mm	
Weight	5.1 kg	
Operating temperature	-20 ~ +60°C	
Protection of enclosure	Degree of protection of electric machines and appliances	
Electromagnetic compatibility	Complied with EN Standards, EN61000-6-2 and EN61000-6-4	



Fig. 2 Data acquisition module

### 4. Flow of operation and diagnosis philosophy

#### 4.1 Observation mode operation

Fig. 3 shows the flow of CMS from installation to operation. As the operating conditions of wind turbines changes from moment to moment, the cause must be determined if the change of vibration comes from the change of operation conditions or damage to the bearings and gears. In order to eliminate the influence of vibration of operating conditions, after CMS is installed, a preliminary measurement called “observation mode operation” is conducted as a preparation of diagnosis, to determine diagnostic operating conditions for the production stage.

With NTN’s CMS, rotational speed and generated power are used as parameters to indicate the operation conditions. In “observation mode operation,” the data acquisition module is regularly activated, and the rotational speed and generated power are recorded.

Fig. 4 shows an example of the main shaft rotational speed and generated power. In general, condition 1, which has large power output around the rated rotation speed, is considered diagnosis operating condition. For diagnosis of lower speed in a

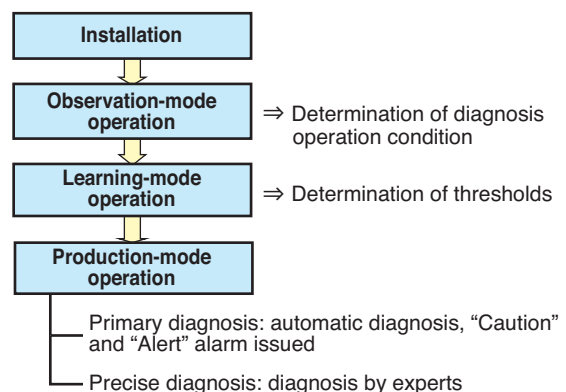


Fig. 3 Flow of NTN's CMS operation

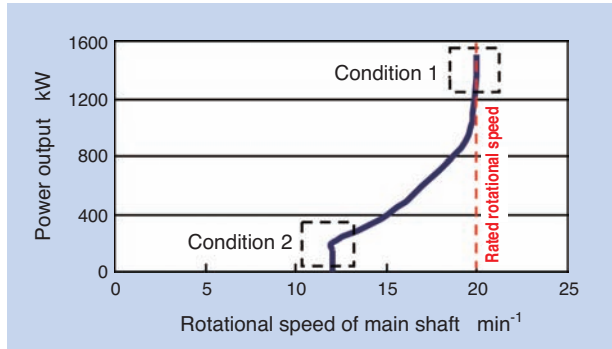


Fig. 4 Main shaft rotational speed and electric power

period of weaker wind conditions, condition 2 with slow rotation speed may be added as a diagnosis operation condition.

#### 4.1 Learning mode operation

After the diagnosis operation conditions are determined, “learning mode operation” is conducted to determine the diagnostic thresholds. In this mode, diagnosis parameters in normal conditions are collected. The data acquisition module is regularly activated in the same way as “observation mode operation,” data is collected only when the rotation speed and generated power match the diagnosis operation conditions.

NTN’s CMS automatically calculates the thresholds for “Caution” and “Alert.” From the relationship between the diagnosis parameters in normal conditions and those in damaged conditions obtained from the past failure cases and the data in normal conditions measured in “learning mode operation,” the thresholds for the diagnosis parameters for the following section 5 are automatically established. In addition, the thresholds can be manually set, as well.

#### 4.3 Production mode operation

Under “production mode operation,” CMS regularly conducts measurement and if a diagnosis parameter exceeds the threshold, it issues two types of alarms, “Caution” and “Alert,” as a “primary diagnosis” in Fig. 3. The alarm can be confirmed on “(3) Monitor/analysis software.” It is also able to automatically notify predetermined personnel via emails.

“Precise diagnosis” in Fig. 3 is diagnosis provided by an expert using analytical tool of “(3) Monitor/analysis software.” “(3) Monitor/analysis software” displays diagnosis parameters, trend analysis, and thresholds, for easy determination of the diagnosis parameter trend. It also provides filter processing, envelope processing, and FFT processing of time waveforms, as well as a function to display

frequencies caused by defects of bearings and gears on the spectrum. It is also possible to compare past waveforms with the current ones.

### 5. Diagnosis parameters

The main components of wind turbines are the blades, main bearings, step-up gears, and generators. NTN’s CMS addresses damage to any of these components. Table 2 shows diagnosis parameters corresponding to the failure modes. The relation between the failure modes and diagnosis parameters are discussed in detail in the following:

#### (1) Imbalance of blades

When blades are damaged, imbalance of mass will cause an increase in vibration. Imbalance appears as a peak in rotational frequency. Imbalance anomaly is detected taking the primary to tertiary components of rotational frequency of the main shaft as the diagnosis parameters.

#### (2) Abnormal vibration of nacelle/tower

This indicates a large vibration out of norm when they receive strong wind, etc. The vibration consists of low frequencies; the sum of spectrum in low frequency band among acceleration vibration is used as the diagnosis parameters.

#### (3) Anomaly in bearings

It is caused by separation or abnormal wear on the raceway surface or rolling surface. The effective value and modulation factor are used as diagnosis parameters. The effective value is an average of vibration and the modulation factor is an effective value of the AC component of accelerated vibration after envelope processing and can be used for determination of vibration caused by a shock.

#### (4) Anomaly in gears

It indicates anomalies of tooth contact surface, such as the pitching and abnormal wear of tooth flank. It is diagnosed by tooth meshing frequency of primary to tertiary components and the sum of spectra of high-frequency band in the acceleration vibration spectra.

Table 2 Failure modes and diagnosis parameters

Failure mode	Diagnosis parameters
Imbalance of blades	Primary to tertiary frequency components of the main shaft rotation
Abnormal vibration of nacelle/tower	Low frequency components of nacelle
Anomaly in bearings (main bearings, step-up gears, generator)	Effective value and modulation factor of vibration in the proximity of bearings
Anomaly of gears (step-up gears)	Primary to tertiary components of tooth meshing frequency and vibration components of high frequency band calculated from specification of the gears

## 6. Case study of diagnosis for generator bearings

Effective values, which are diagnosis parameters, were obtained from the measurement of vibration in bearings with electrical pitting and normal bearings of the actual generator. Fig. 5 shows the relation between main shaft rotational speed of the wind turbine and vibration effective values around the bearings. The effective values are significantly larger due to electrical pitting. The difference from the normal bearings is more significant as the rotational speed becomes higher.

Fig. 6 shows the result of envelope spectrum of vibration. The outer ring defect frequency, which is a frequency that a point on the outer ring raceway surface is in contact with the rolling element, and its higher order components are observed. It is then possible to assume damage on the outer ring raceway surface. This envelope spectrum evaluation result was proven correct after this bearing unit with electrical pitting was disassembled and examined, as it showed repetitive ridge marks on the outer ring raceway, as shown in Fig. 7.

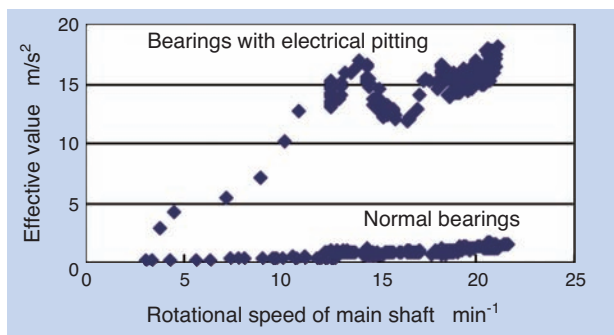


Fig. 5 Main shaft rotational speed and root mean square value of vibration

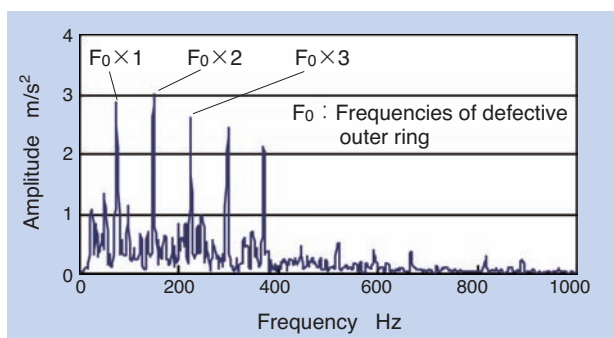


Fig. 6 Envelope spectrum of vibration



Fig. 7 Outer raceway failure by electrical pitting

## 7. Conclusion

Functions expected of CMS for wind turbines include not only an early detection of damages but also the prediction of remaining life. For improving the capacity uptime, it is important to minimize the period of shutdown, and therefore, it is critical for the users to know how long certain components can be used after damage is detected. For highly precise prediction of the remaining life, vibration measurement on the actual machines and accumulation of data from examinations through disassembly are necessary.

We will work together with different players such as wind power providers, windmill facility manufacturers and maintenance service providers to accumulate diagnostic know-how so that the system can provide more useful information for expansion of wind power utilization.

## Reference

- 1) Global Wind Energy Council : Global Wind Report Annual Market Update 2011
- 2) Takeshi Ishihara: Current situation and future perspective of offshore wind power generation, The Journal of the Institute of Electrical Engineers of Japan, Vol. 131 No. 7, 2011
- 3) Germanischer Lloyd Industrial Services GmbH : Guideline for the Certification of Condition Monitoring Systems for Wind Turbines, 2007

## Photo of authors



Akitoshi TAKEUCHI  
New Energy Engineering  
Department  
Industrial Machinery Division

Takashi HASEBA  
New Energy Engineering  
Department  
Industrial Machinery Division

Hiroshi IKEDA  
New Energy Engineering  
Department  
Industrial Machinery Division

# Motorized Linear Module for Tracking System of Solar Light / Solar Heat Power Generation

Tomoyuki OWADA\*  
Masaki KAGAMI\*



NTN is engaged on product development in the renewable energy sector. This article introduces motorized linear modules, which possess the features of low cost, high performance, and easy maintenance for solar tracking systems.

## 1. Introduction

Expectation for renewable energy is increasing, daily, due to growing interest in the reduction of greenhouse gases and the review of electrical power supply. Particularly, solar energy utilization, such as photovoltaic and solar thermal power generation, has attracted attention. However, the reduction of overall cost, including simplified associated equipment, easy maintenance, and reduced running cost, is required, since the investment in facilities reflects the power generation cost.

NTN has developed several motorized cylindrical linear modules with high environmental resistance, thrust power, and resolution.

In this paper, the structure and specifications of these modules are introduced.

## 2. Solar tracking system for solar thermal power generation

As a measure to efficiently utilize solar energy, a mechanism is implemented to ensure that an irradiated surface, such as the mirror in Fig. 1, faces the sun at all times (heliostat). The mechanism consists of a reflective mirror, a linear motion actuator for tracking the solar angle of elevation, and a rotating driver for tracking the horizontal angle.

The sunlight reflected by the heliostat is collected by the solar collector at the central tower, as shown in Fig. 2. The medium inside the heat collector is heated to 500 – 1000°C by the collection of light and used as the heat source for steam-power generation.

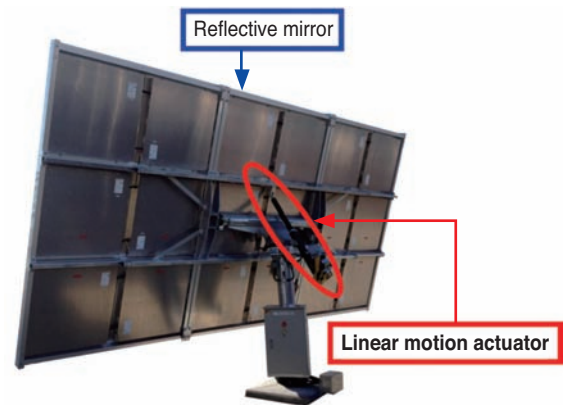


Fig. 1 Heliostat mirror

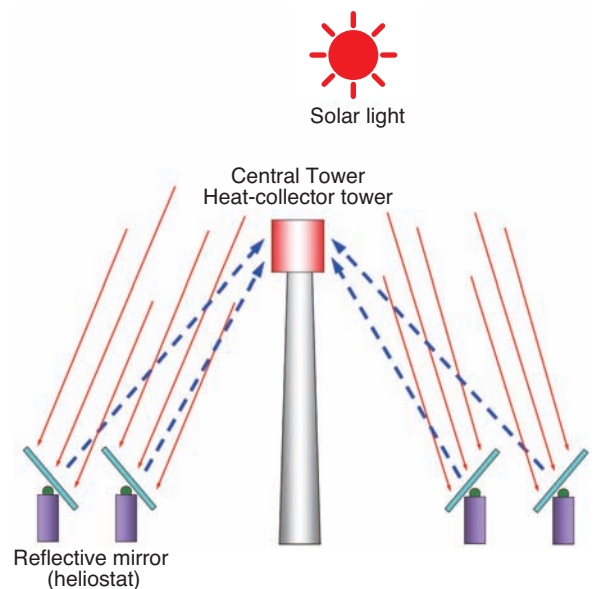


Fig. 2 Central Tower power plants

\* Product Engineering Department, Precision Equipment Division

So far, pneumatic and hydraulic cylinders are used for actuators to control the angle of elevation for tracking the height of the sun, because their structures are simple and suited for mass production. However, since they require ancillary equipment, air and oil may leak from inside the cylinder or hose. Therefore, the use of motors is attracting attention.

### 3. Structure and characteristics of the motorized linear module

Fig. 3 and Fig. 4 show the structure and outer view of the motorized linear module for tracking solar light, respectively.

#### 3.1 Feed screw

To emphasize maximum thrust, long-lasting reliability, and position reproducibility for both forward and backward directions (accuracy of repeatability), ball screws were adopted.

#### 3.2 Linear motion guide

As shown in Fig. 5, a trunnion structure was adopted with bearings installed at the tips of 4 shafts which extended radially from the outer surface of the

nuts for the ball screws. The trunnion bearings are in contact with 4 raceway surfaces inside the housing of the body to obtain a smooth linear guide, as well as to receive uneven load applied to the slide shaft tips in the vertical and horizontal directions.

#### 3.3 Motor, reducer

A 2-phase stepping motor and worm gear reducer were adopted.

#### 3.4 Installation to the body

Rod ends were installed at both ends of the fixed side (motor side) and floating side (slide shaft side) so that the mirror is freely movable within a certain range.

#### 3.5 Other structure

A dust control seal is provided at the inlet/outlet of the slide shaft to prevent dust and foreign objects from entering. In addition, a stainless steel cover is installed for the motor. The sensor areas and wiring are also protected by ultraviolet-resistant and heat-resistant tubes. Finally, a weather-resistant mold agent is used at the connection of exterior components to provide a dustproof and drip-proof property.

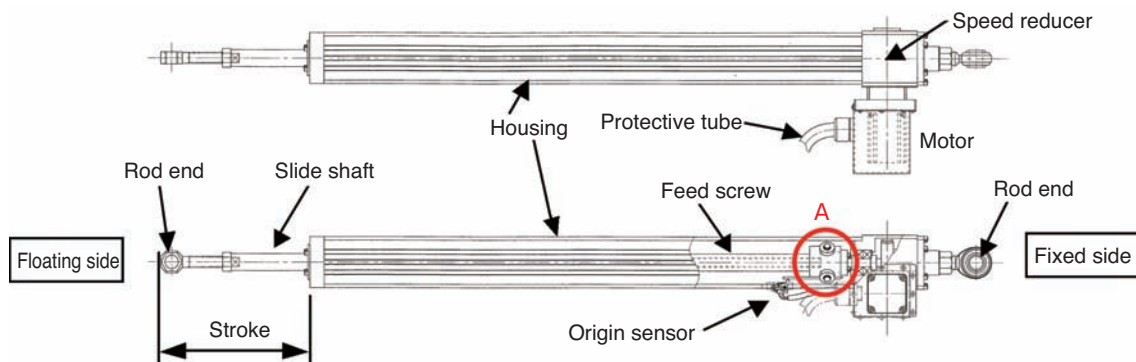


Fig. 3 Structure of motorized linear module

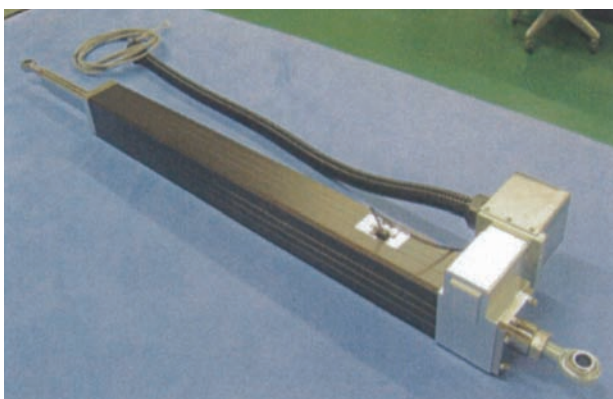


Fig. 4 External appearance of motorized linear module

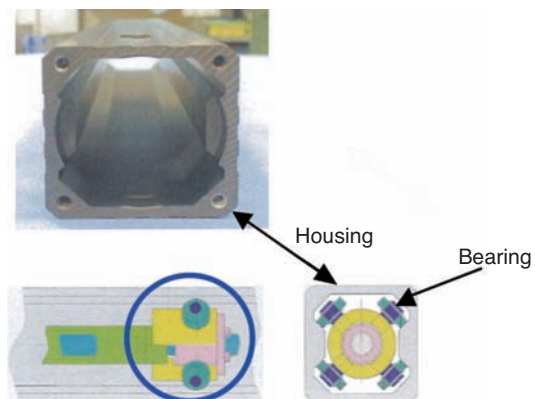


Fig. 5 Part of straight guide (Magnified view A)

## 4. Application of motorized linear module for tracking solar light

### 4.1 Operating conditions

Table 1 shows the operating condition of the motorized linear module. This condition assumes operation in severe environments, such as a desert. Reliability was emphasized for developing this product.

Usually, the reflective mirror changes the direction gradually so that it is precisely synchronized to the orbit of the sun; however, with strong wind, the reflective mirror withdraws at the maximum speed to the horizontal position for protection from danger. The load applied to the tip of the module is considered in this operation.

### 4.2 Product specification and measurement results

Table 2 shows the measurement results of the motorized linear module product (n = 2). This confirmed that the results sufficiently satisfy the overall specifications.

Table 1 Service condition of motorized linear module

Item	Operating condition
Ambient temperature	-10~+45°C
Ambient humidity	40~100%
Condition for maximum thrust as needed	Wind speed 40m/s

Table 2 Specifications and validation result

No.	Measured item	Specification	Developed product No.1	Developed product No.2
1	Resolution	1 μm/p	1	1
2	Maximum speed	2.5mm/s or more	Complied	Complied
3	Accuracy of repeatability of positioning	Less than ±0.1mm以下	±0.004	±0.004
4	Thrust output	40m/s of wind speed equivalent	Complied	Complied
5	Verification of loss of steps of stepping motor	40m/s of wind speed	No loss of steps	No loss of steps
6	Accuracy of positioning	Reference	0.096mm	0.093mm
7	Backlash	Reference	0.002mm	0.016mm
8	Power consumption	Reference	29W	24W

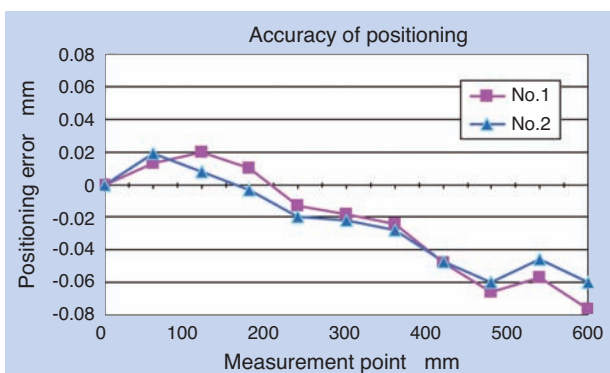


Fig. 6 Result of positioning accuracy

### 4.2.1 Accuracy of positioning

The accuracy of positioning reproducibility was 1/10 or less than the specification.

Also, the accuracy of positioning in the entire stroke range was very high; with 0.10 mm or less as shown in Fig. 6.

### 4.2.2 Verification of thrust performance

The thrust performance required for withdrawal operation under strong wind was evaluated with the measurement equipment shown in Fig. 7. From this test result, the maximum thrust was verified to be adequate.

## 5. Solar tracking system for photovoltaic power generation

There are mainly three different methods for light-collection-type photovoltaic power generation: the fresnel lens method, which utilizes concentrically arranged annular sections of regular lenses which are made thinner than regular lenses but have a jagged cross section (Fig. 8); the reflective mirror method, which collects light at the central focal point by reflecting the sunlight with a concave mirror, and then again with a convex mirror placed above at the center (Fig. 9); and the cassegrain lens method, which collects light at the central point of the bottom part of concave mirror by reflecting the sunlight with the concave part of the bottom of the lens, and then again

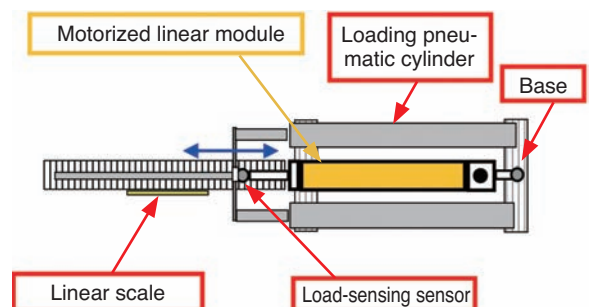


Fig. 7 Thrust force measuring device

with the convex part of the top of the lens (Fig. 10). All of these types require accurate tracking. NTN has developed both a high-accuracy and high-rigidity type motorised linear module so that they can be selected depending on the size and structure of the solar panels. Both of these specifications are currently under evaluation with no problems in continuous operation.

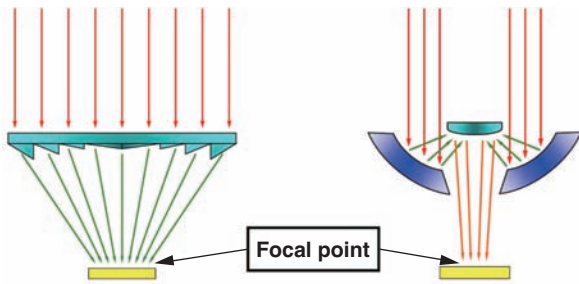


Fig.8 Fresnel lens

Fig.9 Reflective mirror

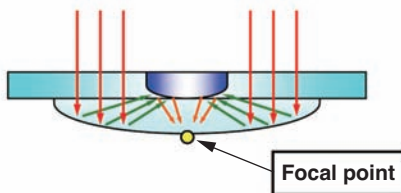


Fig.10 Cassegrain lens

**5.1 High-accuracy specification**

Fig. 11 shows a motorized linear module aiming for moving small panels with high accuracy.

The body of the module is fixed to the base using pins for supporting the body at both sides of the housing; then, the reflective mirror is installed to the clevis at the tip of the slide shaft. The stroke is about 200 mm and a ball screw is used in the actuator for high accuracy, similar to the one for solar thermal power generation. A trunnion structure is adopted for the linear motion guide.

**5.2 High-rigidity specification**

Fig. 12 shows the high-rigidity type solar tracking system for accurate tracking of sunlight while strongly supporting medium to large panels. A trunnion structure is adopted, the same as the other types, for the linear motion guide to cope with uneven loads and high rigidity. The stroke is 500 mm and an accurate trapezoidal screw is used.

In addition, the slide shaft is equipped with bellows for preventing dust and drips from entering.

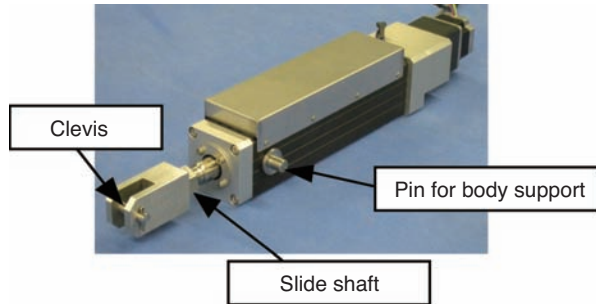


Fig. 11 High precision spec linear module

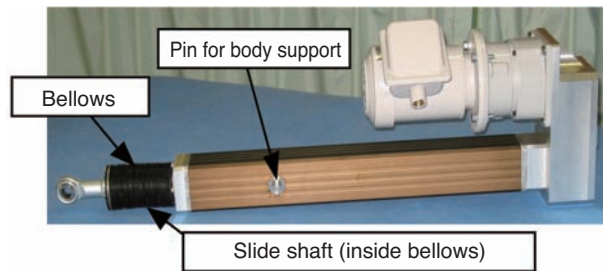


Fig. 12 High stiffness spec linear module

**6. Conclusion**

It is expected that demand for renewable energy will continue to increase.

We have developed motorized linear modules for tracking systems that suit the properties of solar thermal power generation and photovoltaic power generation, respectively.

While they are currently under empirical evaluation, improvement in durability and maintainability is being addressed for product commercialization that meets market demand.

Photo of authors



Tomoyuki OWADA  
Product Engineering  
Department, Precision  
Equipment Division



Masaki KAGAMI  
Product Engineering  
Department, Precision  
Equipment Division

# Development of Induction Through-hardening and Induction Tempering Methods with Temperature Control and Microstructural Control in Bearing Steel

Takumi FUJITA\*  
Nobuyuki SUZUKI\*



In this report, induction through-hardening and induction tempering for bearing rings are introduced. Both technologies determine heat conditions in induction heating by utilizing temperature control and monitoring of carbon solubility in bearing steel. This means the system eliminates the need for qualified expertise in the heat condition design of induction through-hardening and induction tempering. The system

will promote replacements of conventional atmosphere furnaces with induction heating furnaces, and result in a contribution to energy saving in the manufacturing process of rolling bearings and reduction of negative environmental impact.

## 1. Introduction

High-frequency induction heating (hereafter, IH) has advantages in safety, environmental impact, and heating efficiency over other heating methods. It is very safe against fire because no combustion is used, environmentally friendly because there is no heat dissipation, and efficient because no fuel storage facility is required. In addition, since this mechanism offers quick heating taking advantage of electricity, it is suitable for any quick heating application. Recently, cooking devices that take advantage of these characteristics, such as cooking heaters and electric kettles, are found in many homes.

On the other hand, IH is attracting attention in industrial production <sup>1), 2)</sup>, due to many advantages in production facilities, such as piece-by-piece processing, facility space reduction, quick start/stop, and efficient processing of small-lot products. In the area of wheel bearings, selective hardening by IH is applied.

IH has a lot of advantages in industrial production activities. However, there were not many uses in through hardening for general bearings. There are two reasons for this. One is the perception that the selective heating property of IH makes it difficult to uniformly heat the entire product. The other is the concern whether the high temperature and short

heating could make penetration control of carbon into the base metal with good reproducibility, which is necessary for hardening of bearing steel. In order to clear these concerns, a design technique for the heating coil to provide uniform heating conditions and a method to control organization of the entire product are needed.

In this paper, a method for high-frequency through hardening and high-frequency induction tempering (hereafter, IH through hardening/tempering) that can minimize the heating time by controlling the organization of the entire steel bearing raceway ring (JIS-SUJ2, hereafter SUJ2) is discussed.

## 2. IH through-hardening/tempering system

### 2.1 Overview of the system

Preformed material of SUJ2 with 1% carbon is made by spherical disperse precipitation of carbide with 15% of area ratio to improve machinability. When the preformed product is heated to hardening temperature, carbon within the carbide becomes a solid solution in austenite. The hardening temperature needs to be adjusted so that the area ratio of carbide becomes 6–8% for a good balance of fatigue strength, wear resistance, and dimensional stability <sup>3)</sup>. For through hardening of bearing rings made of SUJ2 in

\* Advanced Technology R&D Center

an atmosphere furnace, sufficient soaking time should be secured depending on the thickness so that the overall carbide distribution is kept uniform. On the other hand, with IH, which is basically a selective heating technology, uniform heating is more difficult than with an atmosphere furnace. Therefore, technology to control the entire bearing rings material within the set criteria is necessary. In the following, a method of controlling the entire material based on the result of multiple-point measurement of bearing rings is discussed.

Fig. 1 shows a conceptual diagram of IH system with temperature control.

Two radiation thermometers are set at the heater to measure the temperature at the surface close to the coil and far from the coil. The point closer to the coil is heated faster since more flux penetrates it. On the other hand, the point far from the coil is heated slowly since less flux penetrates it. Now, the position of the radiation thermometer closer to the coil (1) is called the temperature-controlling side and the position of the radiation thermometer far from the coil (2) is called the heating-stop-timing side. The characteristic of this technology is the material prediction method based on the temperature measurement results of the material at these positions. Together with PID control of the temperature at the temperature-controlling side, the material at that position is predicted in real time, with a PC based on the temperature measurement results. In addition, the temperature of the heating stop timing side is also measured to predict the material at that position, as well. If the bearing rings are cooled immediately after the material prediction results of both the positions reach the control criteria of material, hardening can be accomplished in the shortest time. In this system, the material parameter to be predicted at hardening is set to carbide area ratio, and the

material parameter to be predicted at tempering is set to hardness after tempering.

Furthermore, the configuration of PC and controller in Fig. 1 can also be used in the configuration with programmable PLC, fast-response AD and DA conversion unit, controlling unit with PID control, and a touch panel.

**2.2 Prediction of carbide area ratio at IH hardening**

Fig. 2 shows the carbide distribution of SUJ2 hardened product made with an atmosphere furnace. The carbide area ratio in the figure is 6.3%. With this technology, the carbide distribution is predicted from the temperature measurement results using two thermometers. The prediction can be made by solving the diffusion equation <sup>4)</sup> or using empirical formula. The method using empirical formula was adopted for this system. We considered that the prediction accuracy is higher with the method from experimental results than with the diffusion equation model because the latter needs several assumptions. The equations (1) and (2) show the empirical formula.

$$M = M_0 \exp(-kt)^n \dots \dots \dots (1)$$

$$k = A \exp(-E/RT) \dots \dots \dots (2)$$

- M* : Carbide area ratio (%)
- t* : Heating time
- M*<sub>0</sub> : Carbide area ratio (%) of raw material
- T* : Temperature (K), *R*: Gas constant
- A, k, n, E*: Constants obtained from experiment

*A, k, n, and E* in the formula are obtained by regressing the carbide area ratio of the test samples hardened under various conditions with equations (1) and (2).

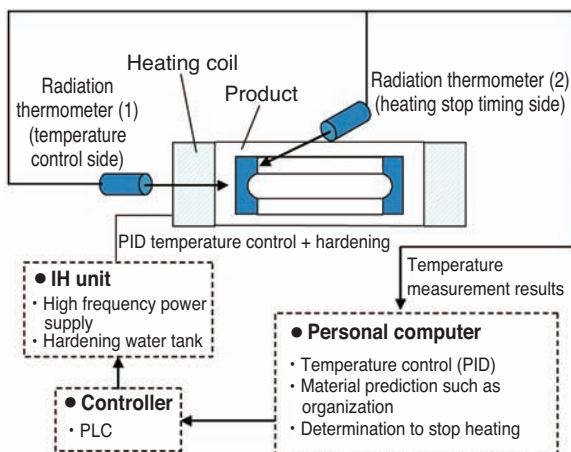


Fig. 1 Schematic of induction heating system with temperature control

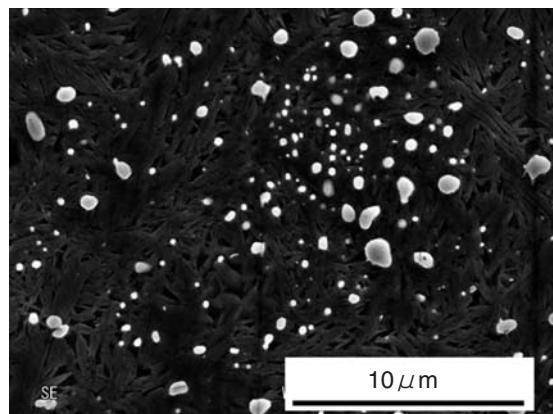


Fig. 2 SEM image of carbide distribution of SUJ2 quenched by atmosphere furnaces

The carbide area ratio is obtained by analyzing the electron microscopic image of the organization of test samples. Fig. 3 shows the results from the calculation of the relation between heating conditions and carbide area ratio, using the regression formula obtained from carbide area ratios of 50 samples of different types. The carbide area ratio significantly reduces in a short time when the heating temperature is higher.

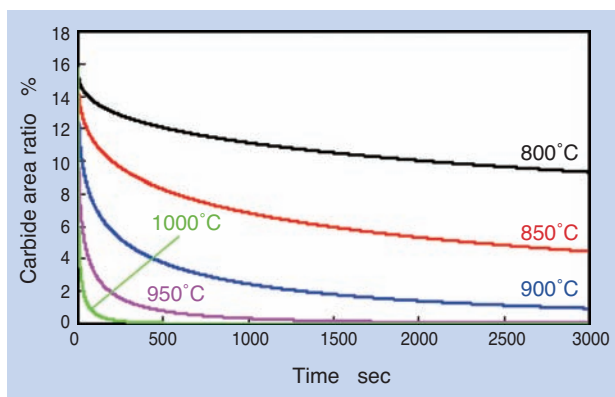


Fig. 3 Carbide area ratio as a function of holding time before quenching of SUJ2

Equations (1) and (2) predict the change of carbide area ratio at constant temperature over time; however, since the temperature of bearing rings while being heated is not constant, some ingenuity is required for calculating the carbide area ratio from the temperature measurement results. Fig. 4 shows the schematic of temperature measurement results. When the graph is enlarged, you can see that the temperature changes in steps. The carbide area ratio  $M_i$  can be calculated using equations (3) and (4) based on temperature  $T_i$  at each step.

$$M_i = M_0 \exp(-(k_i(t_i + \Delta t))^n) \dots\dots\dots (3)$$

$$t_i = \sqrt[n]{\ln(M_0/M_{i-1}) / A^n \exp(nE/RT_i)} \dots\dots\dots (4)$$

$t_i$  indicates the time necessary for heating to reach the temperature of the next step, converted from the change of the carbide area ratio of the current step.  $\Delta t$  is the sampling period for temperature measurement.

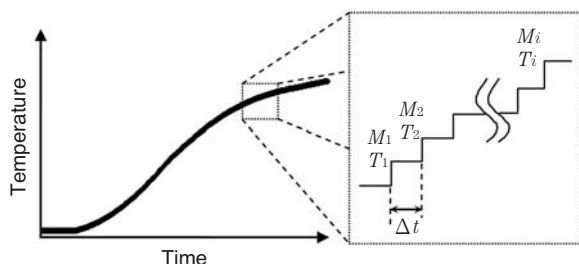


Fig. 4 Schematic of time-temperature chart

In addition, the calculation of the carbide area ratio is started from the austenite temperature when the carbide starts penetrating.

Fig. 5 shows an example of calculation of carbide area ratio from the temperature measurement results at the temperature-controlling side and the heating-stop-timing side. PID is controlled so that the temperature-controlling side remains constant at 880°C. The carbide area ratio decreases after the transformation point is passed along with the rise of temperature. If we set the allowable range of carbide area ratio to 6–10%, the shortest heating time, with which each temperature measurement position reaches the allowable range, is 120 seconds. Fig. 6 shows the carbide distribution of the heating-stop-timing side of the bearing rings hardened under the conditions of Fig. 5. The carbide area ratio of Fig. 6 is 9.5% and matched, in general, with the calculation result of Fig. 5.

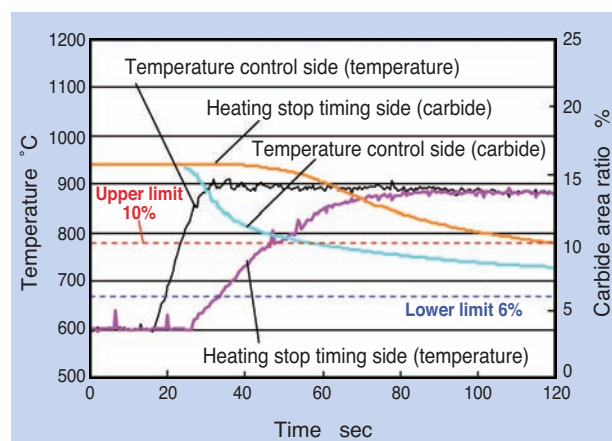


Fig. 5 Specific example of carbide area ratio calculated by equations 3 and 4

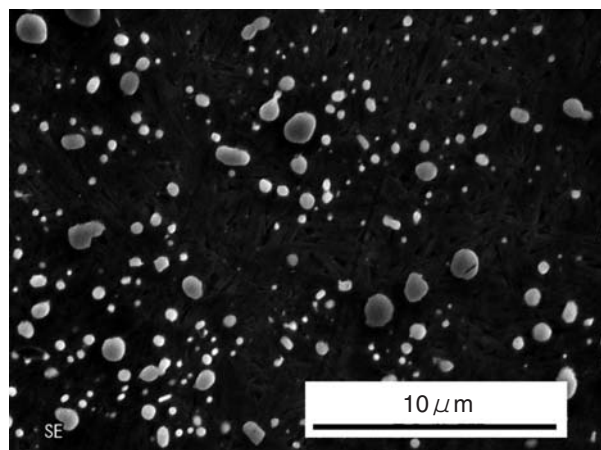


Fig. 6 SEM image of carbide distribution of SUJ2 after quenching. The austenitization condition and the predicted carbide area ratio are shown in Fig. 5

**2.3 Prediction of hardness with IH tempering**

In tempering, the hardness after tempering is estimated in real time from the temperature measurement results <sup>5)</sup>. Equations (5) and (6) show the empirical formula for obtaining hardness after tempering.

$$X = X_0 - (X_0 - X_f)(1 - \exp(-(k' t)^{n'})) \dots\dots\dots (5)$$

$$k' = A' \exp(-E' / RT) \dots\dots\dots (6)$$

- X : Hardness after tempering (HRC)
- t : Heating time
- X<sub>0</sub> : Hardness after hardening (HRC)
- X<sub>f</sub> : Hardness of raw material (HRC)
- T : Temperature (K), R: Gas constant
- A', k', n', E': Constants obtained from experiment

Fig. 7 shows the relation of heating time and hardness after tempering for each tempering temperature. This relation is obtained, in the same way as Fig. 3, by regression analysis of the results of hardness measurement of test samples obtained under systematically changed tempering conditions. In addition, the real time calculation for hardness after tempering for IH is the same as that of case hardening.

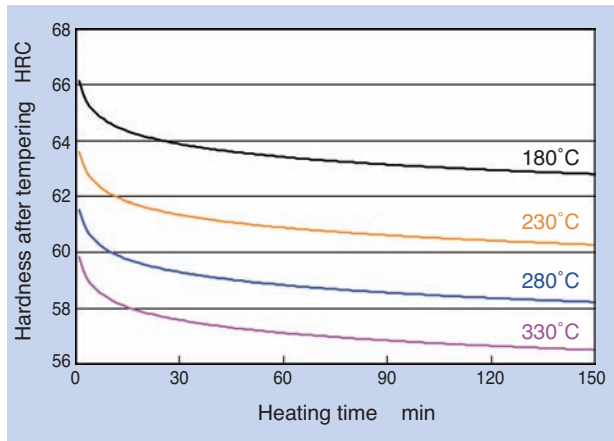


Fig. 7 Relationship between hardness and tempering time

**2.4 Material examination results**

Using this technology, IH through hardening and tempering was applied to 6206 ball bearing inner/outer rings made of SUJ2. Table 1 shows the list of test samples. Vickers hardness of 8 types of test samples in Table 1 was measured at 9 points shown in Fig. 8. Table 2 shows the average hardness and standard deviation at all the measurement points. Standard hardness of bearings made of SUJ2 was, in most cases, HRC 60-63 (HV696-772). The variance of hardness in products was within 2 points in HRC

**Table 1** Heat condition for inner and outer rings of 6206 ball bearing

No	Location	Hardening	Tempering
1	Outer ring	900°C IH heating Carbide area ratio 6-8% Room temperature soluble water cooling	180°C×2h Thermostatic chamber heating
2	Inner ring	↑	↑
3	Outer ring	830 ~ 860°C Atmosphere furnace heating 90°C semi-hot oil cooling	230°C IH uniform heating Hardness HRC62
4	Inner ring	↑	↑
5	Outer ring	900°C IH heating Carbide area ratio 6-8% Room temperature soluble water cooling	230°C IH uniform heating Hardness HRC62
6	Inner ring	↑	↑
7	Outer ring	Standard product (hardening/tempering with atmosphere furnace)	
8	Inner ring		

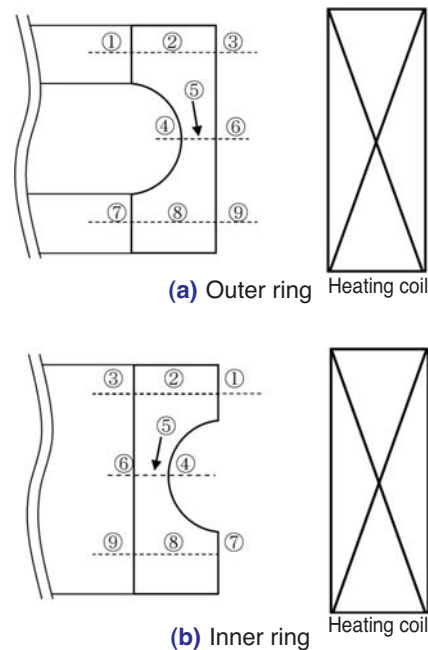


Fig. 8 Measuring position of Vickers hardness

**Table 2** Vickers hardness for inner and outer rings of 6206 ball bearings

No	Location	Hardening	Tempering	Hardness HV	
				Average	Standard deviation
1	Outer ring	IH	Furnace heating	763	7.5
2	Inner ring			734	24.8
3	Outer ring	Furnace heating	IH	710	6.5
4	Inner ring			721	6.1
5	Outer ring	IH	IH	702	5.3
6	Inner ring			710	11.9
7	Outer ring	Furnace heating	Furnace heating	743	8.3
8	Inner ring			738	5.5

(approx. 50 points in HV). The quality of 6206 ball bearing inner/outer rings processed with this technology was good, well within these ranges.

### 3. Characteristics of IH through-hardening/tempering product

#### 3.1 Rolling element fatigue test

Rolling fatigue tests were conducted using the 6206 ball bearing life tester shown in Fig. 9 under the conditions in Table 3. Fig. 10 and 11 show the test results under clean oil lubrication and lubrication with contamination. Under rolling fatigue tests with clean oil lubrication, all three subjects completed testing without any damage for 5984 h. Assuming the Weibull slope is the same as the standard products, 10% life of IH through hardening/tempering is calculated to 2115 h<sup>6), 7)</sup>, with 90% of reliability, and is equivalent to the life level of 1624 h for standard bearings.

Also, the life of IH through-hardening/tempering products under contaminated lubrication showed no difference from the standard products, after the significance test<sup>6), 7)</sup>.

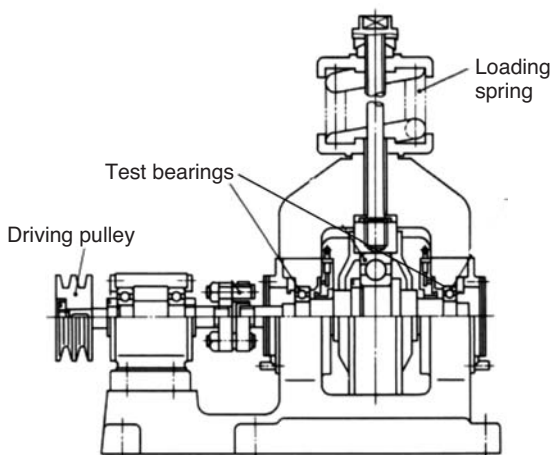


Fig. 9 Rolling contact fatigue (RCF) test rig for 6206 ball bearing

Table 3 Conditions of RCF life testing for 6206 ball bearing

Item	Clean oil lubrication	Lubrication with foreign objects
Bearing		6206C3
Maximum contact surface pressure		3.2GPa
Maximum shear stress depth		$Z_{45^\circ}=0.16\text{mm}$
Rotational speed		$3000\text{min}^{-1}$
Lubrication	Turbine oil with no additives VG56 circulation lubrication	NTN standard foreign objects 0.4g/L Turbine oil with no additives VG56 circulation lubrication
Foreign objects		KHA30 Gas-atomized powder
Size of foreign objects		100~181 $\mu\text{m}$
Hardness of foreign objects		HV700~800
Estimated life		126h (no foreign objects)

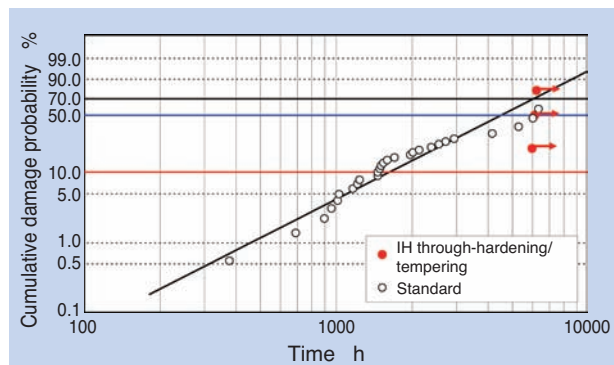


Fig. 10 Comparison of RCF lives for 6206 ball bearing treated by induction heating and conventional heating (clean lubrication)

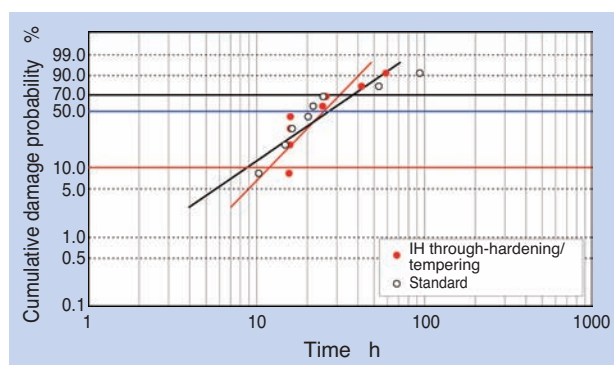


Fig. 11 Comparison of RCF lives for 6206 ball bearing treated by induction heating and conventional heating (contaminated lubrication)

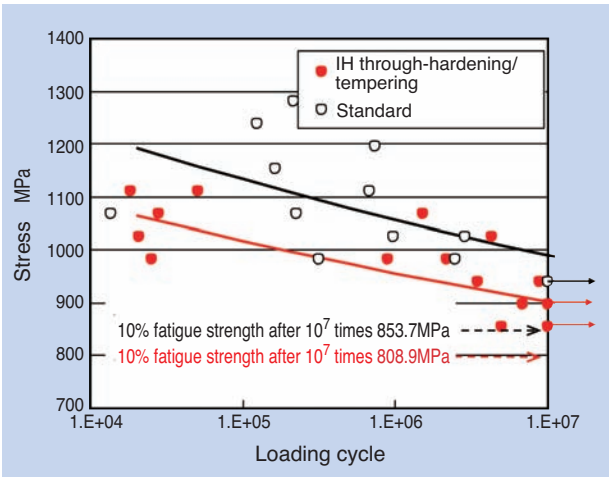
#### 3.2 Static crush test and ring crack fatigue test

Table 4 shows the static crush test result of 6812 ball bearing outer rings. IH through-hardening/tempering products showed the same strength against static crush as the standard products.

Fig. 12 shows the results of a crack fatigue test using rings of 37.8 mm outer diameter  $\times$  29.8 mm inner diameter  $\times$  15 mm width. The continuous drop single logarithm curve model, standard from the Society of Materials Science, Japan,<sup>8)</sup> was applied to the data obtained from the fatigue test for analysis. The 10% fatigue strength of IH through-hardening/tempering product after  $10^7$  times was about 50 MPa lower than the standard product. However, since there was no significant difference with a 5% risk factor, both can be considered the same in strength.

**Table 4** Compressive strengths of SUJ2 rings treated by induction heating and conventional heating

Type	Heat treatment	Strength (kN)	
		Average	Standard deviation
6812 Ball bearing outer ring $\phi 78 \times \phi 60 \times 10$	IH through-hardening/tempering	1.50	0.13
	Standard deviation	1.48	0.02



**Fig. 12** SN Curves of SUJ2 rings treated by induction heating and conventional heating. The stress ratio is 0.1.

**3.3 Peeling test and smearing test**

Under thin lubrication conditions, the rolling elements and raceway rings are in direct contact causing surface damage with small peeling and cracking. Also, in applications with slide bearings, surface damage caused by smearing can be observed. These surface damages are evaluated using a two-cylinder tester shown in **Fig. 13**.

**Table 5** shows the peeling test conditions. The peeling test is conducted by driving the driver-side shaft with a motor, allowing free rotation of the follower side. The resistance against peeling was evaluated with the average of peeling area ratios at three positions on the rolling contact surface of the driving side. **Fig. 14** shows the peeling test results. The peeling area ratio of the IH through-hardening/tempering products was equivalent with the standard products.

**Table 6** shows the smearing test conditions. For the smearing test, the driver side and follower side are driven with different motors, in order to give sliding at the contact surface. The test samples are fixed on both shafts under a predetermined load. Both test samples are driven for 3 min at 200 min<sup>-1</sup> for running in, then maintaining the rotation speed of the follower side at 200 min<sup>-1</sup>. The rotation speed of the driver side

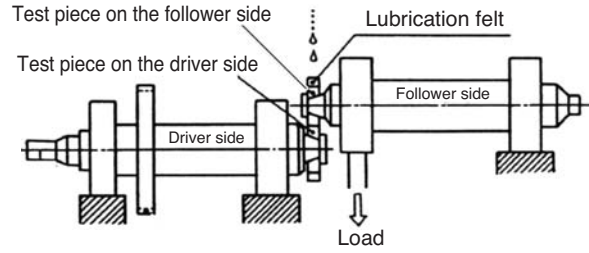


**Fig. 13** Ring to ring type test rig

**Table 5** Condition of peering test

Tester	Two-roller testing machine
Test piece on the driver side	$\phi 40 \times t12$ , Axial curvature R60
Test piece on the follower side	$\phi 40 \times t12$ , Axial straight
Rotational speed	2000 min <sup>-1</sup>
Radial load	1245N
Maximum contact surface pressure	2.3GPa
Contact ellipse	1.48 × 0.71 mm
Loading cycle	4.8 × 10 <sup>5</sup>
Atmosphere temperature	Room temperature
Lubricating oil	Turbine oil with no additives VG46
Oiling method	Felt oiling

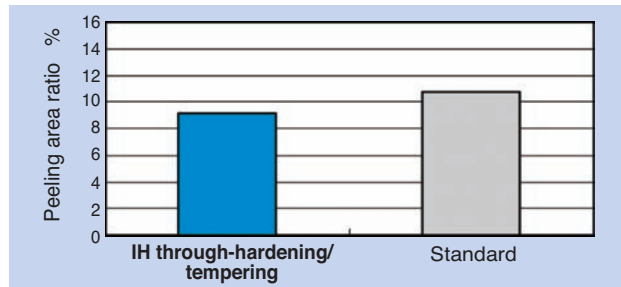


**Fig. 14** Results of peeling test for SUJ2 rings treated by induction heating and conventional heating

**Table 6** Condition of smearing test

Tester	Two-roller testing machine	
Driver side/follower side test piece	$\phi 40 \times t12$ , Axial curvature R60	
Radial load	980N	
Maximum contact surface pressure	2.1GPa	
Contact ellipse	1.37 × 0.66 mm	
Lubricating oil	Turbine oil with no additives VG46	
Oiling method	Felt oiling	
Rotational speed	Driver side	Step up from 200 min <sup>-1</sup> in increments of 100 min <sup>-1</sup>
	Follower side	Constant at 200 min <sup>-1</sup>

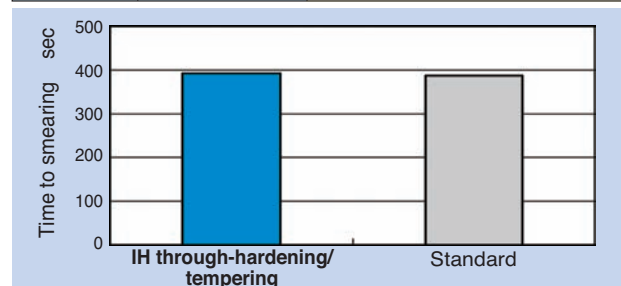


**Fig. 15** Results of smearing test for SUJ2 rings treated by induction heating and conventional heating

is increased from 200 min<sup>-1</sup> in 100-min<sup>-1</sup> steps every 30 seconds. The smearing is detected by vibration, and resistance against smearing was evaluated by the duration of smearing. Fig. 15 shows the smearing test results. The resistance against smearing of IH through-hardening/tempering products was equivalent with the standard product.

### 3.4 Dimensional stability

High-dimensional stability is required for the raceway rings for rolling bearings. Fig. 16 shows the dimensional change due to aging when they were kept at 230°C for two hours. IH through-hardening/tempering products had smaller dimensional change than standard products.

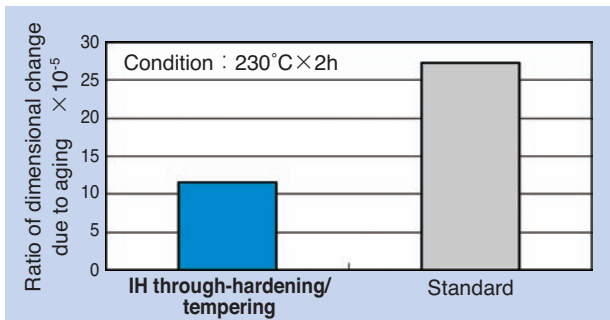


Fig. 16 Dimensional change of SUJ2 rings treated by induction heating and conventional heating

## 4. Consideration

### 4.1 Advantage of IH in production

As shown in Table 7, IH has many advantages over an atmosphere furnace. However, of special note is the fact that the stop/start-up time of the facility is almost zero and that no flammable gas is required. These points open the possibility of elimination of 24-hour operation and elimination of use of flammable gas, which are today instituted in the conventional heat treatment plants of rolling bearings.

The advantages listed in Table 7 assume the production volume, facility cost, and facility space are equivalent to atmosphere furnace. IH shows high productivity of quick heating in applications such as surface hardening, providing equal or more advantages over atmosphere furnace heating. However, for through hardening, since relatively long heating is required, more units are required for production of the same volume. Therefore, reduction of cycle time, reduction of facility cost and compact

Table 7 Merits of induction heating on manufacturing

Features	<ul style="list-style-type: none"> <li>• Inline integration with other facilities</li> <li>• Heat history tracing of each product</li> <li>• Efficient treatment of small-lot products</li> <li>• Short shutdown/star-up time</li> <li>• High freedom of layout</li> </ul>
Safety/environment	<ul style="list-style-type: none"> <li>• Low soot</li> <li>• Flammable gas facilities are not required</li> </ul>

size of facility are required for application to small products.

For larger products, the difference in productivity between IH and atmosphere heating will be reduced; however, it should be noted that different challenges will surface, such as reduced advantages due to larger facilities, decarburization and generation of scale due to increased uniform heating time in the atmosphere, and more difficult uniform heating.

### 4.2 Effect of IH on reduction of environmental load

Table 8 shows the estimates from the energy-saving and CO<sub>2</sub>-reduction viewpoints on the effect of IH on reduction of environmental load. Its power consumption can be reduced to 74% of power consumption of electric furnace per kg of product weight (compared to our existing product). Also, CO<sub>2</sub> emission can be reduced to 56% of the emission of heaters that use city gas. In the calculation, CO<sub>2</sub> emission per consumed electric power unit was assumed to be 0.341 kg/kWh, which is electricity-CO<sub>2</sub> emission equivalent in the Chubu region in FY2010.

Table 8 Reduction effect of using induction heating on negative environmental impact

Heating method	IH	Electrical	City gas
Atmosphere	Nitrogen gas	Nitrogen gas	RX gas
Electricity for heating kWh/kg	0.934	1.261	0
City gas Nm <sup>3</sup> /kg	0	0	0.185
RX gas Nm <sup>3</sup> /kg	0	0	0.464
CO <sub>2</sub> emission g/kg	318	430	566

## 5. Conclusion

In this paper, a method for achieving IH through hardening/tempering in the minimum processing time, while controlling the quality of the entire bearing rings within the control criteria, was discussed. This technology is a proprietary system of NTN, which even allows engineers inexperienced with IH to optimally design the processing conditions. We believe this system will accelerate the use of IH for heat treatment of rolling bearings, resulting in improved environment of production sites and energy saving.

## Reference

- 1) Takao Yamazaki: Review of High Frequency Induction Heat Treating Technology during Past 50 Years, Netsu Shori 50, 6 (2010)580-588.
- 2) Kazuhiro Kawasaki, Yoshitaka Misaka, Fumiaki Ikuta: Towards the High Performance Induction Heat-Treatment Accompanied with W-Eco (Ecological & Economical) Effect, Netsu Shori, 50, 4 (2010) 368-376.
- 3) Saburo Shiko, Kazuo Okamoto, Shozo Watanabe: Effect of Metallographical Factors on the Rolling Fatigue Life of Ball Bearing Steel, Tetsu- to – Hagane, 54, 13 (1968)1355-1366.
- 4) Takumi Fujita, Nobuyuki Suzuki: High Frequency Overall Heating Hardening Method for Bearing Race under Temperature Control, 61st Meeting of the Japan Society of Heat Treatment, presentation material, (2005) 41-42.
- 5) Takumi Fujita, Nobuyuki Suzuki: High Frequency Overall Heating Hardening Method for Bearing Race made of SUJ2 under Temperature Control, 62nd Meeting of the Japan Society of Heat Treatment, presentation material, (2006) 25-26.
- 6) Takumi Fujita: Rolling Contact Fatigue Life Test Design and Result Interpretation Methods Maintaining Compatibility of Efficiency and Reliability, NTN Technical Review, 76 (2008) 31-38.
- 7) T. Fujita: Rolling contact fatigue life test design and result interpretation methods maintaining compatibility of efficiency and reliability, J. ASTM international, 7, 6 (2010)Paper ID JAI102492.
- 8) The Society of Materials Science, Japan, Committee on Fatigue of Materials, Committee on Reliability Engineering, Metal Materials Fatigue Reliability Evaluation Standard JSMSSD-6-02 –SN Curve Regression Method, The Society of Materials Science, Japan (2002).

Photo of authors (titles are at the time of development)



Takumi FUJITA  
Advanced Technology  
R&D Center



Nobuyuki SUZUKI  
Advanced Technology  
R&D Center

## Rolling Bearing for Environments of Ultrahigh Temperatures



**Miki ARIHANA\***

**Takayuki KAWAMURA\*\***

In recent years the demand of bearings which are used at 400 degree C for tenter clips, glassmaking facility for solar panels etc., has been increasing. Usually, plain bearings are used for such ultra-high temperature application in atmosphere.

NTN developed the “ULTAGE Deep Groove Ball Bearings for Ultrahigh Temperature Environment” instead of plane bearings, which has the advantage of low torque and efficient operation because of rolling bearing. On the other hand in vacuum environment, NTN adopts “Ultra-clean WB Bearing” by using the application is under 300 degree C. NTN is now developing new products to achieve 400 degree C for higher performance. This report introduces the design, feature and performance of “ULTAGE Deep Groove Ball Bearings for Ultrahigh Temperature Environment” in atmosphere environment, “Ultra-clean WB Bearing” in vacuum environment and current further study of it.

### 1. Introduction

Recently, demand for heat resistance is increasing for bearings used in tenter clips and glassmaking facilities, etc. and today, their use at around 400°C is particularly increasing.

Traditionally, bearings used in 150 to 250°C of temperature have heat resistance by adoption of a shield plate made of steel and a seal made of fluoro rubber, or injection of heat resistant fluorinated grease, etc. Plain bearings are mainly used for high temperature environments at around 400°C; however, requirement for rolling bearings are increasing for lower torque.

In addition, demand for bearings for use in vacuum and ultrahigh temperatures for manufacturing

equipment of solar panels is increasing as the global market for solar cells expands. Operating temperature of products for this use can reach up to 400°C; therefore we have worked to establish forward-looking and superb bearing specifications that withstand vacuum and 400°C environments.

In this paper, we introduce you to “ULTAGE Deep Groove Ball Bearings for Ultrahigh Temperature Environment” of Ultrahigh Temperature Graphite (UTG) type for atmosphere environment and “Ultra-clean WB Bearing” for ultrahigh temperature vacuum environment, which are already introduced in a series and their current improvement development status.

\* ULTAGE is a name created from the combination of “ultimate,” signifying refinement, and “stage,” signifying NTN’s intention that this series of products be employed in diverse applications and is the general name for NTN’s new generation of bearings that are noted for their industry-leading performance.

\*Industrial Machinery Engineering Dept., Industrial Machinery Division

\*\*Advanced Technology R&D Center

## 2. ULTAGE Deep Groove Ball Bearings for Ultrahigh Temperature Atmosphere Environment

### 2.1 Features

#### (1) Long life under atmosphere/ultrahigh environment

Approximately double the durability compared to fluorinated grease for high temperature specification, due to the adoption of solid lubricant of special composition blend and internal structure for supplying adequate amount of solid lubricant

#### (2) Lower torque

Approximately a quarter of the starting torque and half of the dynamic torque compared to fluorinated grease by adoption of ceramic balls and consistent supply of solid lubricant

#### (3) Improved handling with sealed structure

Reduced leakage of solid lubricant from inside bearings by side ring and non-contact shield plate installed inside the bearings (cannot be used in a clean environment)

### 2.2 Structure

Fig. 1 shows the structure of ULTAGE Deep Groove Ball Bearings for Ultrahigh Temperature Atmosphere Environment. These bearings use a graphite solid lubricant with a special composition blend and optimized lubricant amount to achieve long life. Also, its structure prevents balls from being offset causing inner/outer rings to be dislocated even when the solid lubricant wears out, by installation of a U-shaped metal cover. In addition, the optimum shape of solid lubricant, and shield plate and lubricant side rings for guiding rotation of the solid lubricant make it ideal for the solid lubricant to remain in contact for

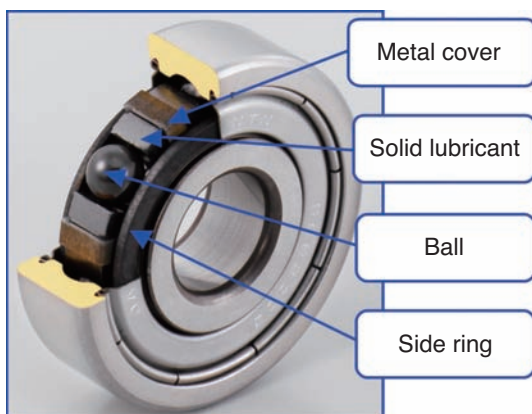


Fig. 1 ULTAGE Deep groove ball bearings for the atmosphere and ultrahigh temperature environment

ensuring smooth rotation.

However, because of the graphite solid lubricant, bearings must not be dropped or exposed to a shock load.

### 2.3 Solid lubrication mechanism

A solid lubricant with the longest life was selected after the essential testing of different types and blends of solid lubricants under the conditions listed in Table 1. In this test, the life was determined when the total bearing torque reached 147 mN·m. The test results are shown in Fig. 2. The adopted lubricant was confirmed to have more than 4 times longer life compared with WS<sub>2</sub> (tungsten disulfide). Fig. 3 shows the supply mechanism of solid lubricant.

As the bearings rotate, the transfer film transferred from solid lubricant to the balls, and then from the balls to the raceway surface of the inner/outer rings keeps adequate lubrication.<sup>1)</sup>

Table 1 Evaluation test condition of lubricant

Test bearings	608 (φ8×φ22×7)
Load	196N
Rotational speed	1000min <sup>-1</sup>
Temperature	400°C

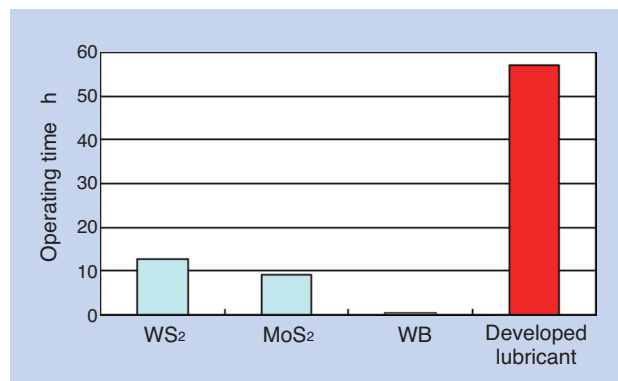


Fig. 2 Evaluation results of solid lubricants

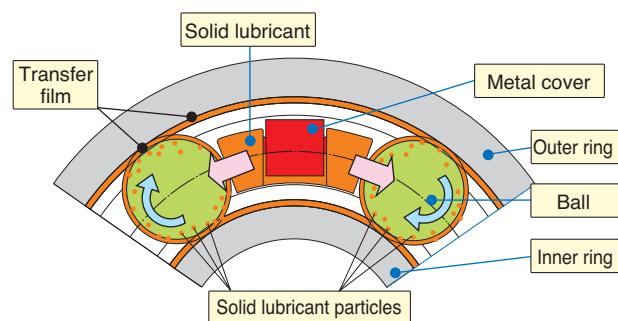


Fig. 3 The supply mechanism of solid lubricant

2.4 Various performance tests

2.4.1 High temperature durability evaluation test

The high temperature durability of ULTAGE Deep Groove Ball Bearings for Ultrahigh Temperature Atmosphere Environment was evaluated as shown in Table 2 and Fig. 4. As a result, they were proven to double the life of conventional fluorinated grease type at its operating limit of 350°C.

Also, even in the atmosphere and a temperature of 400°C, where the fluorinated grease type cannot be used, they were proven to have an equivalent durability as the fluorinated grease type at 350°C.

Table 2 Test condition of high temperature durability

Test bearings	6200 (φ 10×φ 30×9)
Load	49N
Rotational speed	530min <sup>-1</sup>
Rotation type	Outer ring rotation
Temperature	350, 400°C

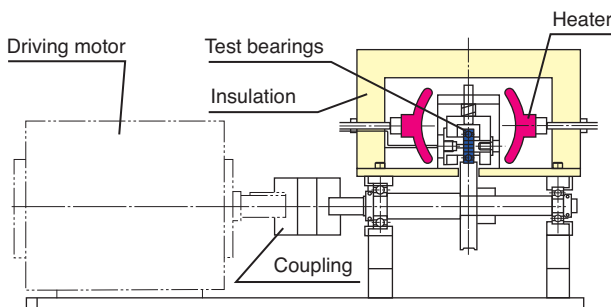


Fig. 4 High temperature endurance testing machine

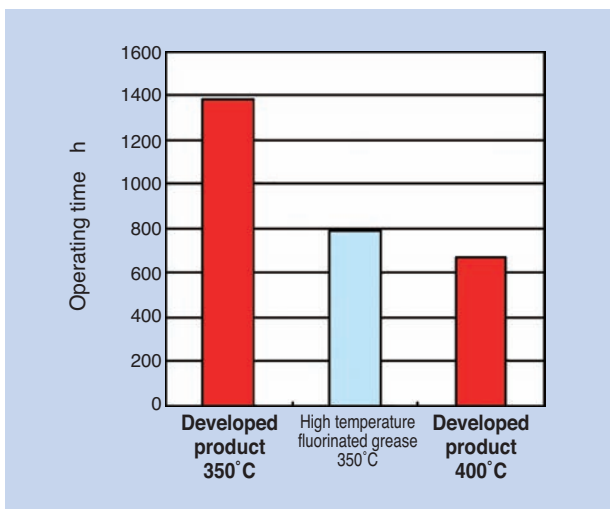


Fig. 5 Test results of high temperature durability

2.4.2 Running torque test

The running torque of ULTAGE Deep Groove Ball Bearings for Ultrahigh Temperature Atmosphere Environment was evaluated under the conditions shown in Table 3. As a result, as shown in the torque chart of Fig. 6, the starting torque was found to be about one-fourth and the dynamic torque was about half, respectively, compared to the conventional high temperature fluorinated grease type.

Table 3 Measurement conditions of rotating torque

Test bearings	6200 (φ 10×φ 30×9)
Load	98N
Rotational speed	530min <sup>-1</sup>
Rotation type	Inner ring operation
Temperature	Room temperature

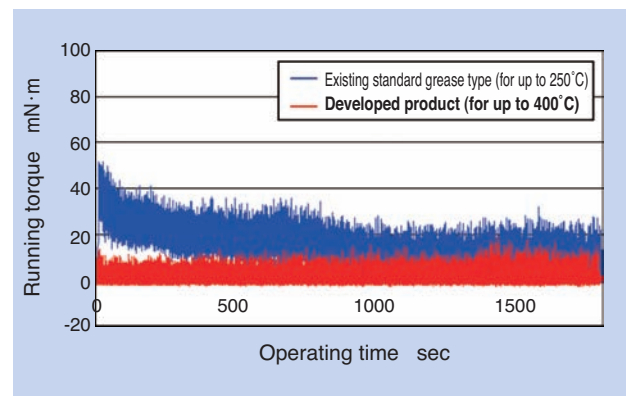


Fig. 6 Results of rotating torque

3. Introduction to rolling bearings for use in vacuum and ultrahigh temperature (Ultra-clean WB Bearings and their improved version)

Since oil and grease cannot be used for lubricating rolling bearings for use in high temperature and vacuum environments, a solid lubricant is used. A method of forming solid lubricant film directly on the raceway through spattering, etc. has been used for supplying solid lubricant to rolling elements. This method is widely used because it works from the beginning of the bearing operation; however, the bearings start wearing quickly when the film on the raceway surface wears out, which ultimate results in seizure. Therefore, long life cannot be expected.

NTN uses a sintered tungsten disulfide ball (hereafter WS<sub>2</sub> ball) replacing a steel ball for continuous supply of solid lubricant and created “Ultra-clean WB Bearings” (Fig. 7).<sup>2)</sup>

In this section, these Ultra-clean WB Bearings and the current status of development for improved durability under vacuum and high temperature (400°C) conditions are introduced.



Fig. 7 Ultra-clean WB bearing

### 3.1 Durability under high temperature for solid lubricant sintered balls

Different types of solid lubricants and blends were reviewed for bearings with solid lubricant sintered balls as shown in Table 4. The result showed that the WS<sub>2</sub> balls surpassed MoS<sub>2</sub> balls in durability against high temperature and 95% mix of WS<sub>2</sub> proved to provide the longest life.<sup>3)</sup>

Table 4 Test conditions of endurance test for solid lubricants

Test bearings	608 (φ8×φ22×7)
Vacuum level	10 <sup>-5</sup> Pa
Rotational speed	1550min <sup>-1</sup>
Temperature	200°C
Thrust load	83.4N
Determination of life	When abrupt increase of torque is observed

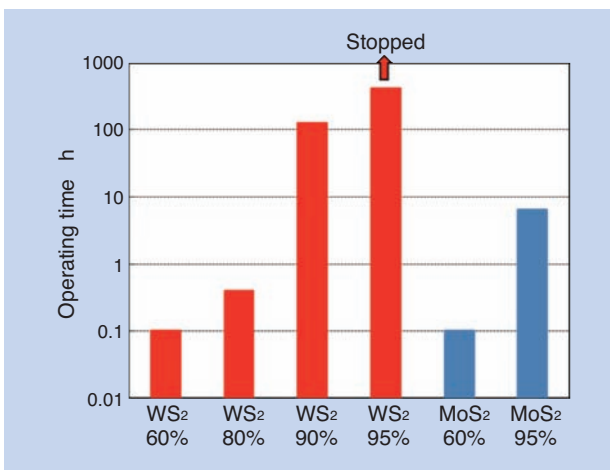


Fig. 8 Test results of endurance test for solid lubricants

### 3.2 Various performance tests

In this section, results from various performance tests for Ultra-clean WB Bearings with sintered balls of the best mix of WS<sub>2</sub> are provided.

#### 3.2.1 Running torque

The running torque for Ultra-clean WB Bearings was tested in a vacuum environment under the conditions in Table 5. The result indicated that it provides lower torque than the conventional special PTFE film type, as shown in Fig. 9.

Table 5 Measurement conditions of rotating torque

Test bearings	608 (φ8×φ22×7)
Vacuum level	10 <sup>-5</sup> Pa
Rotational speed	500min <sup>-1</sup>
Temperature	Room temperature
Thrust load	196N

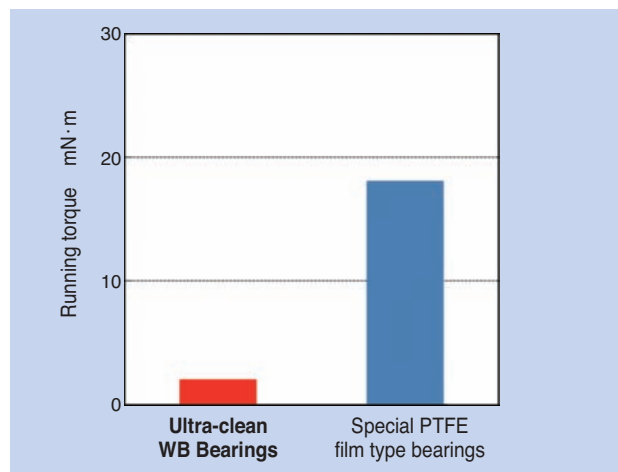


Fig. 9 Results of rotating torque

#### 3.2.2 Durability under high temperature (300°C)

Durability under high temperature of Ultra-clean WB Bearings was evaluated under the test conditions in Table 6. The result showed that the high temperature durability of Ultra-clean WB Bearings was 5 times higher than the conventional special PTFE film type, as shown in Fig. 10.

Table 6 High temperature endurance test conditions

Test bearings	608 (φ8×φ22×7)
Vacuum level	10 <sup>-5</sup> Pa
Rotational speed	1550min <sup>-1</sup>
Temperature	300°C
Thrust load	9.8N
Determination of life	When abrupt increase of torque is observed

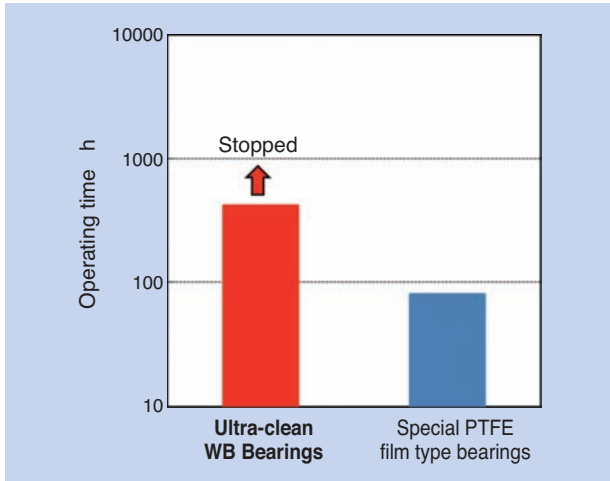


Fig. 10 Results of high temperature endurance tests

### 3.2.3 Heavy load endurance

Heavy load endurance of Ultra-clean WB Bearings was evaluated under the test conditions in Table 7. The result showed that the heavy load endurance of Ultra-clean WB Bearings was 9 times higher than the conventional special PTFE film type, as shown in Fig. 11.

Table 7 Heavy load endurance test conditions

Test bearings	608 ( $\phi 8 \times \phi 22 \times 7$ )
Vacuum level	$10^{-5}$ Pa
Rotational speed	$500 \text{min}^{-1}$
Temperature	Room temperature
Thrust load	256N
Determination of life	When abrupt increase of torque is observed

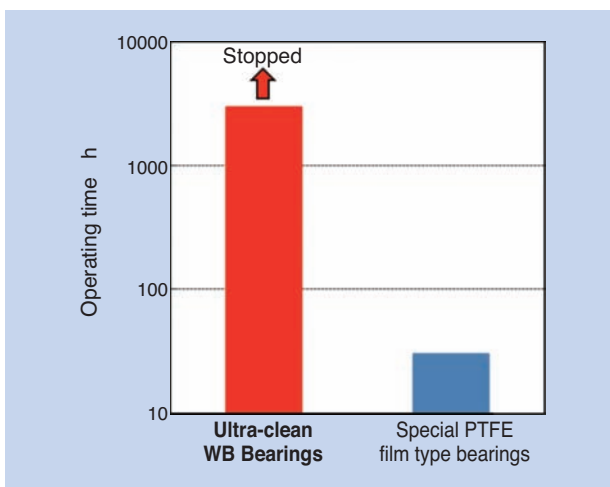


Fig. 11 Results of heavy load endurance tests

### 3.3 Development of Ultra-clean WB for improvement

It is expected that the operating temperature of bearings for vacuum/high temperature conditions for use in solar panel manufacturing equipment will reach up to  $400^{\circ}\text{C}$ . Since the Ultra-clean WB Bearings developed and marketed by NTN (hereafter, conventional product) can only be used in continuous operation up to  $300^{\circ}\text{C}$  under vacuum condition, NTN is developing bearings that can be used under  $400^{\circ}\text{C}$ .

#### 3.3.1 Specification of bearings

Endurance was evaluated in the following two specifications:

- Specification (1): Replaced a conventional stainless steel ball with a ceramic ball (one  $\text{WS}_2$  sintered ball)
- Specification (2): Added another  $\text{WS}_2$  sintered ball of the Specification (1) so two balls are used (see Fig. 12)

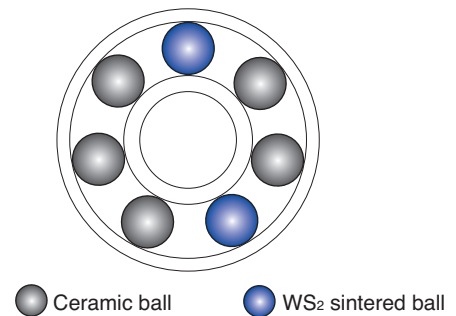


Fig. 12 Arrangement of ceramic balls and  $\text{WS}_2$  balls of development bearing ②

#### 3.3.2 Endurance under ultrahigh temperature ( $400^{\circ}\text{C}$ )

The newly developed product and conventional product were evaluated under the test conditions shown in Table 8. The result showed that the developed product was more than double in Specification (1) and more than 60 times in Specification (2) in endurance compared to the conventional product, as shown in Fig. 13.

Table 8 Ultra-high temperature endurance test conditions

Test bearings	608 ( $\phi 8 \times \phi 22 \times 7$ )
Vacuum level	$10^{-5}$ Pa
Rotational speed	$1000 \text{min}^{-1}$
Temperature	$400^{\circ}\text{C}$
Thrust load	196N
Determination of life	When abrupt increase of torque is observed

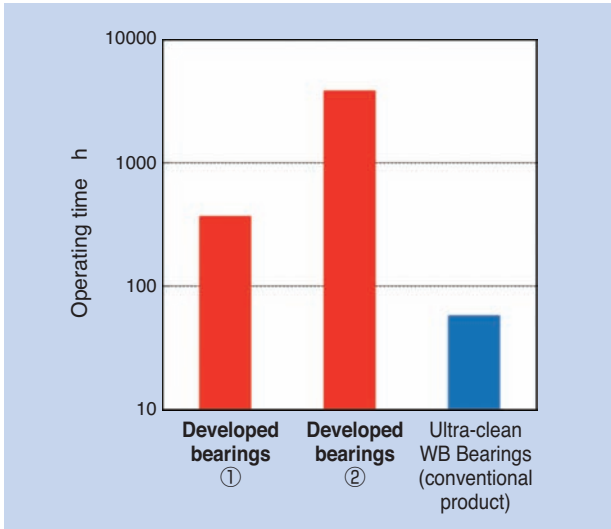


**Fig. 13** Results of ultra-high temperature endurance test at 400°C

## 4. Summary

In this paper, we have introduced ULTAGE Deep Groove Ball Bearings for Ultrahigh Temperature Atmosphere Environment, which can be used in atmosphere and ultrahigh temperature of 400°C. We will proceed to develop bearings for further applications such as tenter clips and glassmaking facilities.

We have also introduced Ultra-clean WB Bearings and bearings for use in vacuum and ultrahigh temperature of 400°C, currently under development, to be used in solar panel manufacturing equipment, the market for which is globally expanding.

NTN strives to contribute to extending maintenance intervals, improving reliability, and saving energy of various systems for use in ultrahigh temperature by developing new products that match the requirements of the market.

## Reference

- 1) Japanese Society of Tribologists, Solid Lubricant Technical Committee, New Edition Solid Lubrication Handbook, 1st edition, Yokendo, P56 (2010)
- 2) Ryouichi Nakajima, Masaaki Honda: Ultra-Clean Bearings for Clean Environment, NTN TECHNICAL REVIEW No. 74 (2006) 76–81
- 3) Hideyuki Tsutsui, Masakazu : Endurance of bearings with sintered tungsten disulfide balls in vacuum, Japanese Society of Tribologists, Tribology Conference 2007-5 Proceedings (2007) 173–174

## Photo of authors



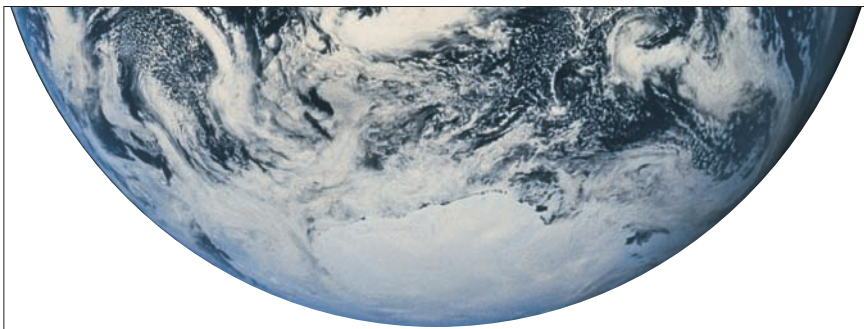
Miki ARIHANA

Industrial Machinery  
Engineering Dept.,  
Industrial Machinery Division



Takayuki KAWAMURA

Advanced Technology  
R&D Center



## NTN Bearings Turning our World “Blue”

Bearings are the “eco products” that reduce energy loss from rotating parts in all types of machinery from household appliances, medical equipment, and machine tools, to automobiles, trains, and aircraft.

At NTN, we are actively involved in an “eco” approach throughout the bearing manufacturing process, such as eliminating the use of hazardous substances, using clean natural energy, reducing CO<sub>2</sub> emission, and thoroughly recycling on a global level.

Working to keep the earth blue forever.

For a symbiotic relationship between humankind and the global environment, NTN continues to pursue the possibilities in “MONOZUKURI\*” for the future.

\*MONOZUKURI: A comprehensive concept of creating value throughout NTN's entire business process



NTN Blue = Ecology Blue

**NTN**®

[www.ntn.co.jp](http://www.ntn.co.jp)



# Machine Tool Main Spindle Bearings with “Air Cooling Spacer”



Yuushi ONDA\*  
Mamoru MIZUTANI\*  
Masatsugu MORI\*\*

High speed and high rigidity performances are always required for high precision bearings for machine tool main spindles. However, since both high speed and high rigidity increase operating temperature, it has been very difficult to achieve high speed and high rigidity performance at the same time. In this paper new “air cooling spacer” technology, which will be able to decrease the operating temperature of bearings by applying cooling air onto the outside diameter of inner ring spacer located, is introduced.

## 1. Introduction

Machine tools are used for machining parts of automobiles, aircrafts, and construction equipment. Therefore, machine tools are called “mother machines,” and are under constant pressure to increase machining efficiency and improve quality of machined products.

In order to improve machining efficiency, increase of rotational speed of the main spindles is effective. However, when the bearings run in high speed, the centrifugal force on the rolling elements will increase. Therefore, lightweight ceramics are used for rolling elements to reduce this centrifugal force. <sup>1)</sup>

Also, for quality improvement of machined products, bearings are required to improve rotational precision and increase shaft rigidity. For improving rotational precision, it is effective to increase the number of rolling elements and improve dimensional precision for inner/outer rings. On the other hand, for higher rigidity of bearings, it is effective to increase the size of rolling elements and raise the pressurized amount.

These improvements tend to increase temperature in the bearings; therefore, it is difficult to achieve high speed and high rigidity at the same time. However, for recent machining centers and field-assisted machining, both high speed and high rigidity are desired for space saving and process integration.

Technology for fulfilling high speed and high rigidity has been realized by supplying coolant in the spindle

(core-cooling main spindle) and a device to adjust running bearing pressurization; however, these methods require complex main spindle designs. <sup>2)</sup>

To cope with this issue, NTN is developing air cooling spacer technology, which will be able to decrease the operating temperature of bearings by applying cooling air onto the outside diameter of inner ring spacer. This technology can be used to achieve high speed or high rigidity of machine tools, or both, without complicating the main spindle design. In this paper, the performance of this air cooling spacer is introduced.

## 2. Structure of bearings with air cooling spacer

Fig. 1 shows the structure of bearings with air cooling spacer. The outer ring spacer installed in the center of a back-to-back (DB) arrangement is provided with environment friendly nozzles, which are air cooling nozzles, independent from the air oil supplying nozzle for lubricating bearings. The air cooling nozzles are offset from the spindle center at three locations on the circumference of the ring, pointing toward the direction of rotation. Room temperature air injected from the air cooling nozzles passes between the inner ring spacer and outer ring spacer, and through the bearings swirling toward the direction of the rotation to cool off the bearings.

\*Machining Tool/Aerospace Engineering Dept., Industrial Machinery Division

\*\*Advanced Technology R&D Center

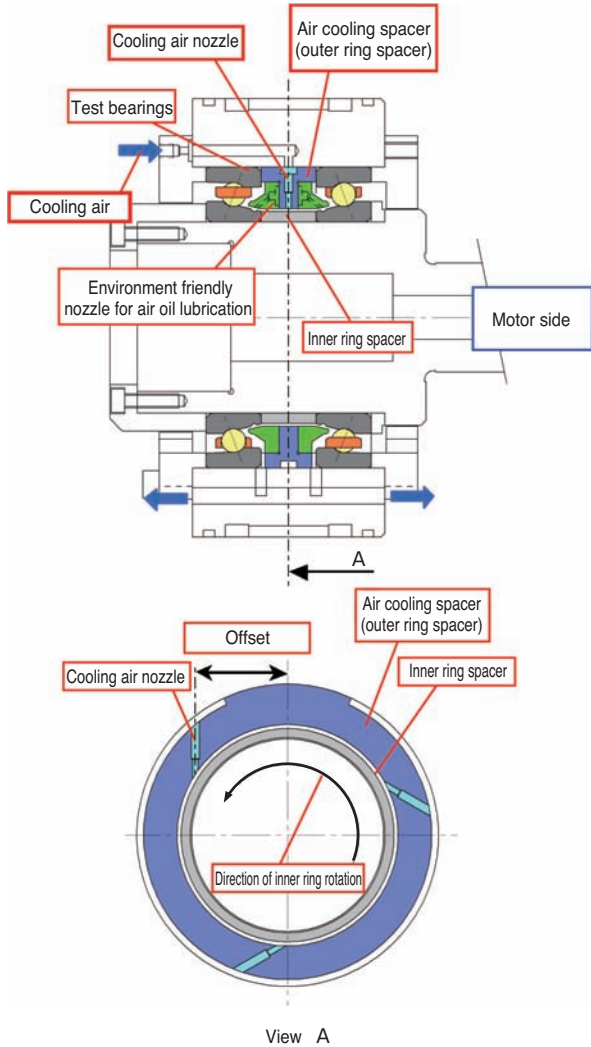


Fig. 1 Structure of the bearing with air cooling spacer

### 3. Evaluation of bearings with air cooling spacer

#### 3.1 Comparison of temperature

##### 3.1.1 Evaluation of air cooling spacer setting

Fig. 2 shows an overview of the test machine used for the evaluation and Table 1 shows the test conditions. The bearings under test are arranged back-to-back (DB) and driven by a motor. The outer ring of the bearings and outer tube of the motor are cooled by circulating oil during the test.

The effect of the air cooling spacer was confirmed by the temperature of inner/outer rings.

First, the impact of the injection points of the cooling air nozzles and amount of cooling air on the temperature of bearings was evaluated. Fig. 3 shows the injection points of the nozzles in four different positions from (1) to (4), with different offset amount (hereafter, offset amount) from the center of the spindle. In the evaluation test, the spindle was sped

up to 17,000 min<sup>-1</sup> without air cooling, then while the speed was maintained at 17,000 min<sup>-1</sup>, pressure of cooling air was gradually increased to examine its relation with the temperature of the bearings. The result is shown in Fig. 4. The higher the cooling air pressure, the more the temperature dropped. The slope of the temperature drop depended on the offset amount.

The condition for the least temperature drop was when the offset amount was 0, which is to inject air at the right angle to the inner ring spacer. The more the offset amount, the lower the temperature becomes.

Also, to confirm the relation between the offset amount and the temperature drop, the air pressure was maintained at 400 kPa. From Fig. 4, the optimum offset amount was assumed to be between 25 and 34.5 mm; therefore, offset amount of 33 mm was also evaluated. The result is shown in Fig. 5. The maximum temperature drop, which is the best air cooling effect, was found to be at the offset amount of approx. 30 mm, which is at about 80% of the radius of the inner ring spacer outer diameter.

In addition, if the direction of air injection is set backward to the rotation the temperature drop of the inner ring was about 3°C even though it was cooled at 400kPa; therefore, it is important to match the direction of cooling air injection with the direction of

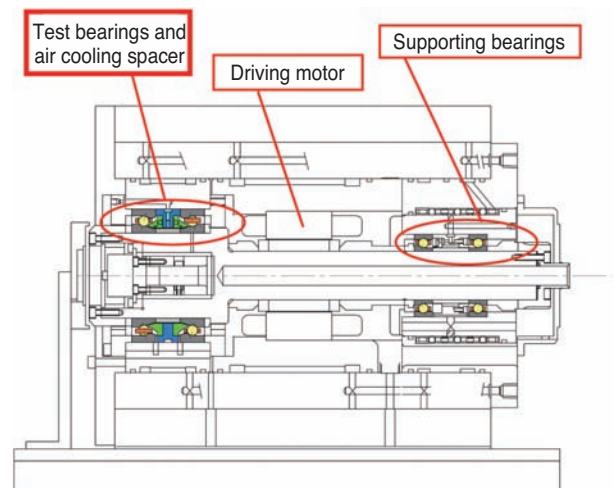


Fig. 2 Structure of testing equipment

Table 1 Test conditions

Test bearings	70×1 10×20 5S-2LA-HSE014 equivalent
Pressurization method	Fixed position pressurization (ON after incorporation)
Lubrication	Method: Air oil Supply oil amount: 0.03mL/5min Lubricating oil: ISO VG32 Air flow: 40NL/min
Outer cylinder cooling	Yes, tuned to room temperature (21±1 °C)

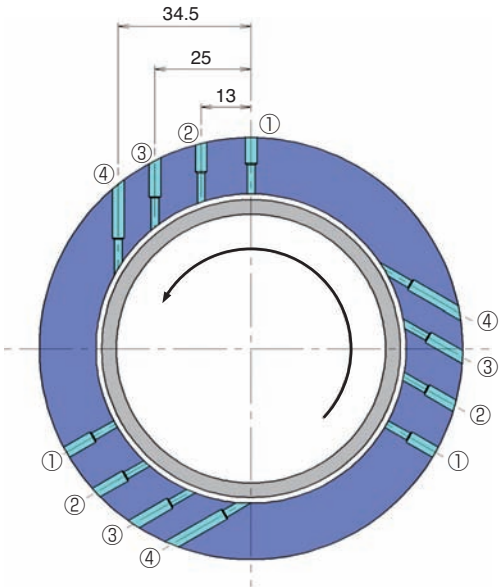


Fig. 3 Off set amount of cooling nozzles from the center

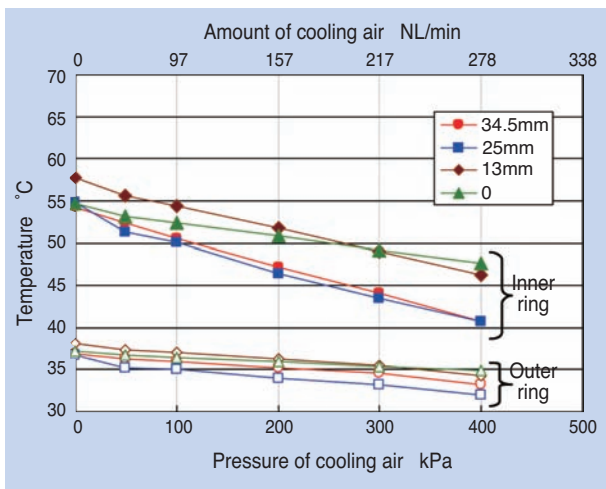


Fig. 4 Air pressure (amount of cooling air) vs. temperature by each offset amount

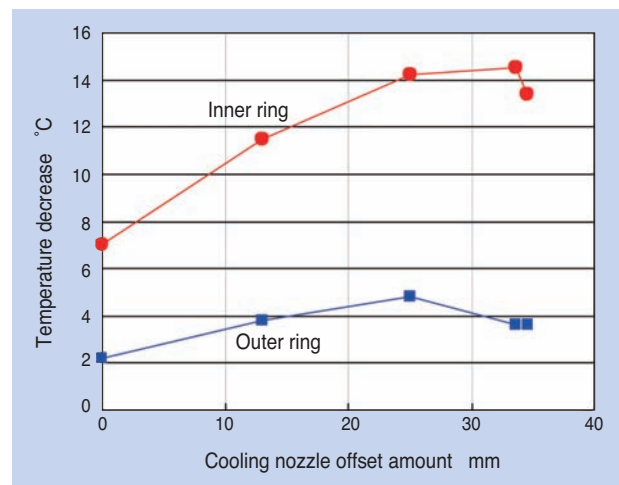


Fig. 5 Temperature decrease by cooling nozzle offset amount

the rotation and to inject air to the surface of the rotational spacer, in order to increase the cooling effect.

### 3.1.2 Combined test with the air oil lubrication nozzle

Next, air cooling effect was examined between standard nozzles widely used for air oil lubrication shown in Fig.6 and environment friendly nozzles. The result showed that even with the standard nozzles, air cooling effect could be confirmed, in the same way as the environment friendly nozzles, as shown in Fig. 7. In addition, the rotational speed for the inner ring temperature to reach 60°C was 20,500 min<sup>-1</sup> when cooling air was injected, compared to 16,000 min<sup>-1</sup>

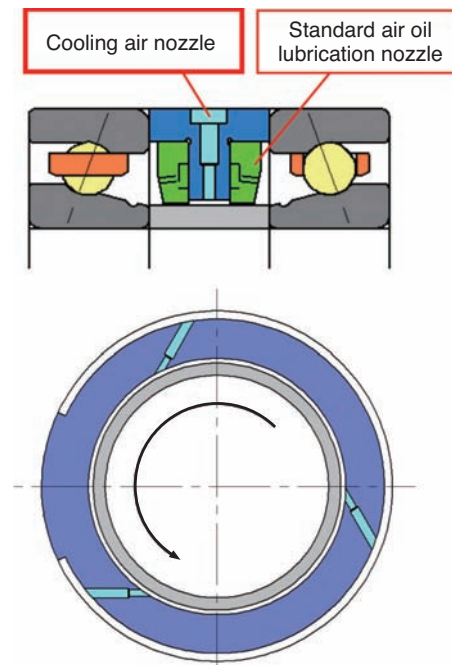


Fig. 6 Assembly with standard nozzles

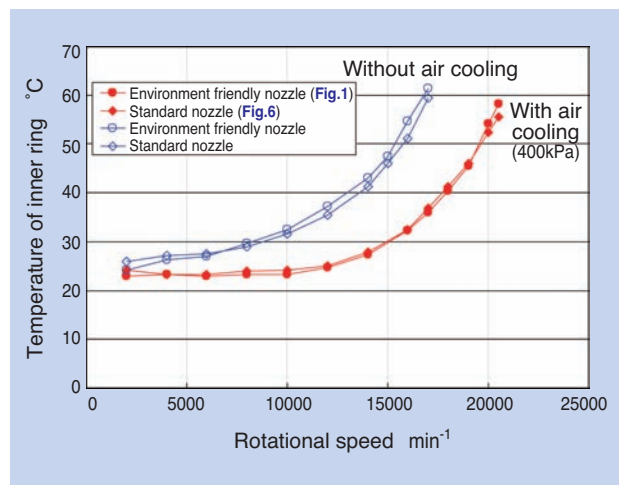


Fig. 7 Test result of inner ring temperature

without cooling air, meaning that an increase in operating speed of 28% was achieved with cooling air injection.

### 3.2 Comparison of generated noise

Noise level of standard air oil lubrication nozzle and environment friendly nozzle are compared with or without cooling air from the cooling air nozzle. The noise was measured with a broadband precision sound-level meter placed at  $45^\circ \times 1$  m high. Fig. 8 shows the rotational speed and results from measurement of A-weighting sound level.

With no air cooling, the standard nozzle generated 82–86 dBA as opposed to the lower 76–79 dBA of the environment friendly nozzle. With the standard nozzle, the injected high-speed air directly hits the rolling elements, while the environment friendly nozzle injects air to the inner ring; therefore, it was evident that the environment friendly nozzle produces less noise from the past experiments.<sup>3)</sup>

On the other hand, with air cooling, the standard nozzle generated 81–86 dBA while the environment friendly nozzle produced 87–97 dBA. Due to massive cooling air, the environment friendly nozzle produced more noise; however, no difference was recognized with or without cooling air with the standard nozzle, resulting in lower noise level than the environment friendly nozzle.

It is conceivable that the reason for the lower noise level with the standard nozzle is that the opening between the air oil nozzle’s inner cylindrical surface and inner ring spacer outer cylindrical surface is smaller than in the case of the environment friendly nozzle, and that the cooling air is diffused at a position more distant from the rolling elements due to the difference of the position of the nozzle tips.

We will study and evaluate further for reducing the noise.

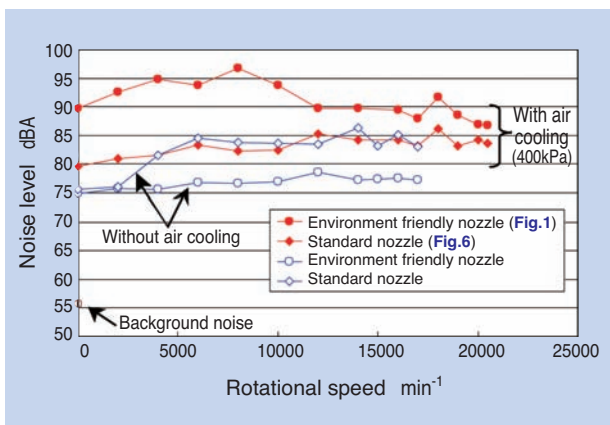


Fig. 8 Noise level with inner ring spacers with different type

## 4. Summary

We have introduced bearings with air cooling spacer for high speed and high rigidity for bearings of machining tool main spindles. Air cooling spacer can be applied not only to angular contact ball bearings evaluated in this paper, but also cylindrical roller bearings and, with some more improvement, bearings with grease lubrication, contributing to the reduction of temperature for the entire main spindle.

NTN will continue evaluating this air cooling spacer to concurrently achieve high speed and high rigidity of machine tool main spindles.

## Reference

- 1) NTN Catalog: Precision Rolling Bearings, CAT. No. 2260-IV/J 11.06.03
- 2) Kenji Fujii, Masatsugu Mori: Pressurization Switch Unit, NTN TECHNICAL REVIEW No. 60 (1992)
- 3) Kenji Fujii, Masatsugu Mori, Yoshimi Ota: Noise Reduction for Machine Tool Main Spindle Air Oil Lubrication Bearings, The Japan Society for Precision Engineering, Autumn Meeting 2000 Proceedings (2000) 449.

## Authors



Yuushi ONDA

Machining Tool/Aerospace  
Engineering Dept.,  
Industrial Machinery Division



Mamoru MIZUTANI

Machining Tool/Aerospace  
Engineering Dept.,  
Industrial Machinery Division



Masatsugu MORI

Advanced Technology  
R&D Center

# Parallel Link High Speed Angle Control Equipment (PHACE)

Hiroshi ISOBE\*  
Yukihiro NISHIO\*



NTN has developed a Parallel link High speed Angle Control Equipment (PHACE) that can control the angle with two-degrees-of-freedom quickly and over a wide range (max bend angle : 90 deg.). Adapting the unique parallel link mechanism enables both compact size and wide operating range. In addition, by developing the drive

mechanism and control methods, positioning accuracy is improved by more than ten times compared to conventional equipment, and higher speed control is realized.. Furthermore, we have developed a teaching console that facilitates equipment implementation on the production line.

## 1. Preface

NTN has been developing angle control equipment that can control tip angle by actuators at high speed and with two degrees of freedom, through improvements to the constant velocity joint link mechanism.<sup>1)</sup>

By increasing the number of axial drives of the Parallel Link High-Speed Angle Control Equipment (hereafter referred to as PHACE) from 2 axes to 3 axes, positioning accuracy is improved to  $\pm 0.05$  mm or less, and backlash is eliminated from the driving mechanism. In addition, we have developed a highly maneuverable teaching console anticipating its introduction to production lines.

This paper will introduce the features of PHACE, explain the measurement method for accuracy of position reproducibility, and provide an example of implementation on grease application equipment.

## 2. Parallel link mechanism

In general, a parallel link mechanism is a mechanism to connect base and end effector with multiple links in parallel, with different types of implementation such as the Steward-Gough type, the rotational type, and the linear fixed type.<sup>2)</sup> The parallel link mechanism adopted in PHACE is different from those widely used, and includes a unique structure described as follows.

This parallel link mechanism, as shown in **Fig. 1**, places three rows of link systems (1st link system, 2nd link system, 3rd link system) each consisting of base-side arm member, central link member, and tip-side arm member, in parallel, between the base-side link hub and the tip-side link hub. The joints of these link members are arranged in turning pairs, which use rolling bearings such as deep groove ball bearings and angular ball bearings to reduce rotational resistance. In addition, backlash in the joints is eliminated by applying pressure to the bearings. Also, as shown in **Fig. 2**, the rotational axes of central link member and arm member, and the rotational axes of link hub and arm members are arranged so that they meet at one point, to enable a configuration that combines two spherical link mechanisms (mechanism to allow each link to operate around the sphere) as shown in **Fig. 3**. As a result, high speed and broad operation range are achieved because the constant distance between the center of the base-side link hub and the tip-side link hub is maintained, and the base side and the tip side operate symmetrically against the intersecting plane of two spherical links. Also, cables and tubes can be inserted through an ample space in the center and those cables, etc. are not twisted even when the turn is repeated on one direction.

\*New Product Development R&D Center

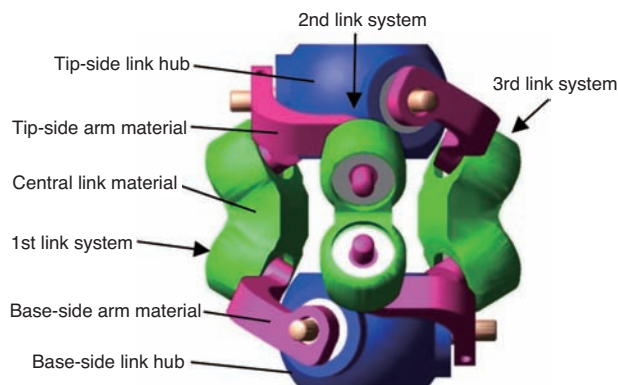


**Fig. 1** Unique parallel link mechanism

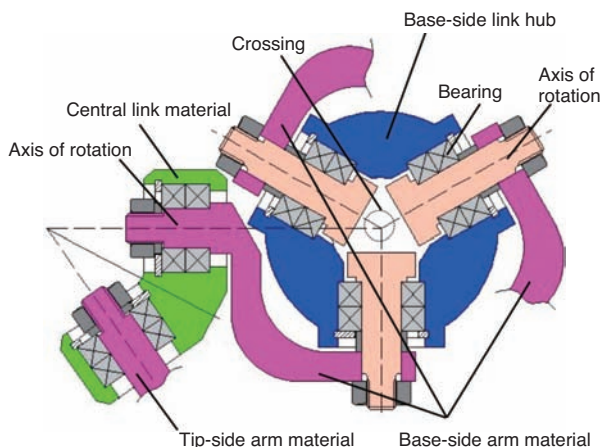


**Fig. 2** Connecting Section between each part

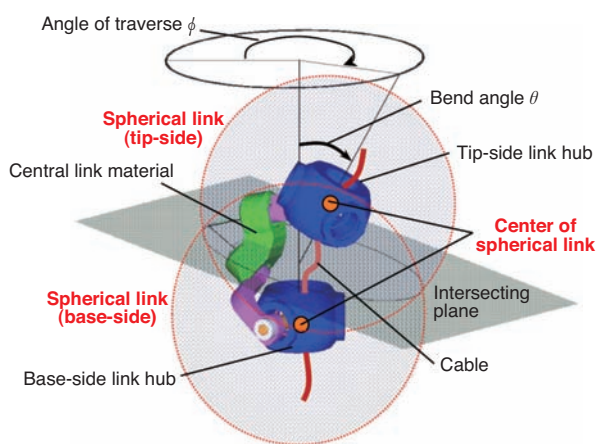


**Fig. 3** Spherical link mechanism

### 3. Structure and features of the developed product

**Fig. 4** shows the developed PHACE. PHACE consists of a fixed driving mechanism and movable parallel link high-speed angle displacement mechanism (hereafter, high-speed angle displacement mechanism) and is installed with the tip side of the high-speed angle displacement mechanism downward. Also, teaching operation is conducted using the dedicated teaching console shown in **Fig. 5**.

This product was designed for applying grease and therefore, the bend angle  $\theta$  (see **Fig. 3**) is limited to 45° or less; however, it has capability of up to 90°.

**Table 1** shows the main specifications of PHACE.

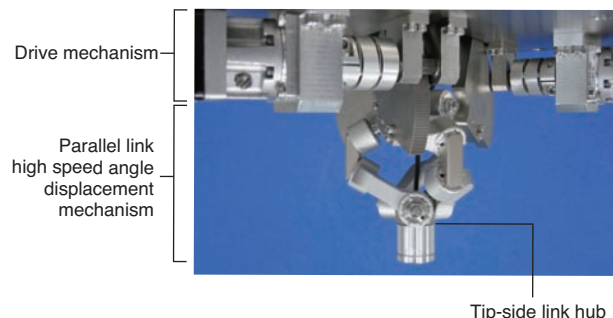


**Fig. 4** PHACE



**Fig. 5** The dedicated teaching console

**Table 1** PHACE specification

Item	Specification
Weight	10kg
Maximum payload (inertia moment)	Max. 1.0kg (6300kg·mm <sup>2</sup> )
Operating range	Bend angle $\theta$ : $\pm 45$ deg Angle of traverse $\phi$ : 360deg(unlimited)
Accuracy of positioning reproducibility	$\pm 0.05$ mm or less
Motor output	50W×3

### 3.1 Parallel link high-speed angle displacement mechanism

Fig. 6 shows the high-speed angle displacement mechanism and Table 2 shows its main specifications. Angular ball bearings are set for each turning pair and pressure is applied to eliminate backlash in the joint.

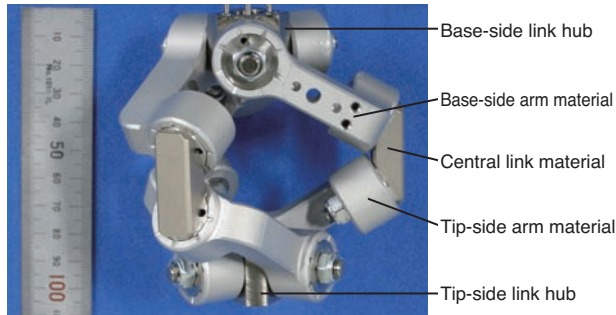


Fig. 6 Parallel link angle displacement mechanism

Table 2 Specification for the parallel link angle displacement mechanism

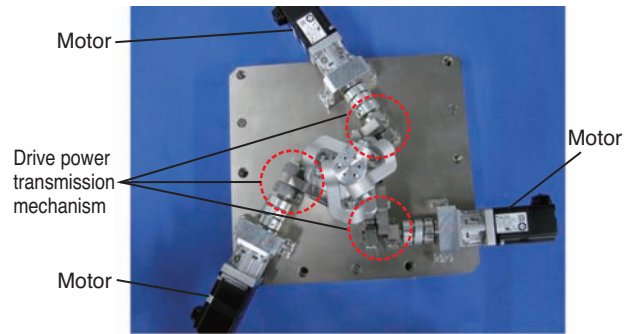
Item	Specification
Size (outer diameter×height)	100×90mm
Weight	560g
Material	Aluminum + steel

### 3.2 Driving mechanism

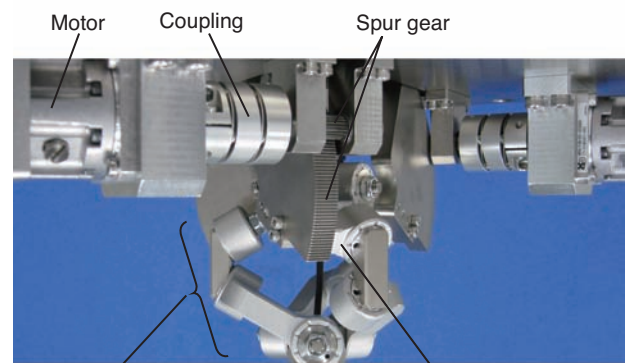
Fig. 7 shows the driving mechanism. As shown in Fig. 7 (a), each of the three link systems is equipped with a motor and the size of the driving mechanism is about 450 mm including the motor. Also, the motors are placed horizontally to achieve a low profile structure. The drive power transmission mechanism, as shown in Fig. 7 (b), transmits power from the motor to the base-side arm member through a spur gear attached to the base-side member.

### 3.3 Control method

PHACE controls the attitude using relational expression between the arm rotational angles  $\beta_1$  to  $\beta_3$  of the base-side arm member and the attitude of the link hub at the tip side (bend angle  $\theta$ , angle of traverse  $\phi$ ). As shown in Fig. 8, the inverse transformation of this relational expression can give the arm rotational angles  $\beta_1$  to  $\beta_3$  from the command of the tip-side link hub attitude (bend angle  $\theta$ , angle of traverse  $\phi$ ) and control the arm rotational angles  $\beta_1$  to  $\beta_3$  with three motors. As a result, the positioning speed can be increased even with small motors. In addition, we have improved the positioning accuracy by adopting a control method to cancel out backlash of the drive mechanism by allowing small mutual interference of three base-side arm members.



(a) Flat structure of the drive mechanism



(b) Driving force transmission mechanism

Fig. 7 Drive mechanism

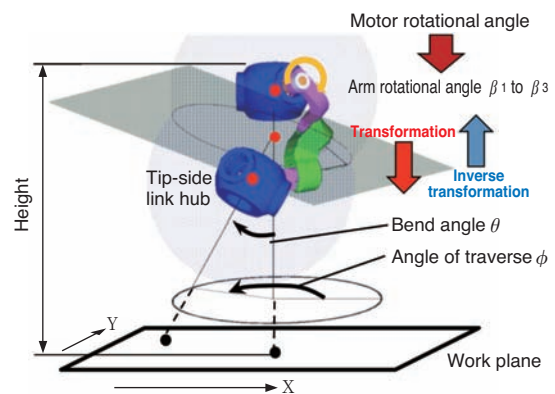


Fig. 8 Control method

### 3.4 Dedicated teaching console

Here is an overview of the dedicated teaching console developed for introduction to production lines. Table 3 shows the key specifications. This console enables command input for the tip-side link hub attitude by inputting the bend angle  $\theta$  and angle of traverse  $\phi$ , and in addition, allows teaching by inputting position with the XY coordinates of the actual work plane, as shown in Fig. 8. Furthermore, it includes a teaching function that can memorize the position adjusted by fine tuning operation of the

control buttons on the console, shown in Fig. 9, which brings improved efficiency when the work order is changed on the shop floor and prevents operational errors. Other operations such as setting conditions for each motor gain and registered pattern, and XY stage teaching as described below (see 5. Examples of application) are also available.

**Table 3** Console specification

Item	Specification
Size (W×L×H)	224×174×87.1mm
Weight	1kg or less

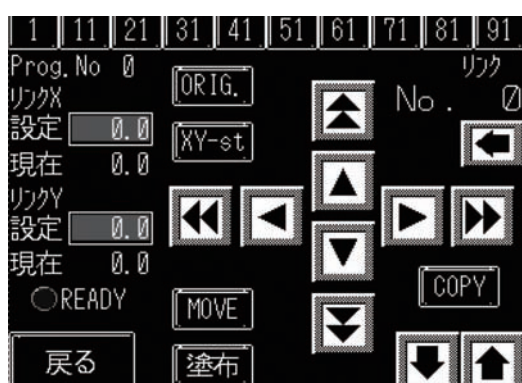


**Fig. 9** Operation screen of the teaching console

#### 4. Measurement of accuracy of position reproducibility by inclination angle sensor

As shown in Fig. 10, a 2-axis inclination angle sensor is installed at the tip of PHACE to measure accuracy of position reproducibility of the tip position. The measurement method and condition was based on JIS B 8432 “Manipulating Industrial Robots – Performance Criteria And Related Test Methods.”<sup>3)</sup>

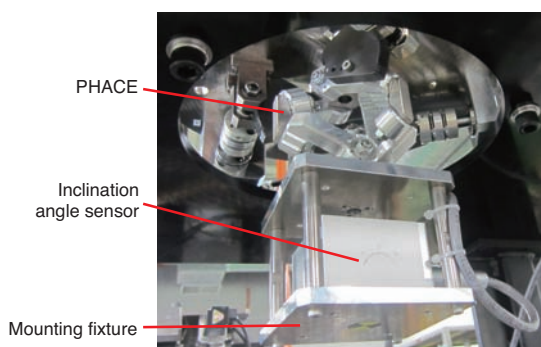


**Fig. 10** Device for the measurement of the positioning accuracy

#### 4.1 Measurement method

As shown in Fig. 11, for an arbitrary command pose, positioning from 16 directions was conducted for 10 cycles each, and accuracy of positioning reproducibility of the tip of the tip-side link hub was calculated.

As shown in Fig. 12, a virtual plane is defined as a plane perpendicular to the center axis of the tip-side link hub, at the distance D from the rotational center of the tip-side link hub (equivalent to the position of the tip of the tip-side link hub). The attained pose  $(P_x, P_y)$  is defined as the position where the center axis of the tip-side link hub and the virtual plane intersect. As shown in Fig. 13, accuracy of positioning reproducibility is defined as the average of the attained poses and two times the maximum distance between each attained pose  $(P_x, P_y)$  and the average (“±maximum distance”). The attained pose  $(P_x, P_y)$  is calculated by the following equation (1).

$$(P_x, P_y) = (D \times \tan(\alpha_y - \bar{\alpha}_y), D \times \tan(\alpha_x - \bar{\alpha}_x)) \dots\dots(1)$$

where,  $\alpha_x, \alpha_y$  : inclination angles around axis X, Y

$\bar{\alpha}_x, \bar{\alpha}_y$  : average of  $\alpha_x, \alpha_y$  of each command pose

The output signal of this inclination angle sensor varies by very small vibration. Therefore, the output signals were passed through low-pass filter and to an

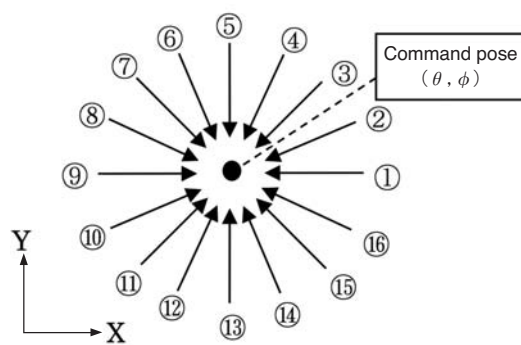


**Fig. 11** Positioning direction

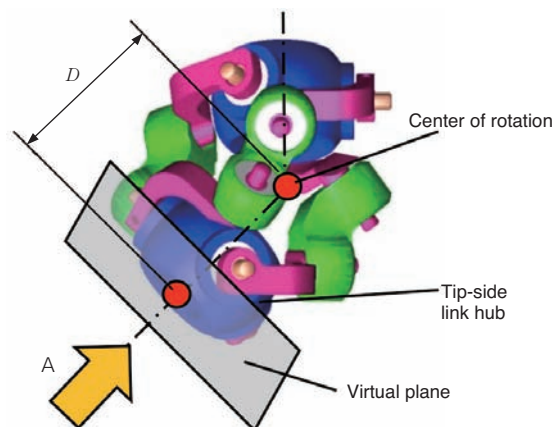


**Fig. 12** Measuring method

analog meter as differential inputs then the moving average was calculated (fluctuation of measured values:  $\pm 0.01$  mm or less).

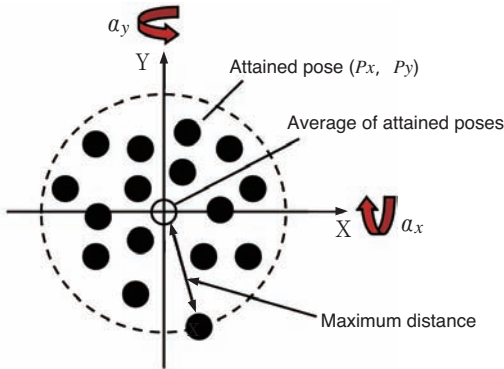


Fig. 13 Repeat positioning accuracy

4.2 Measurement condition

Table 4 shows the measurement conditions. The maximum values of this equipment were used for load and rotational speed.

Table 4 Measurement condition

Item	Condition	Remark
Weight of load	1 kg	Sensor + mounting fixture
Command rotational speed	8min <sup>-1</sup>	Equivalent to synthesized rotational speed for base-side arm materials
Direction of positioning	16 (9)	Value in parentheses is for $\theta = 45^\circ$
Measurement points	9	See command pose in Table 5
Number of measurements	160 (90)	Value in parentheses is for $\theta = 45^\circ$

4.3 Measurement results

Table 5 shows the measurement results of accuracy of positioning reproducibility. The accuracy of positioning reproducibility is max.  $\pm 0.025$  mm.

Table 5 Measurement result

Command pose		Accuracy of positioning reproducibility (mm)
$\theta$ [deg]	$\phi$ [deg]	
0	0	$\pm 0.012$
25	0	$\pm 0.017$
25	90	$\pm 0.023$
25	180	$\pm 0.019$
25	270	$\pm 0.018$
45	45	$\pm 0.014$
45	135	$\pm 0.018$
45	225	$\pm 0.025$
45	315	$\pm 0.021$

4.4 Consideration

The validity of the measurement of accuracy of positioning reproducibility of this equipment using an inclination angle sensor was considered. The unidirectional accuracy of reproducibility,<sup>3)</sup> separately measured, was about twice the accuracy of multidirectional accuracy of positioning reproducibility shown in Table 5. Therefore, we determined that the accuracy of positioning reproducibility of this equipment is represented by multidirectional accuracy of positioning reproducibility.

We also verified the results with the accuracy measurement by image processing shown in Fig. 14. Measurement by image processing can be highly accurate by taking an enlarged image of a 4-quadrant circle marker and calculating to the resolution less than the image pixel size (fluctuation of measured values:  $\pm 0.005$  mm or less). When comparing the accuracies of positioning reproducibility by these measurement methods, we verified that they were equivalent.

This measurement method using an inclination angle sensor does not require changing settings of measurement equipment for each command pose and the measurement can be made automatic by indicating the recording timing of the sensor output signals with trigger signals, etc., resulting in a shorter testing period.

Therefore, we decided to select the measurement method of using an inclination angle sensor for measuring accuracy of positioning reproducibility of this equipment, based on the above consideration.

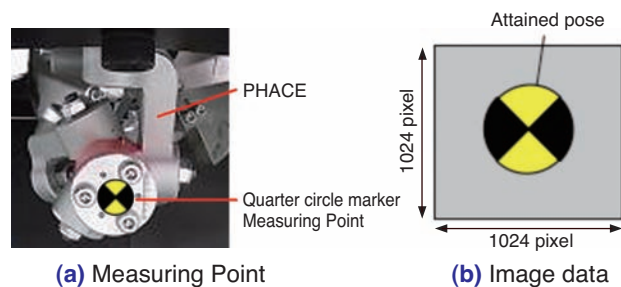


Fig. 14 The measuring method using image processing

5. An example of implementation (Grease Applicator)

An example of grease application equipment configuration using PHACE is shown in Fig. 15 and Fig. 16. With this configuration, a dispenser (constant liquid delivery equipment) is attached at the tip of the tip-side link hub of PHACE, which is installed downward against the stand, so the dispenser can apply grease on the work-piece placed on the XY

stage. This dispenser can discharge grease at a distance by controlling high pressure air with an electromagnetic valve. Three motors used by PHACE and two motors used by the XY stage are collectively regulated by one controller. With this configuration, one dedicated teaching console can perform the teaching operation and parameter setting for both the PHACE and the XY stage.

The advantages of the grease application equipment in this configuration are as follows:

**(1) Reduction of tact time**

About 10 points of grease application per second can be made resulting in reduction of tact time.

**(2) Compact footprint**

As the movable components of PHACE are small, the equipment can be made compact.

**(3) Enables grease application for components with complex shape**

Grease can be applied from a slanted orientation by controlling the dispenser attitude by PHACE; therefore, grease can be applied to objects that are not directly seen from the top as in Fig. 17 (a) and the vertical side of column-like objects as in Fig. 17 (b).

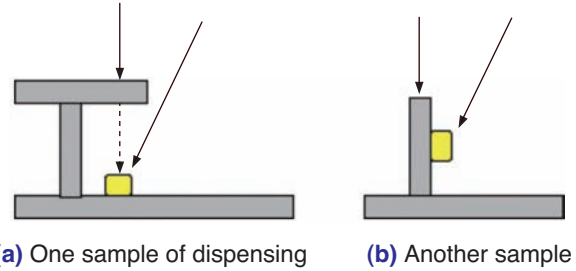


Fig. 17 Sample of dispensing

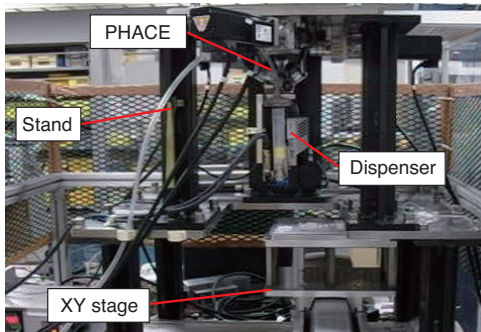


Fig. 15 System configuration example of grease dispensing

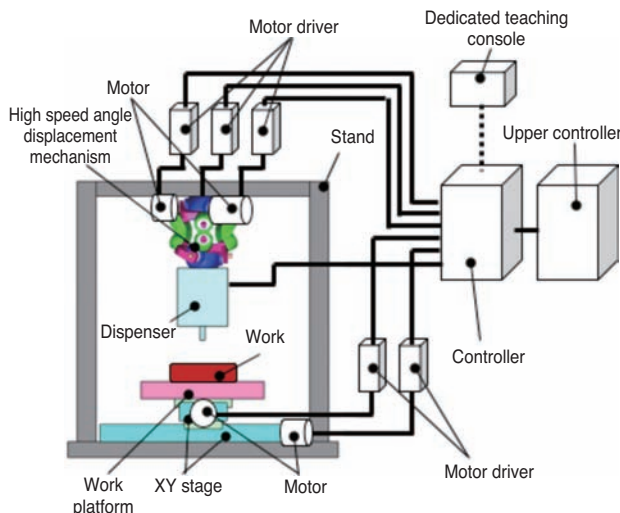


Fig. 16 System configuration

**6. Summary**

This paper has introduced the structure of Parallel Link High-Speed Angle Control Equipment (PHACE) with two degrees of freedom, described the measurement method of positioning accuracy, and provided an application example.

NTN is planning to expand the market of this device in addition to grease application equipment, for such purposes as adhesive applicators camera or laser inspection devices, camera platforms, and so on by expanding functions and reducing cost.

**Reference**

- 1) Keisuke Sone, Hiroshi Isobe, Koji Yamada: High Angle Active Link Equipment, NTN TECHNICAL REVIEW No. 71 (2003) 70–73
- 2) The Robotics Society of Japan, Robotics Hand Book, New Edition, Corona Publishing, 297, 2005
- 3) Japanese Standards Association, JIS Handbook 14, 2011 edition, 1585–1662, 2011

Photo of authors



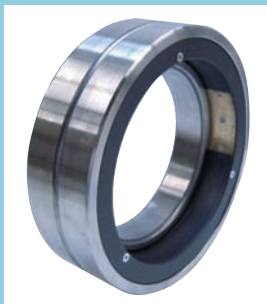
Hiroshi ISOBE  
New Product Development  
R&D Center



Yukihiro NISHIO  
New Product Development  
R&D Center

## Development of the Lubricating Oil Supply Unit with Self-generating Power Supply

Kaoru OMOTO\*  
Hiroyoshi ITO\*



For the purpose of life time extension of the grease lubricated bearing for machine tool spindle, NTN developed a lubricating oil supply unit with the self-generating power supply.

This lubricating oil supply unit, which includes a self-generating power supply, pump, and lubricating oil, is built into the outer ring spacer. Testing on angular contact ball bearings confirmed that it is possible to supply adequate lubrication by using a standalone lubrication supply unit.

### 1. Introduction

For bearings with grease lubrication, maintaining an oil film for a long time with minimum grease is a critical task. NTN has been developing a “New grease lubrication system, MQGS (Minimum Quantity base oil of Grease Supply lubrication),”<sup>1)</sup> which supplies a small quantity of grease base oil while maintaining oil films.

Based on the minimum oil supply technology we have cultivated, we have added an electronic application technology to develop a lubrication supply unit with a self-generating power supply which supplies grease lubrication to the bearings.

This unit lubricates itself without any external power supply or external control. In this paper, we will discuss this lubricating oil supply unit with self-power generation (hereafter referred to as the “lubricating oil supply unit”).

### 2. Configuration

#### 2.1 Overall structure

Fig. 1 shows the external view of the lubricating oil supply unit with self-generating power supply. The lubricating oil supply unit is installed on the inside of the outer ring fixed spacer and can be separated from the bearings, as shown in Fig. 2 (a). Also, as shown in Fig. 2 (b), power generator (thermoelectric

converter), power supply/controller, pump, and lubrication oil tank are built-in inside of the unit to draw lubrication oil out with the pump and supply oil to the bearing raceway through the nozzle using the generated power.

The nozzle is installed near the bearing outer ring raceway, as shown in Fig. 2 (a). Fig. 3 shows the nozzle hole and (a) and (b) show the status before and after discharge of lubricating oil.

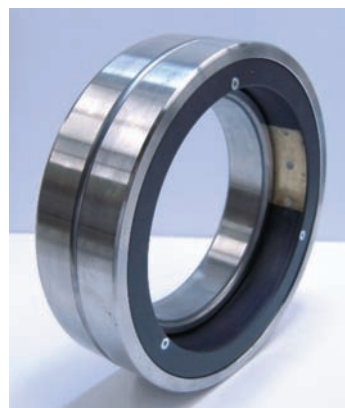
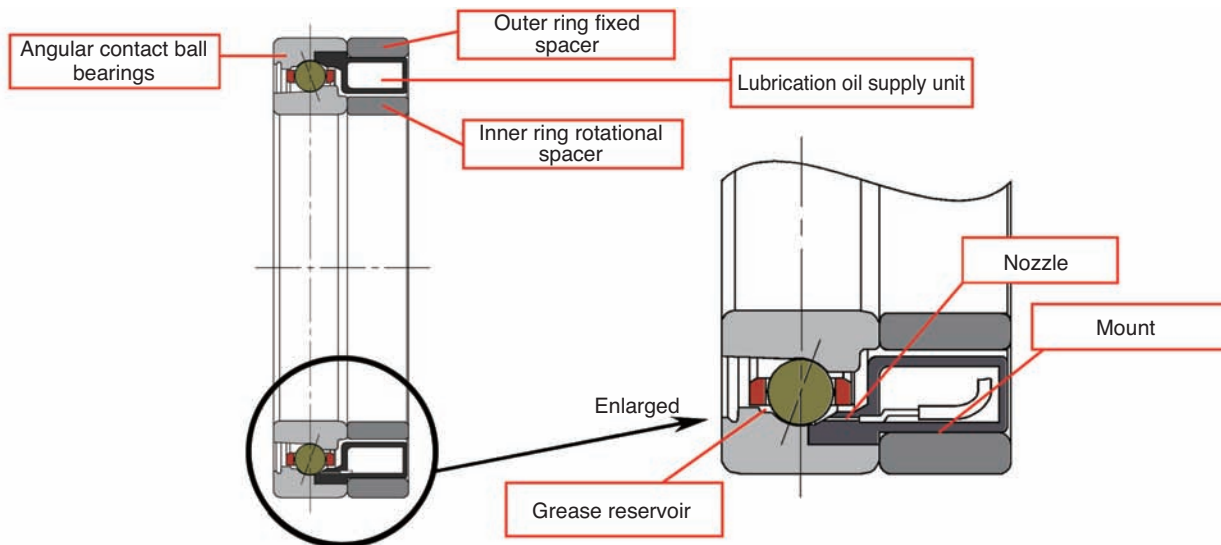
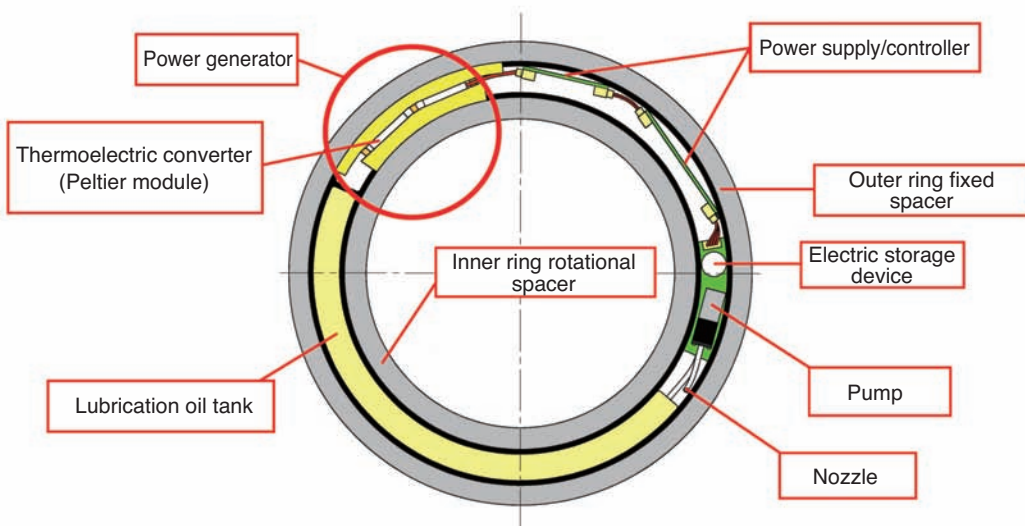


Fig. 1 Lubricating oil supply unit with self-power generator

\*Industrial Machinery Engineering Dept., Industrial Machinery Division



(a) Section view of lubricating oil supply unit and bearing



(b) Inside of lubricating oil supply unit

Fig. 2 Schematic structure of lubricating oil supply unit with self-power generator



(a) before discharge

(b) after discharge

Fig. 3 Discharge of lubricating oil

## 2.2 Power generator and power generation method

The electrical control block of this unit is shown in Fig. 4. A power generation method to obtain sufficient energy for powering the control devices and charging the electric storage device is necessary.

In general, heat, vibration, magnetism (electromagnetic induction) are used for power generation. This lubricating oil supply unit adopts a method of converting differences in the temperature between the inner and outer rings (thermal energy) generated by the rotation of bearings into electrical energy by using a thermoelectric converter.

The thermoelectric converter used in this unit is the Peltier module, which generates electricity when there is temperature difference between side A and side B in Fig. 5. Since the Peltier module is small, it can be installed between the inner ring spacer and the outer ring spacer of the bearings.

## 2.3 Controller

The amount and interval of lubricating oil supplied to the bearings are controlled by the program of the controller.

## 2.4 Electric storage device

The electric storage device stores power generated by the Peltier module and ensure the pump operates consistently by maintaining a constant voltage.

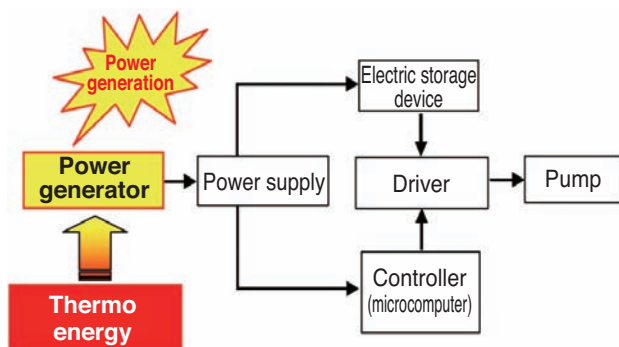


Fig. 4 Block diagram of electrical control

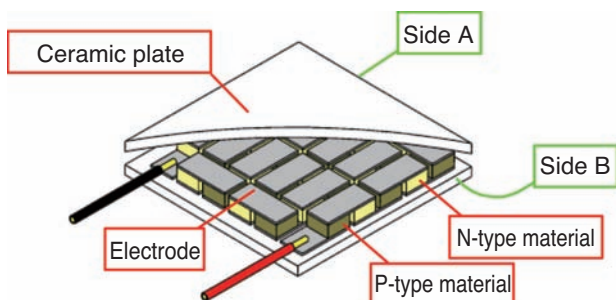


Fig. 5 Structure of peltier module

## 3. Features

- (1) No external power or lubrication is necessary since the self-generating power supply and lubrication reservoir are built-in.
- (2) Same configuration of bearings and spacers as the conventional unit.
- (3) Lubricant supply is minimized by utilizing microcomputer control to disperse the optimum amount of lubricant at the appropriate intervals.

## 4. Performance evaluation

### 4.1 Power generation characteristics

By installing the power generator in the spindle shown in Fig. 6, the relationship between charging voltage and charging time from power generated using the difference in temperature between the inner/outer rings of the bearings was verified. The bearing specification of this test is shown in Table 1 and the power generation test conditions are shown in Table 2. A double layer capacitor was used as the electric storage device and the time needed to reach an arbitrary charging voltage target was evaluated.

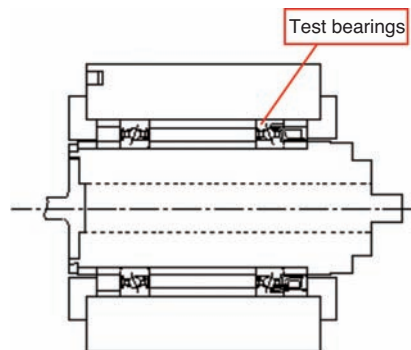


Fig. 6 Spindle for test

Table 1 Specifications of test bearing

Test bearings	$\phi 100 \times \phi 150 \times 24$
Contact angle	20°
Rolling element material	Si <sub>3</sub> N <sub>4</sub>
Cage material	Laminated phenolic resin
Sealed bearing grease	MP-1 (9g contained)

Table 2 Conditions of power generator

Attitude of axis	Horizontal axis
Pressure when incorporated into bearings	100 N (pressure at fixed position)
Rotational speed	10,000min <sup>-1</sup> , 15,000min <sup>-1</sup>
Outer cylinder cooling temperature	Room temperature $\pm 1^\circ\text{C}$
Electric storage device	Electrical double layer capacitor (rated 0.1 F)

Fig. 7 shows the power generation characteristics. It can be seen that the charging time is reduced when the temperature difference between the inner and outer rings is larger.

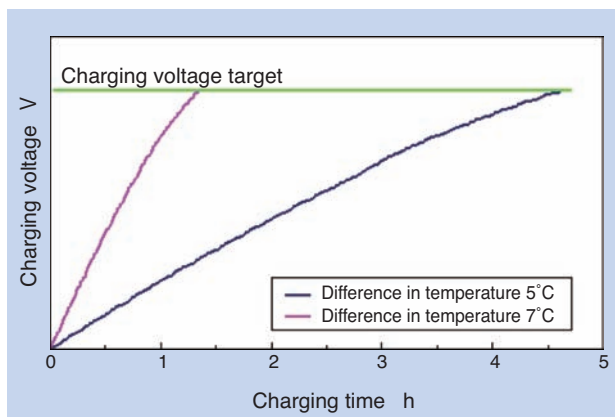


Fig. 7 Characteristic of power generation

#### 4.2 Dispenser operation

In order to verify the diffusion of the lubricating oil, the oil was colored red and the dispenser was installed in the spindle shown in Fig. 6. The test conditions are shown in Table 3.

Fig. 8 (a) shows the grease condition before dispensing lubricating oil and (b) shows the grease condition after lubricating oil is dispensed. It was verified that the grease became red overall after lubricating oil was dispensed. The lubricating oil supply unit was verified to operate correctly as the oil was uniformly diffused in the grease reservoir close to the bearing raceway indicated in Fig. 2 (a).

Table 3 Conditions of lubricating oil supply

Attitude of axis	Horizontal axis
Pressure when incorporated into bearings	100 N (pressure at fixed position)
Rotational speed	15,000min <sup>-1</sup>
Outer cylinder cooling temperature	Room temperature ±1°C
Sealed bearing grease	MP-1 (9 g contained)
Supply lubrication oil	MP-1 base oil
Operating time	Approx. 100 hours



(a) Before lubricating oil discharge (b) After lubricating oil discharge

Fig. 8 State of grease before and after discharge

#### 4.3 Durability evaluation

Bearings for machine tool main spindles with grease lubrication are required to have a durability of 20,000 hours or more. Therefore, we are currently continuing a durability test based on conditions listed in Tables 4 and 5, setting the optimum amount and interval of lubricating oil supply.

Table 4 Specifications of test bearing and lubricating oil supply unit

Test bearings	φ 100×φ 150×24
Contact angle	20°
Rolling element material	Si <sub>3</sub> N <sub>4</sub>
Cage material	Laminated phenolic resin
Sealed bearing grease	MP-1 (9 g contained)
Supply lubrication oil	MP-1 base oil
Amount and interval of supply oil	Automatically adjusted depending on the bearing conditions.

Table 5 Conditions of endurance test

Attitude of axis	Horizontal axis
Pressure when incorporated into bearings	100 N (pressure at fixed position)
Rotational speed	15,000min <sup>-1</sup>
Outer cylinder cooling temperature	Room temperature ±1°C

### 5. Summary

In this paper, we have discussed the lubricating oil supply unit with self-generating power supply that operates using the difference in temperature between the inner and outer rings in the bearings. Traditionally, with grease lubrication, it was difficult to maintain a long and optimum lubrication environment; however, we have solved this issue with the developed lubricating oil supply unit. We will extend this technology to general industrial machines for energy saving and reduction of environmental load.

#### Reference

- 1) Sun-Woo Lee, Tadaaki Maeda: Minimum Quantity base oil of Grease Supply Lubrication Angular Contact Ball Bearings, NTN TECHNICAL REVIEW No. 76 (2008) 88–93

#### Photo of authors



Kaoru OMOTO  
Industrial Machinery  
Engineering Dept.,  
Industrial Machinery Division



Hiroyoshi ITO  
Industrial Machinery  
Engineering Dept.,  
Industrial Machinery Division

# NTN Linear Modules Series



Ulrich GIMPEL\*  
 Michael WILLE\*  
 Tomoyuki OWADA\*\*  
 Masaki KAGAMI\*\*

NTN linear modules are establishing credibility from customers as supplying best suited products. In this document, the feature and applications of NTN linear module series are introduced.

## 1. Introduction

Automated facilities are being implemented in more diverse sectors, such as automobile, machine/parts, semiconductors, flat panels, food, and medicine, for increased productivity, increased efficiency, and cost reduction. This paper introduces the features and applications of the NTN linear module for use in carrying mechanisms, positioning devices, and lifts.

## 2. NTN linear module products

Table 1 shows an overview of NTN linear modules and Table 2 shows their dimensions. Four series are available, which are (1) small type, (2) parallel type, (3) large type, and (4) table type. They offer a fast operation of up to 10 m/s, driven by a timing belt, and a long stroke of up to 10 m with the large-type AXS series.

Table 1 Outline of NTN linear modules

		(1) Small type: AXC Series	(2) Parallel type: AXDL Series	(3) Large type: AXS Series	(4) Table type: AXLT Series
Features		Small, compact	Small, high load capacity	Supports transport of heavy object	Supports highly accurate positioning
Number of rows of incorporated linear motion guide		Single row	Multi-row	Multi-row	Multi-row
Linear motion guide	Linear guide	Applicable	Applicable	Applicable	Applicable
	Roller guide	Applicable	Applicable	—	—
Driving method	Feed screw drive	Applicable	Applicable	—	Only ball screw drive
	Timing belt drive	Applicable	Applicable	Applicable	—
	Omega drive	Applicable	—	Applicable	—
	Rack and pinion drive	—	—	Applicable	—
Maximum speed	m/s	10.0	10.0	10.0	2.5
Maximum length	m	8.00	6.35	10.00	3.50
Maximum static permissible moment	N · m	5.900 ( Frame size 120 × 120mm )	3.550 ( Frame size 240 × 100mm )	21.000 ( Frame size 400 × 300mm )	10.000 ( Frame size 455 × 70mm )

\*NTN-SNR ROULEMENTS Engineering Bielefeld

\*\*Product Engineering Department, Precision Equipment Division

**Table 2** Lineup of NTN linear modules

Type	Series/model	Frame size A×B mm				
(1) Small type	AXC	40	40 × 40			6.00
		60	60 × 60			8.00
		80	80 × 80			8.00
		120	120 × 120			8.00
(2) Parallel type	AXDL	110	110 × 50			6.10
		160	160 × 66			6.10
		240	240 × 100			6.35
(3) Large type	AXS	120	120 × 120			3.00
		200	200 × 100			6.00
		230	200 × 160			10.00
		280	280 × 170			10.00
		460	400 × 300			10.00
(4) Table type	AXLT	155	155 × 30			3.50
		225	225 × 40			3.50
		325	325 × 50			3.20
		455	455 × 70			3.20

They have a large static permissible moment that is suitable for carrying large or heavy materials and making compact equipment. They also provide diverse motor couplings, which allow a combination of different motor types.

NTN linear modules can be combined with those of different series or frame sizes, linear motion guides, or driving methods in order to address required operation conditions such as applications, loads, or installation positions.

### 2.1 Small type: AXC Series

The outer view of AXC80Z is shown in Fig. 1. It is equipped with a single-row linear motion guide and a driver in the slim and light aluminum frame. Its small form-factor provides the same load capacity as the larger competitive products due to the adoption of a highly rigid linear motion guide, which helps the users to realize smaller equipment.

A linear motion guide can be selected from two types, which are the ball-circulating-type linear guide or roller guide, which consists of a shaft and bearings, depending on the application. A driving method can be

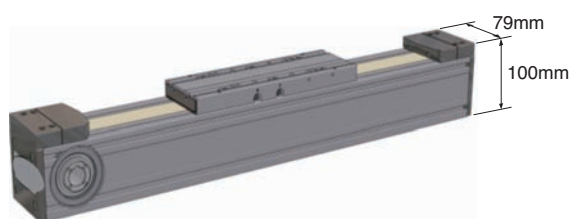


**Fig. 1** AXC Series AXC80Z

selected from three types, feed-screw drive, timing belt drive, or omega drive. The details are discussed in Section 4.

The standard equipment now includes a dust control seal to prevent foreign objects from entering the frame, as well as a mechanism for facilitating easy greasing and exchange of the timing belt, which all contribute to the improved maintainability.

This series can be used not only as a uniaxial application, but also as a part of multi-axial systems combined with other products of the same AXC series or different series.

### 2.2 Parallel type: AXDL Series

The outer view of AXDL110S is shown in Fig. 2. This series is equipped with two linear motion guides on both sides of the driver to provide larger load capacity and rigidity. Particularly, it provides increased pitch and yaw rigidity, making it possible to be used for a long time under severe conditions, such as uneven loading.

It also provides the same dust control and maintainability as the AXC Series. A linear motion guide can be selected from two either linear guide or roller guide and a driving method can be selected from feed-screw drive or timing-belt drive. This series is considered the by the users as most well rounded among the size, load capacity, rigidity, and accuracy.

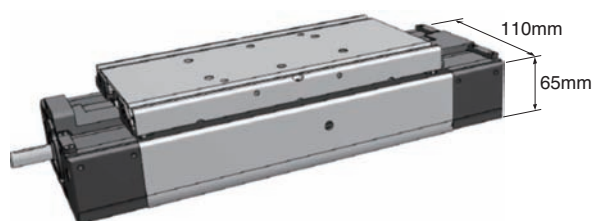


**Fig. 2** AXDL Series AXDL110S

### 2.3 Large type: AXS Series

Fig. 3 shows an example of combined use with AXS280Z as a horizontal axis. High rigidity and high load capacity are achieved by the large aluminum frame and high-performance linear guide. It is mainly used for horizontal transportation of heavy loads over 100 kg, as an upper axis of a gantry structure called a beam, and for lifting heavy loads with vertical axes.

This series includes an ultra-large size type that other competitors do not manufacture. The frame size of AXS460 is 400 mm wide × 300 mm high. A drive method can be selected from rack-and-pinion drive, timing-belt drive, or omega drive, with 10 m of maximum stroke, 10 m/s of maximum speed, and

1000 kg of maximum transport weight supported. (See 5.2 An example of application to a machine tool)

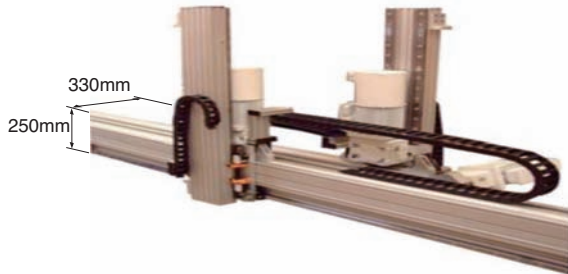


Fig. 3 Application of AXS280Z

### 2.4 Table type: AXLT Series

AXLT155, shown in Fig. 4, uses aluminum extruded material of positioning table type for the frame. The linear module products from other manufacturers are mostly limited to transportation; however, this series can also be used as an accurate positioning device, as it combines precision ball screws and multi-row high-performance linear guides.

Although the bellows are equipped to prevent foreign objects from entering the frame, maintenance can be conducted without removing them since the lubrication hole is provided on the side of the stage.

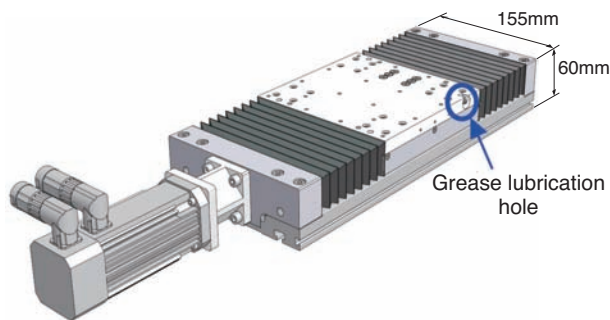


Fig. 4 AXLT Series AXLT155

## 3. Linear motion guide

The linear motion guide to be incorporated into NTN linear modules can be selected from linear guide and roller guide, depending on the operating conditions such as load, speed, accuracy, and the required cost.

### 3.1 Linear guide

Fig. 5 shows the internal structure of a ball-circulating-type linear guide. The linear module is

required to operate consistently for a long time. This product achieved low heat, low noise, long life, and long maintenance-free operation by adopting a ball retainer with grease pockets, as shown in Fig. 6.

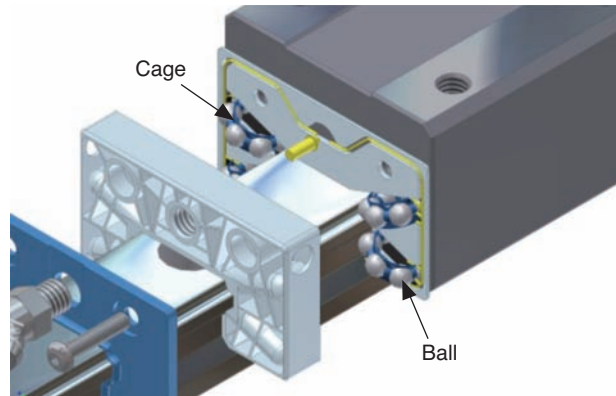


Fig. 5 Linear guide

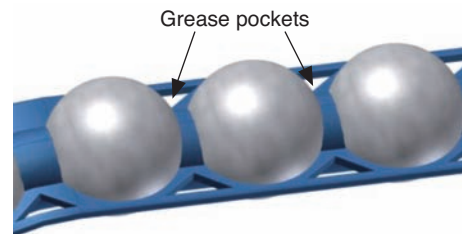


Fig. 6 Retainer with grease pocket

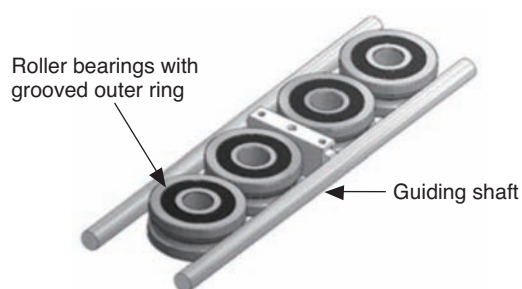
### 3.2 Roller guide

Fig. 7 shows the roller guide as installed into the AXC Series in transparent view. A roller guide can also be selected with the AXDL Series.

As shown in Fig. 8, it has a simple structure where rolling bearings with grooved outer rings traverse between two rod-shaped guiding shafts in the aluminum frame, yet it has high load capacity with a maximum operating speed is 10 m/s.



Fig. 7 Roller guide



**Fig. 8** Guiding system of roller guide

## 4. Driving method

There are 4 types of driving methods that can be combined with the module, i.e., (1) feed screw drive by a ball screw or trapezoidal screw, (2) timing-belt drive, (3) rack-and-pinion drive, and (4) omega drive using a timing belt.

### 4.1 Feed screw drive

This method can be applied to AXC, AXDL, and AXLT Series (not AXS Series), selecting either a ball screw or trapezoidal screw depending on the load, speed, and application.

The standard specification of the ball screw is JIS accuracy class Ct7 with lead typical motion error of 52  $\mu\text{m}/300\text{ mm}$  or less. If even higher accuracy is required, a precision grinding ball screw can also be selected.

A trapezoidal screw is mainly used in a simplified positioning device where cost is emphasized. The lead typical motion error is 100  $\mu\text{m}/300\text{ mm}$  (or 200  $\mu\text{m}/300\text{ mm}$  depending on the size), which is inferior to the ball screw; however, the accuracy of positioning reproducibility after it is incorporated into the module is  $\pm 0.100\text{ mm}$  or less and the supported maximum speed is 115 mm/s. Therefore, it has a high-cost performance.

### 4.2 Timing-belt drive

This can be selected for AXC, AXDL, and AXS Series (not AXLT) and is a driving method appropriate for high-speed transport. **Fig. 9** shows the timing-belt drive

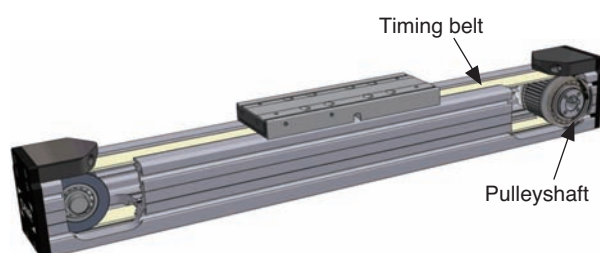


**Fig. 9** Timing belt drive

drive AXC Series. It uses a highly durable timing belt that does not stretch even after a lengthy operation. Its responsiveness is improved by adjusting the belt tension to the optimum value when it is assembled into the module.

### 4.3 Omega drive

This driving method, which can be applied to AXC and AXS Series, uses a driving pulley and a motor (omitted from the figure) on the stage (carriage), with both ends of the timing belt fixed on the frame, as shown in **Fig. 10**. It is called “omega drive” because the shape of the driving pulley wrapped by the timing belt looks like the Greek letter  $\Omega$  (omega). It is used to provide independent motions of multiple omega driving stages installed on the module of a single axis, or to move the frame by fixing the stage, for example.

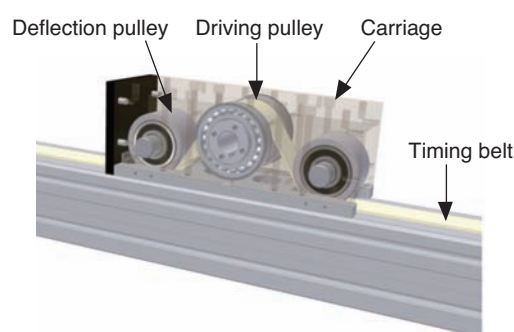


**Fig. 10** OMEGA drive

### 4.4 Rack-and-pinion drive

The rack-and-pinion drive, which is only applicable to AXS Series, is used for lifting load in vertical motion or as a beam in the gantry structure. It is able to transport a maximum of 1000 kg of load due to its high power transmission capability despite the simple and light structure.



**Fig. 11** Rack-and-pinion drive

## 5. Applications of NTN linear modules

### 5.1 Combined approach

Fig. 12 shows a gantry structure combining several NTN linear modules.

Small-type AXC Series are used for the two bottom axes to reduce the size of the overall equipment. In order to drive both axes at the same time, the connecting shaft is used to transmit the power of the motor rotation in this mechanism. The parallel-type AXDL Series is used as the beam axis to support the overhang moment load of the Z-axis driving module and the large type AXS Series is used for Z-axis to enhance the lifting performance.

As shown in this example, it is possible to configure a system taking advantage of features of each module.

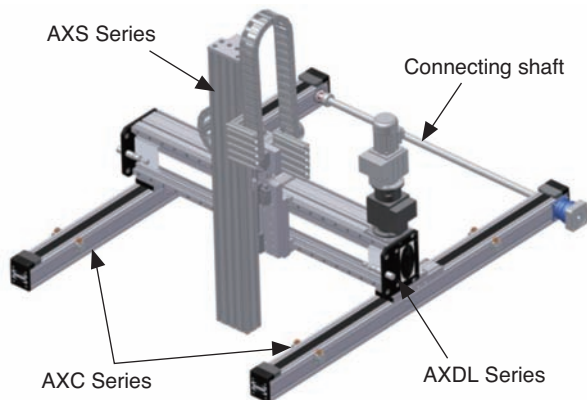


Fig. 12 Combination reference example

### 5.2 An example of application to a machine tool

Fig. 13 shows an example of using a timing belt drive AXS Series for the work automatic attach/detach loader. In order for a robot exceeding 100 kg in weight, which is suspended from the beam, to attach/detach the work quickly and accurately after its position is determined, it is necessary to keep the displacement of the tip of the hand caused by the robot operation and movement of the load within the required accuracy. This was achieved by the AXS Series with high rigidity.

### 5.3 Special applications

Fig. 14 shows its application on the lateral slide mechanism for the operator cockpit of a road pavement service vehicle.

The linear modules have been used in very large applications such as automatic sprayer equipment of pesticide and water in greenhouses and planting facility and gantry-type cranes for transporting

construction material (large wall panels) as well as small applications such as industrial products and in food and medical sectors, due to their many variations.

NTN Linear Module AXS Series  
(length 6000; stroke 3000; width 280 mm)



Fig. 13 Example of use for loader



Fig. 14 Example of use for service vehicle

## 6. Summary

NTN linear modules are excellent for rigidity and reliability and have an extremely proven track record, especially in Europe.

We will continue to contribute to the facility automation by proposing solutions with high cost performance to the new user requirements for their facilities and new development challenges using NTN linear modules.

## Reference

Ulrich Gimpel, Michael Wille, NTN-SNR High Performance and Flexible Linear Modules Series AXDL, NTN TECHNICAL REVIEW No.78 (2010) 64-69

### Photo of authors



Ulrich GIMPEL  
NTN-SNR ROULEMENTS  
Engineering Bielefeld



Michael WILLE  
NTN-SNR ROULEMENTS  
Engineering Bielefeld



Tomoyuki OWADA  
Product Engineering  
Department,  
Precision Equipment Division



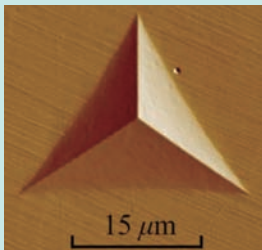
Masaki KAGAMI  
Product Engineering  
Department,  
Precision Equipment Division

# Evaluation of Local Mechanical Properties of High Strength Steels by Indentation Method

Takeshi OGAWA\*

Noriaki SAKANAKA\*\*

Yukio MATSUBARA\*\*



High strength steels are used for important components such as rolling bearings, for which surface treatments such as induction and carburized hardenings are applied. Strength designs for these components require material properties at the local areas, since the material properties are different at the treated locations. The objective of the present study is to evaluate the local mechanical properties of high strength steels by the dual indenter method. Non-dimensional  $\Pi$  function is developed for 118 degree trigonal pyramid indenter using finite element method. Dual-indenter method is conducted by indenters with the apex angles of 115 and 118 degrees for JIS-SUJ2 and JIS-SUJ3. The results reveal that good agreements are achieved between stress-strain curves of tensile testing and those of the dual-indenter method. The local mechanical properties are evaluated by the dual-indenter method for induction-hardened and carburized components. There are some differences in stress strain curves at the locations of the components by the influence of the heat treatments.

## 1. Introduction

For important components such as rolling bearings, hardening is applied for either all the components or only local areas where high strength is needed by surface treatments such as induction and carburized hardenings. Since the local areas where surface treatment is applied have different material properties, local evaluation for those local areas is required when mechanical properties are evaluated. A dual indenter method<sup>1)</sup> has been proposed for evaluating local mechanical properties as an indentation method. One of the authors (Ogawa) has been applying the dual indenter method to diverse materials for the mechanical evaluation<sup>2)</sup>. However, it was revealed that the prediction on high-strength-bearing steel did not always match the tensile testing results. Therefore, in this study, a method of estimating mechanical properties of high-strength materials was studied using the indentation method and finite element method (FEM).

## 2 Material under test and test piece

The chemical components of materials under test, high-carbon chrome-bearing steel JIS-SUJ2 and JIS-SUJ3, are shown in **Table 1**. The standard overall hardening was applied to the materials under test, and then, they were tempered at 180–350°C and used as test pieces. Induction-hardened and carburized materials were also used as test pieces. The surface of test pieces was treated with emery paper polishing, buffing, and lapping with diamond paste.

**Table 1** Chemical compositions (mass %)

	C	Si	Mn	P	S	Ni	Cr	Cu
<b>SUJ2</b>	1.02	0.27	0.43	0.014	0.007	0.05	1.48	0.09
<b>SUJ3</b>	0.99	0.47	1.06	0.014	0.006	0.07	1.06	0.14

\*Professor, Department of Mechanical Engineering, College of Science and Engineering, Aoyama Gakuin University

\*\*Advanced Technology R&D Center

### 3. Testing machine and conditions

Six indentation tests were conducted for each condition, using Dynamic Ultra Micro Hardness Tester DUH-W201 of Shimadzu Corporation. Tests were all conducted at room temperature (approximately 20°C) with the loading/unloading speed of 10.1 mN/s and the maximum test force of 1961 mN. In addition, trigonal pyramid indenters with apex angles  $\phi$  of 100°, 115°, and 118° were used for the testing.

### 4. Indentation test

#### 4.1 Dual indenter method

In this study, a trigonal pyramid indenter with apex angle of 118°, which has relatively small plastic deformation, is used in addition to  $\phi = 100^\circ$  and  $115^\circ$ , as the dual-indenter method is applied.<sup>3)</sup> The following analysis was conducted using a conical indenter with apex angle  $\theta$ , where the ratio of projected area and h of the indenter is the same. In general, indentation force  $F$  and indentation depth  $h$  are in the relationship of  $F = Ch^2$  and can be expressed as follows after a dimension analysis:

$$F = F(E^*, n, \sigma_r, \theta, h) \dots\dots\dots (1)$$

Where  $E^*$  is the complex Young's modulus,  $n$  is the work-hardening exponent including influence of elastic deformation of indenter.  $\sigma_r$  is called the typical stress that characterizes the plastic deformation region. When the  $\Pi$  theory is applied to the equation (1), the following is obtained<sup>3)</sup>.

$$\frac{F}{\sigma_r h^2} = \frac{C}{\sigma_r} = \Pi\left(\frac{E^*}{\sigma_r}, n, \theta\right) \dots\dots\dots (2)$$

The typical stress-strain relationship for each indenter can be obtained by finding this  $\Pi$  function for each of the indenters of apex angles  $\phi$  and testing two types of indenters, and using the  $\Pi$  function and the experiment result, that is, the slope  $C$ , which is  $F$  against  $h^2$  in the load process.  $n$  is determined from the relationship of these two points. Also, from the generally known stress-strain relationship, the yield stress  $\sigma_y$  and the strength coefficient  $K$  can be obtained from the following equation: where  $\epsilon_r$  is the typical strain.

$$\sigma_r = K \epsilon_r^n \quad \sigma_r = \sigma_y \left(1 + \frac{E}{\sigma_y} \epsilon_r\right)^n \dots\dots\dots (3)$$

#### 4.2 Finite Element Method (FEM) analysis

A general-purpose non-linear structural analysis program, MSC.MARC Mentat 2005, was used for analyzing newly generated  $\Pi$  functions in this mechanical property evaluation using dual-indenter method. In the previous indentation tests with trigonal pyramid indenters, it has been verified that the three-dimensional analysis result of trigonal pyramid indenters is equivalent to the analysis result from the axisymmetric model of conical indenters with the same depth-projected ratio<sup>3)</sup>. Axisymmetric model with 2549 elements and 2658 nodes simulating conical indenter of apex angle  $\theta = 77.37^\circ$  was used for the indenter of  $\phi = 118^\circ$  in the FEM analysis. Fig. 1 shows the analysis model. For generating new  $\Pi$  functions, total of 72 combinations were analyzed with a range of material parameters, namely, Young's modulus  $E = 50$  to 300 GPa, yield stress  $\sigma_y = 0.1$  to 5.0 GPa, and work-hardening exponent  $n = 0.1$  to 0.5. The Poisson's ratio was set to  $\nu = 0.3$  for all combinations.

The relationship of  $E^*/\sigma_r$  and  $C/\sigma_r$  obtained from this analysis is shown in Fig. 2. The analysis result is indicated by one curve for each value of work-hardening exponent  $n$  in the analysis conditions. For

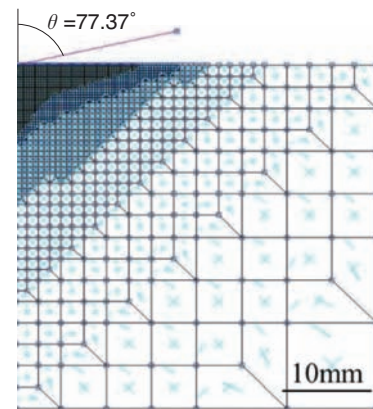


Fig. 1 Model for FEM analysis

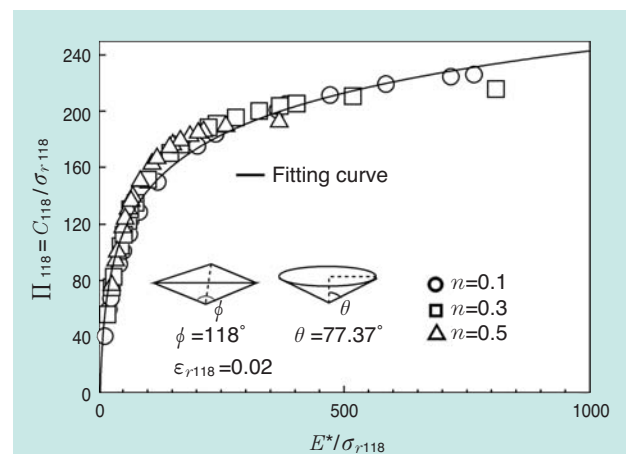


Fig. 2 Dimensionless function of 118° indenter

the determination of  $\varepsilon_r$ , the fitting to the curve is tested in  $\varepsilon_r = 0.001$  increments to obtain  $\varepsilon_r = 0.020$  for the indenter of  $\phi = 118^\circ$ . As a result, the relationship of  $E^*/\sigma_r$  and  $C/\sigma_r$  is expressed by one curve independent from the work-hardening exponent  $n$  and the non-dimensional function  $\Pi_{118}$  is obtained by the following equation:

$$\Pi_{118} = \frac{C_{118}}{\sigma_{r118}} = 43.25 \ln \left( \frac{E^*}{\sigma_{r118}} \right) - 55.90 \dots\dots (4)$$

## 5. Test result and observation

### 5.1 Evaluation of mechanical properties of bearing steel

Mechanical properties were evaluated by the dual-indenter method using the newly generated  $\Pi$  function for the  $118^\circ$  indenter. Fig. 3 shows the evaluation results of SUJ2 and SUJ3, tempered at  $180^\circ\text{C}$ , using indenters of  $\phi = 115^\circ$  and  $118^\circ$ , and  $\phi = 100^\circ$  and  $115^\circ$ . It can be seen that the evaluation tests using the  $115^\circ$  and  $118^\circ$  indenters provide similar results as the tensile test results. On the other hand, the dual-indenter method using the  $100^\circ$  and  $115^\circ$

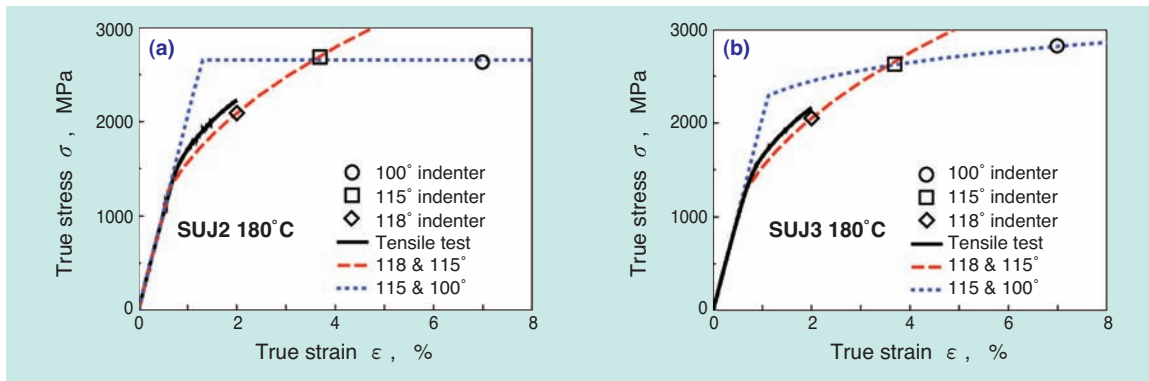


Fig. 3 Stress-strain curves obtained by tensile testing and dual-indenter method for SUJ2 (a) and SUJ3 (b)

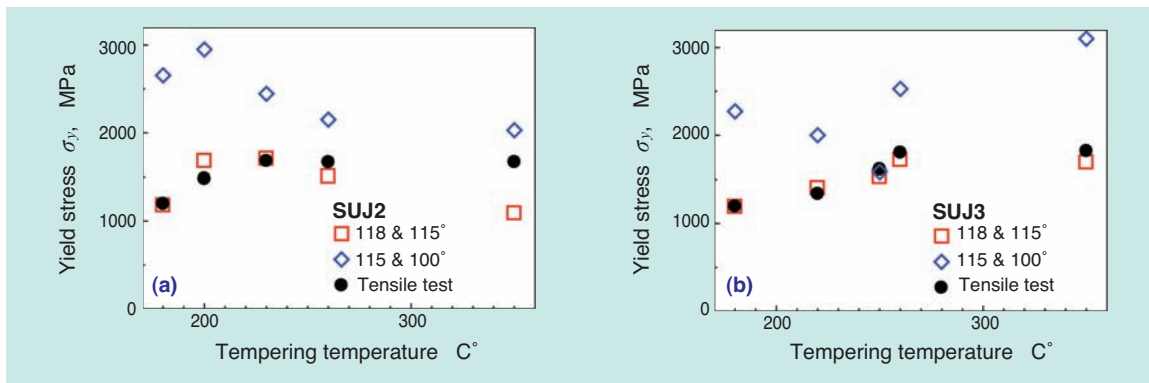


Fig. 4 Results of yield stresses for SUJ2 (a) and SUJ3 (b)

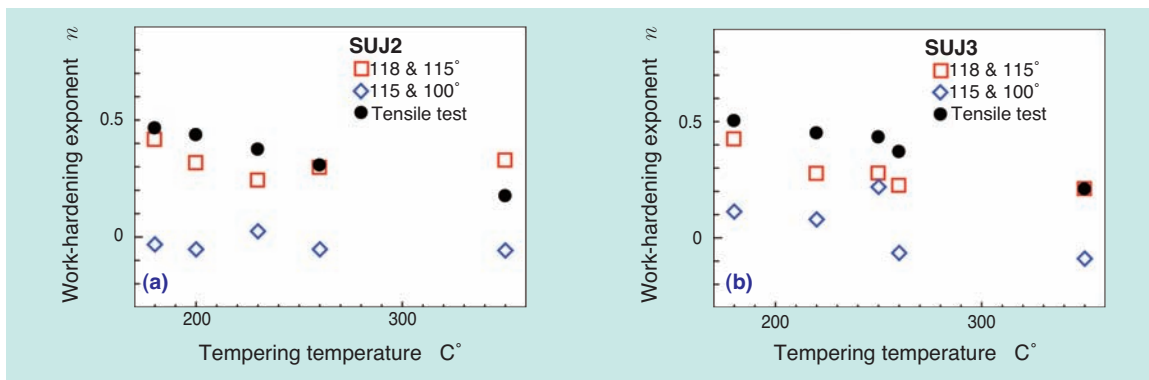


Fig. 5 Results of work hardening exponents for SUJ2 (a) and SUJ3 (b)

indenters gave significantly different results from the tensile tests. Fig. 4 and Fig. 5 show the yield stress  $\sigma_y$  and work-hardening exponent  $n$  obtained from the dual-indenter method. Since the indenters of  $115^\circ$  and  $118^\circ$  provided similar values as the tensile test results, evaluating correct tempering temperature dependency of the mechanical properties, the validity of the dual-indenter method using those  $115^\circ$  and  $118^\circ$  indenters is verified.

In order to review the cause of the significant difference between the test results using the indenters of  $100^\circ$  and  $115^\circ$  and the tensile tests, impressions were observed. Fig. 6 shows the photo of impressions of each  $\phi$  and AFM observation result. It can be observed that the smaller the apex angle  $\phi$ , the larger the pile-up around the impressions. As the pile-up is

not well simulated with the FEM analysis that generates  $\Pi$  functions, it is assumed that the significant pile-up prevented valid results to be generated in the dual-indenter method using indenter of  $100^\circ$ .

### 5.2 Evaluation of mechanical properties of surface treated components

The local mechanical properties were evaluated for test pieces cut out from the induction-hardened carbon steel S53C and carburized chrome steel SCr420 components. In order to evaluate local mechanical properties on these test pieces, hardness distribution was verified to identify the range of effect of the respective heat treatments. The distribution of Vickers hardness HV is shown in Fig. 7 and Fig. 8. The measurement was carried out with Vickers micro-

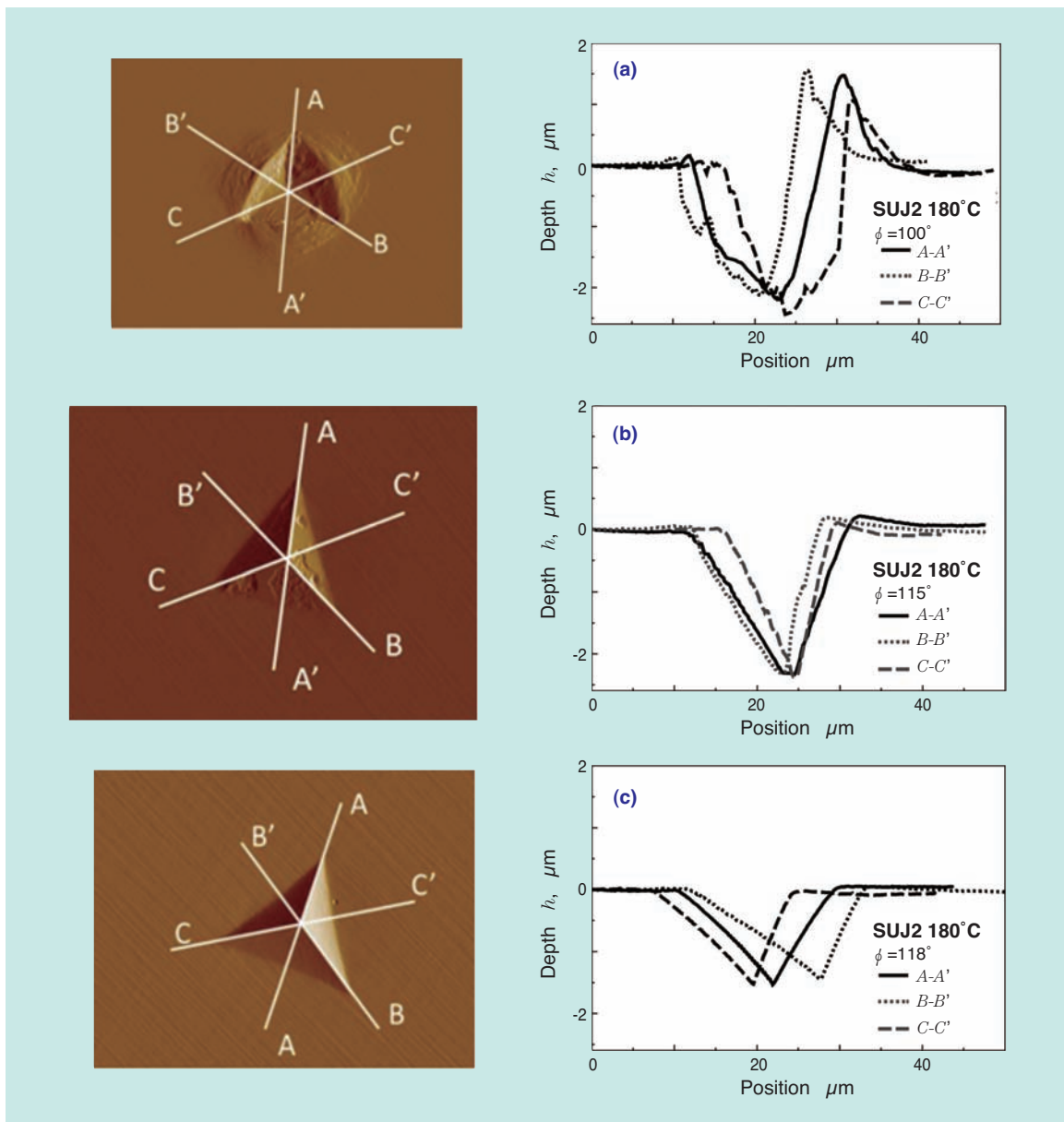


Fig. 6 Shapes of impressions and height profiles measured by AFM formed by  $100^\circ$ (a),  $115^\circ$ (b) and  $118^\circ$ (c) indenters

hardness tester MVK-G3, made by Akashi. The test force is 2940 mN (300 gf) and measurement was taken toward the direction of the arrow in the picture at the same intervals. HV of induction-hardened component in Fig. 7 shows distribution of 304 to 746. In contrast, HV of carburized hardened component in Fig. 8 shows distribution of 383 to 744. As such, the difference of HV by heat treatment methods can be confirmed.

Defining the region of 700 or higher of HV as “high hardness” and 450 and lower as “low hardness”, the local mechanical properties were evaluated using the

dual-indenter method. The 115° and 118° indenters were used for indentation test. The results are shown in Fig. 9 and 10. In the high-hardness region, the test result shows large yield stress and it is possible to confirm the relationship between the hardness and the yield stress. When the induction-hardened components and carburized-hardened components are compared in the high-hardness region, the hardness of the induction-hardened components is higher and the yield stress is also larger. In the low-hardness region, however, different from the high-hardness region, the carburized-hardened

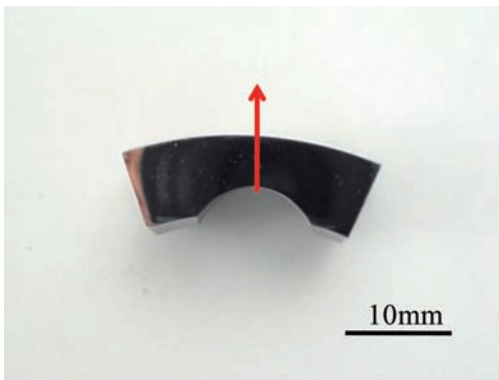


Fig. 7 Shape and hardness distribution chart of induction-hardened specimen

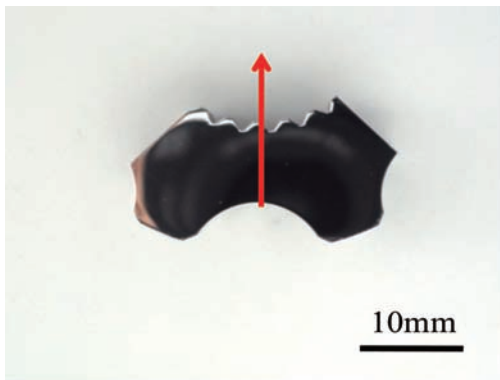
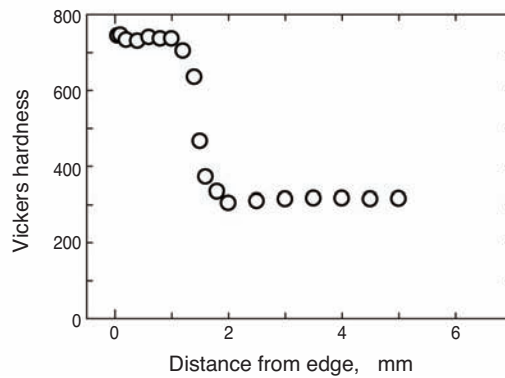


Fig. 8 Shape and hardness distribution chart of carburized specimen

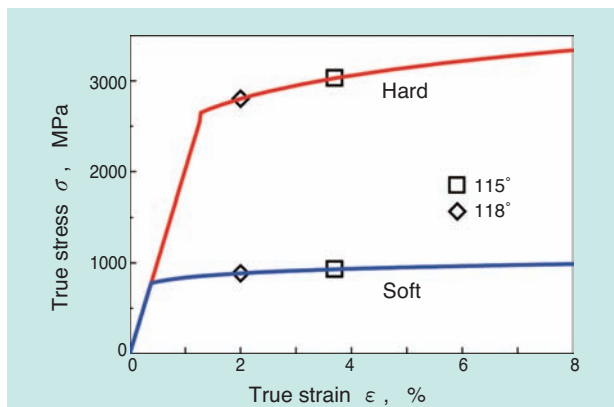
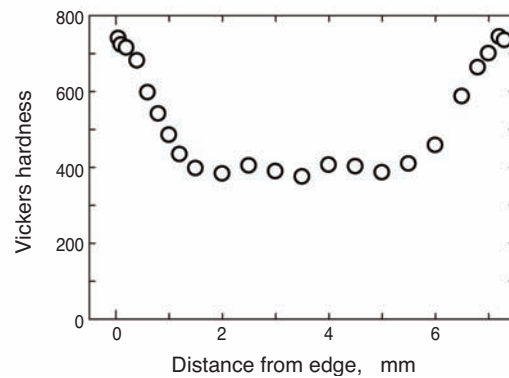


Fig. 9 Stress-strain curves of induction hardened specimen

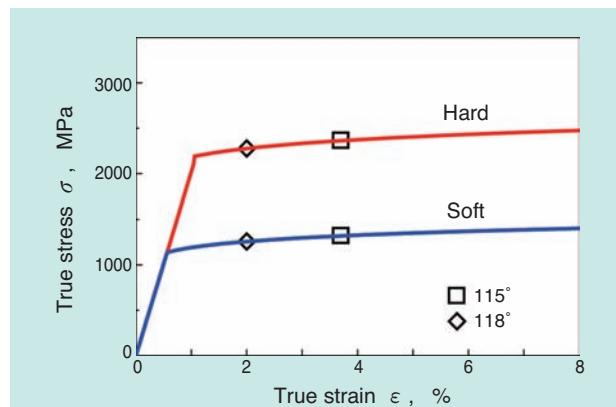


Fig. 10 Stress-strain curves of carburized specimen

components are superior in both hardness and yield stress.

Induction hardening has a hardening effect only on the surface but the internal organization remains the same. On the other hand, carburized hardening hardens the surface and also the internal organization to some extent. The test result clearly shows these characteristics of the respective heat processes, indicating the clear difference of the impact of the heat processes in  $\sigma - \varepsilon$  curve of the local areas.

## 5. Summary

The dual-indenter method using trigonal pyramid indenters of apex angles of  $115^\circ$  and  $118^\circ$  applied to the test pieces of high-strength steel with different heat processes revealed equivalent stress-strain properties as the test results of tensile tests.

With the evaluation of mechanical properties of surface-hardened components, the difference of induction-hardened and carburized-hardened heat processes was verified from the stress-strain properties of the local areas.

Also, pile-up was confirmed around the impressions of the  $100^\circ$  indenter. When pile-up is formed, the relationship between the indentation force and depth is affected and the dual-indenter method cannot be applied.

When stress-strain properties obtained from the dual-indenter method are used for the analysis of the actual machines, it is possible to conduct more detailed elastic/plastic analysis than conventional methods.

## Reference

- 1) Nagahisa Ogasawara, Wakako Makiguchi, Norimasa Chiba, "Plastic Properties Determination Method for Power-Law Hardening Material Using Plural Triangular Pyramid Indenters", Transactions of the Japan Society of Mechanical Engineers. A, Vol. 70, No. 698 (2004), pp. 1529-1534.
- 2) Akio Yonezu, Takeshi Ogawa and Mikio Takemoto, Key Engineering Materials, Vols. 353-358, pp.2223-2226 (2007).
- 3) Takashi Ono, Akio Yonezu, Takeshi Ogawa, Jun Akimitsu, "Evaluation of Mechanical Properties and Strength Characteristics of Micro Region Using Indentation Method", Journal of Material Testing Research Association of Japan, Vol. 49, No. 3 (2004), pp. 149-156.

## Photo of authors



Takeshi OGAWA

Professor,  
Department of Mechanical Engineering,  
College of Science and Engineering,  
Aoyama Gakuin University



Noriaki SAKANAKA

Advanced Technology  
R&D Center



Yukio MATSUBARA

Advanced Technology  
R&D Center

# TMR: A New Frontier for Magnetic Sensing

Christophe DURET\*  
Shintarou UENO\*



We present here a new linear magnetic sensing technology, based on Tunnel Magneto Resistance (TMR). The TMR principle derives from Spintronics, a new branch of Physics which received the 2007 Nobel Prize in Physics. Contrary to “traditional” electronics, a Magnetic Tunnel Junction (MTJ) uses not only the electric charge of the electron, but also its quantum spin value.

During the CAMEL project, we have designed MTJs for sensor applications, i.e. for having, compared to other existing technologies, greater performances, extended working ranges and design capabilities, the robustness needed for harsh mounting and working conditions and of course a cost compatible with a market introduction. The fascinating properties of the TMR sensing elements we have developed open the door to many new possibilities of magnetic sensing.

## 1. NTN-SNR magnetic sensing technology

### 1.1 Bearings with active sensor ASB®

NTN-SNR has developed the active sensor bearings, ASB®, the technology for detecting wheel speed used for Antilock Brake System (ABS) and Electronic Stability Program (ESP) for vehicles, as shown in Fig. 1. The ASB®, which helps in reducing the weight and space of vehicles and improves the robustness and zero velocity detection in the severe conditions, is a defacto global standard for detecting wheel velocity in the automobile industry. The following shows the configuration of an ASB®:

- **Target magnet**

Multi-pole ring magnet integrated with the bearing seal. It generates an alternating magnetic field with frequencies proportional to the rotational speed of the wheel.

- **Detection device**

This uses the magnetoresistance effect or Hall effect. It measures the alternating magnetic field that the target magnet generates with no contact and calculates the wheel rotation speed to be used by the ABS and ESP.



Fig. 1 Example of ASB integration in a roller bearing unit

### 1.2 Development and applications of high-resolution rotation sensor MPS40S

After the development of the ASB®, continuing with the research of a low-cost sensor for accurately detecting angles of rotation and for controlling rudder angle of the steering wheel and electric motor, we developed the special-purpose IC MPS40S<sup>1)</sup> with a built-in Hall effect device and signal processing circuit. As shown in Fig. 2. MPS40S is applicable for a wide

\*NTN-SNR ROULEMENTS Research & Innovation Mechatronics

range of pole widths, has the capability of outputting high-resolution pulse signals and origin position signals, and satisfies the quality standard AEC-Q100 as the electronic device for automobile use.

MPS40S is also targeted at industry machines such as the rotational control of servo motors. Fig. 3 shows the high-resolution sensor bearing with origin signal output<sup>3)</sup>, which integrates MPS40S and bearings for improving ease of assembly with target equipment.

As an application of MPS40S, Fig. 4 shows a high-precision magnetic angle sensor<sup>4)</sup>, which detects the absolute angle using the Vernier principle. This sensor is applicable to tubular shafts, where the existing sensors shaft end placements was not applicable. By integrating the multi-pole ring magnet and the bearing rotating ring and placing the detection device with a built-in signal processing circuit to the fixed ring, the axial space adjustment is not required when assembled. The absolute angle can be accurately measured even in high-speed rotation. This is done by setting the dedicated multi-pole ring magnet, which has two rows of concentric magnetic patterns with a different number of magnetic poles inside and outside, and calculating the relative displacement of the patterns from the magnetic sensor signals.



Fig. 2 Appearance of MPS40S

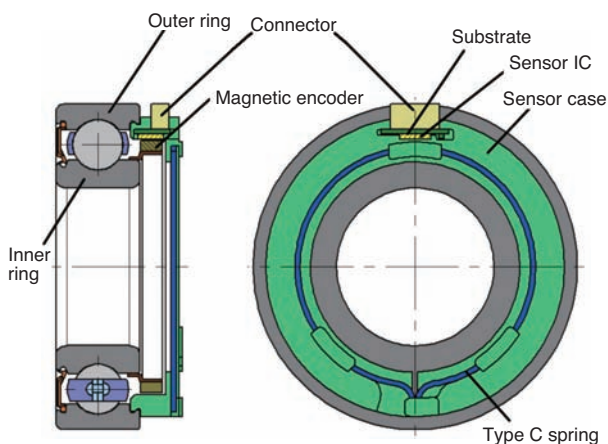


Fig. 3 High resolution sensor bearing

## 2. Characteristics of various magnetic sensors

In order to apply magnetic sensing technology to a wide range of applications, it is necessary to consider basic performance of magnetic detection sensors (such as output accuracy, frequency bandwidth, and power consumption), as well as operation range against air gap and temperature, size of the sensor, installation allowance, robustness, and cost. Sensors in severe operating environments such as automobile and industrial machine applications typically use the Hall device, anisotropic magnetoresistance (AMR) device, and giant magnetoresistance (GMR) device for magnetic field detection<sup>5)</sup>. The following shows their respective characteristics:

### • Hall device

It is of very good linearity and is inexpensive. On the other hand, it has limited sensitivity and large power consumption and offset drift.

### • AMR element

It has better sensitivity than the Hall device and the hysteresis is small. Linearity, offset-free operation, and high magnetic field detection can be achieved by a barber pole sensor structure, flip driving method, and arranging a stabilizing magnet. However, in a high-temperature environment, slight deterioration of sensitivity and linearity is observed.



Fig. 4 High precision magnetic angle sensor

### • GMR element

It has the highest sensitivity and widest permissible range of input magnetic field strength. However, the performance, such as linearity, significantly deteriorates as soon as the temperature or input magnetic field strength exceeds the operating range.

## 3. Tunnel Magneto Resistance (TMR) effect

The basic theory of the MTJ element<sup>\*1</sup> is based on spintronics that uses the quantum spin condition in addition to the electric property of the electron based on the existing electronics theory. When Pr. A. Fert and Pr. P. Grünberg received the Nobel Prize in Physics in 2007, Spintronics attracted immediate attention.

As shown in Fig. 5, the MTJ element generally has the structure of an insulation layer of aluminum oxide ( $\text{Al}_2\text{O}_3$ ) or magnesium oxide ( $\text{MgO}$ ) in the middle of two stacked ferromagnetic layers, similar to a GMR element. With the MTJ element, the current flows vertically through these layers while the electrons in a ferromagnetic layer pass through the insulator by quantum-mechanical effect and are injected to the other ferromagnetic layer by the tunneling effect. In this case, the electric resistance to the current changes significantly depends on the relative angular difference of the magnetized direction of two ferromagnetic layers. When the magnetized direction of two layers is antiparallel, it indicates high

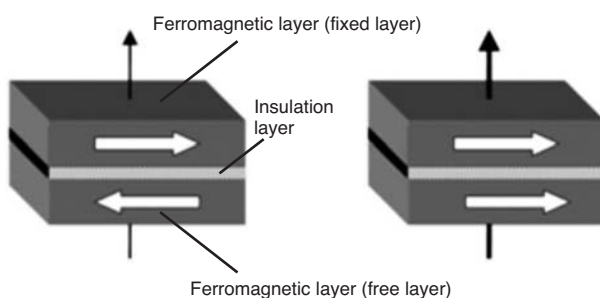


**Fig. 5** Representation of a MTJ in an antiparallel magnetization configuration (left) and in a parallel magnetization configuration (right). The black arrow represents the current going through the junction

resistance, and when it is parallel, it indicates low resistance. That is, the resistance changes depending on the relative angle of magnetization direction of two layers. This phenomenon is called the Tunnel Magneto Resistance (TMR) effect<sup>\*2</sup>. In order to detect an external magnetic field using this effect, the device is configured keeping the magnetized direction of one ferromagnetic material layer (called fixed or pin layer) fixed and allowing the magnetized direction of the other ferromagnetic material layer (called free layer) to change depending on the external magnetic field.

The TMR effect under low temperature was discovered in 1975<sup>6)</sup>; however, it did not attract attention, at that time, as the application was difficult. However, in 1995, when a change of almost 20% of magnetic resistance was achieved (the maximum value at that time) at room temperature in the low magnetic field, the TMR effect was immediately placed under spotlight<sup>7) 8)</sup>.

A recent research reports that using crystalline  $\text{MgO}$  (100) for the insulation layer as an alternative to amorphous  $\text{Al}_2\text{O}_3$  yields very high magnetoresistance change of about 600%<sup>9)</sup> in room temperature<sup>10) 11)</sup>. While the TMR effect has been recently used in the hard disk read head, application development for magnetoresistance memory (MRAM<sup>12)</sup>) for read/write of quantum information of 0 and 1 and for magnetic sensor has just begun<sup>13) 14)</sup>. Also, in order to apply the MTJ element to a magnetic sensor, the resistance needs to be changed depending on the external magnetic field strength and direction, as opposed to the MRAM and hard disk head.

## 4. CAMEL Project

NTN-SNR has been focusing on the research and development of the TMR effect since 2000<sup>15) 16) 17)</sup>, and has filed several patents such as laminated structure of the MTJ element and sensor structure. It also accelerated technology development and application from 2005 to 2010 in the CAMEL (CApteur Magnétique à effet tunnEL) project. Sponsored by the French National Research Agency (ANR), the project was conducted as an academic-industry partnership of NTN-SNR (end-user project leader), Sensitec (making of MTJ element), and two public research institutions.

The project established the MTJ element aimed at sensor applications and linear magnetic sensing technology. It evaluated how they would adapt to the production and high-volume production using the existing production line of AMR/GMR elements owned by Sensitec<sup>18)</sup>. An example of the linear magnetic

\*1 MTJ element: Magnetic Tunnel Junction element.  
An element made of a stack of layers with an insulation layer of a few nm of thickness called a barrier layer or tunnel barrier in the middle, and two ferromagnetic layers made of ferromagnetic metal on both sides.

\*2 TMR Effect: Tunnel Magnetoresistance Effect.  
A phenomenon that resistance changes by MTJ element.

sensing using the TMR effect is shown in Fig. 6. As shown in the graph to the right, it was determined that the measured result mostly matched with the linear approximation and the hysteresis was sufficiently small.

In addition, this project received the Yves Rocard prize in 2010 from the French Physics Society for its achievement in advancing the basic technology to practical utilization.

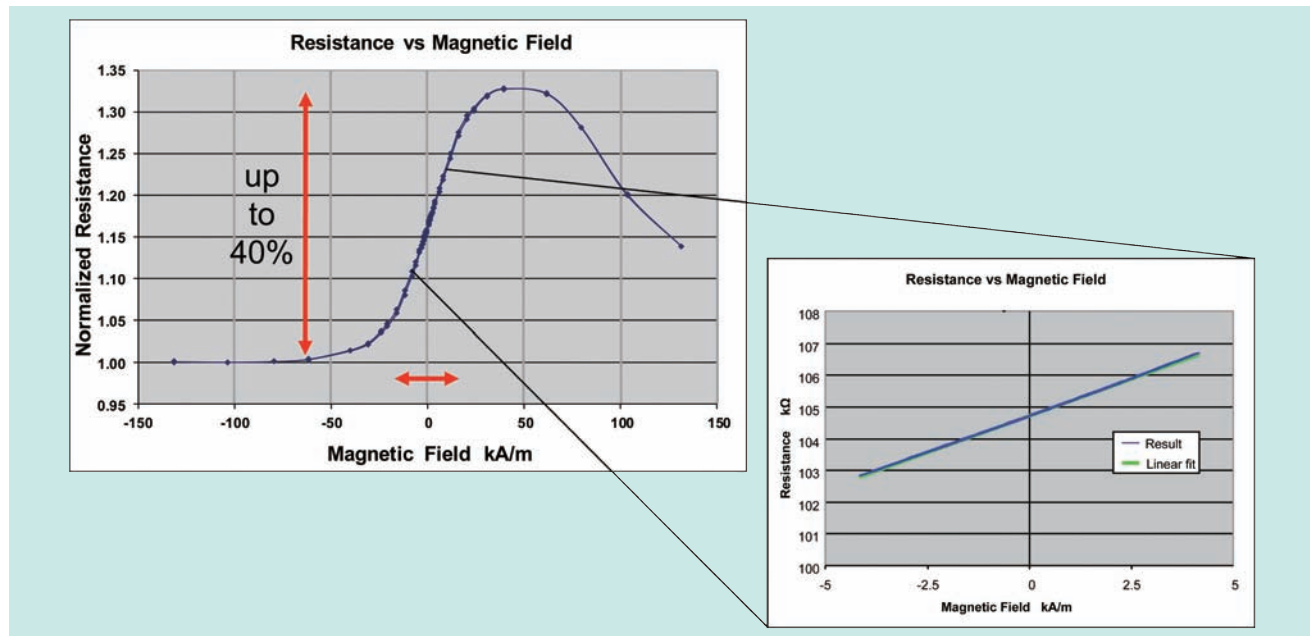


Fig. 6 Example of transfer curve for a MTJ with the following structure

## 5. State-of-the-art magnetic sensing using the TMR effect

The following discusses important properties of the sensor using the TMR effect (hereafter, “TMR Sensor”), which was developed applying this technology. The details of the structure and test results are omitted in this paper. For more information, refer to the references <sup>17) 18) 19)</sup>.

### 5.1 Basic performance

#### 1) Low power consumption

The power consumption of the TMR Sensor is 1/100th of the AMR sensors and 1/1000th of the Hall sensors <sup>19)</sup>, since the internal resistance of the MTJ element is high. Even when the peripheral signal processing circuits are considered, the power consumption is still sufficiently low which enables long operation over the system product life with small batteries or energy harvesting devices. Therefore, it is expected to be used in self-supported wireless sensors. As an example, a comparison image of the number of button cells required for six-month continuous operation is shown in Fig. 7.

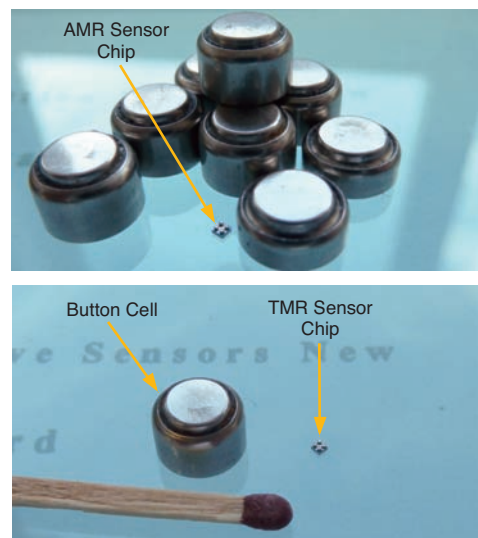


Fig. 7 Power and Cost comparison of an AMR and a TMR sensor after 6 months of continuous use

## 2) High detection accuracy

The sensor detection accuracy is determined by the combination of linearity, hysteresis property, sensitivity, and S/N ratio. The newly developed TMR sensor has the following characteristics compared to the sensors using the existing AMR/GMR/Hall devices.

The linearity of a Hall sensor for detecting high magnetic field and the hysteresis property of an AMR/GMR sensor for detecting low magnetic field are both at a very high level. However, they are not always good across all the properties because they exhibit both advantages and disadvantages. On the other hand, the TMR sensor exhibits a high level of performance across all the properties compared to other sensors, and thus, it can be used for detecting a wide range of magnetic fields. Also, it is possible to verify the position sensing accuracy by the evaluation kit discussed in the next Chapter.

When used for detection of absolute angles, the AMR sensor can only detect a range of 180° of external magnetic field, while the TMR sensor can detect a range of 360° (one full rotation). The TMR sensor can be applied to angle detection placed on the shaft end by using its superior properties of wide-range of input magnetic field strength, good linearity, and low hysteresis.

For magnetic detection sensitivity, although the performance of SQUID<sup>\*3</sup> is superior, it is proven that the 1/f noise and thermal noise of MTJ element can be reduced to the  $\ln T/\text{Hz}^{1/2}$  level. This implies realization of high space resolution and low cost for medical and non-destructive test applications<sup>20)</sup>.

## 5.2 Operating range

### 1) Wide operating temperature range

In high-temperature life test, it is confirmed that there is no atom diffusion within the MTJ element even in high temperature of over 150°C. Also, different from other sensors, the TMR sensor can be designed to increase sensitivity as the temperature rises to compensate the reduction of magnetic field in high temperature. Therefore, it can detect a magnetic field even in the high temperature range with the same air gap as in room temperature.

### 2) Wide air gap range<sup>\*4</sup>

Air gap setting for the AMR sensor for detecting wheel speed in ABS, etc., is usually set at 2 mm or even at 1 mm or less when higher resolution or accuracy is required.

The sensitivity of the TMR sensor is 10 times that of the AMR sensor and 3 times that of the GMR sensor. Its internal noise is so small that it can also be used for magnetic field measurement of geomagnetism in  $\mu\text{T}$  scale. Therefore, as shown in Fig 8, detection with maximum of 5 mm of air gap is possible, which significantly expands the freedom of design. For example, a wall of non-magnetic material such as stainless steel, aluminum, or plastic can be installed between the sensor and the ring magnet for improving dust-, oil-, or heat-resistant properties.

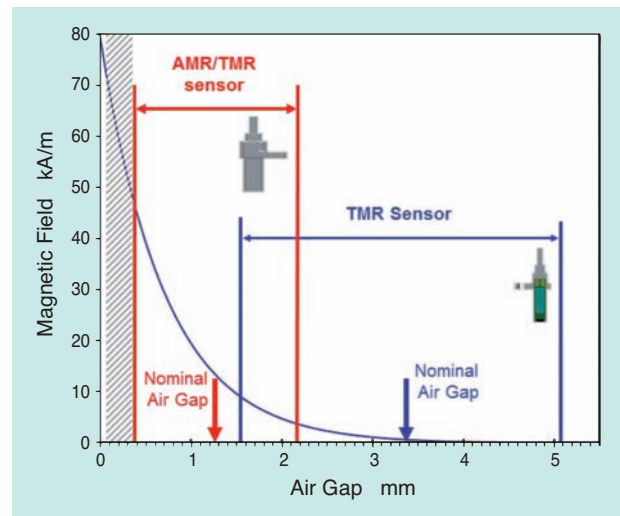


Fig. 8 Magnetic field generated by an elastoferrite pole ring as a function of the air gap

## 5.3 Freedom of design

### 1) Small size

Different from the AMR element and GMR element, the MTJ element uses electric current that flows vertically through the layers that compose the device. Therefore, it is possible to significantly reduce the area of the sensor by improving the manufacturing process such as the etching machining performance and side-etching performance. MRAM, where the recording density is the most critical parameter, can be configured with 1  $\mu\text{m}^2$  or less of area per MTJ element. On the other hand, for sensor application, it is necessary to ensure the operation by securing the minimum dimension in the bonding pad. That is also possible with about 30% less space than the AMR sensor.

### 2) Larger installation tolerance

Magnetic sensors for speed and position detection are susceptible to inaccuracy of sensor and magnet installation. When they are not properly installed, signals may not be detected or the detection accuracy may be deteriorated.

\*3 SQUID: Superconducting Quantum Interference Device

\*4 Air gap: Distance between sensor and magnetic target

The TMR sensor operates from a low magnetic field of -0.5 to 0.5 kA/m to a high magnetic field of -15 to 15 kA/m, as shown in Fig.6. It is possible to apply the most appropriate design for the application and the installation tolerance can be larger.

**5.4 Robustness**

**1) Electrostatic discharge (ESD) capability**

The MTJ element can be regarded as a capacitor with a very thin insulator of nanometer scale susceptible to high insulation breakdown risk.

However, the risk is reduced as follows:

- To increase dielectric strength voltage by improving the quality of the insulation layer
- To distribute ESD voltage per MTJ element by serially connecting multiple MTJ elements
- To reduce the risk of ESD by controlling the process of connecting the TMR sensor and signal processing circuit for quick handling, as the ESD is mostly found in the sensor packaging process.

After introducing the above measures, the testing based on the machine model after installation onto the printed wiring board revealed improvement in insulation breakdown risk.

**2) Tolerance against high magnetic field**

As shown in Fig.6, the resistance of the TMR has reversed property against the external magnetic field; therefore, the TMR sensor does not break down even when it is exposed to a strong magnetic field produced by a rare-earth magnet.

**5.5 Cost**

**1) Facility investment cost**

As previously noted, the MTJ element is made by the same manufacturing facility as the AMR/GMR elements that Sensitec owns. In other words, the TMR sensors can be manufactured by using similar process and materials as the manufacturing for the GMR elements, and any special facility investment for the volume production is not required.

**2) Cost reduction effect by TMR sensor**

The following shows the cost reduction effects:

- Sensor chips can be made smaller so that more chips can be manufactured from one wafer.
- Inexpensive ferrite magnets can be deployed instead of expensive rare-earth magnets since a very low magnetic field can be detected.
- Low power consumption drive is possible due to simplified signal processing circuit, as the resistance of the device itself is high and amplifying circuitry is not required.

**3) Cost reduction of the entire system**

In applications such as electric motors and ABS, consideration for assembly and installation of the entire system configuration including peripheral components is required, not only the sensing functionality.

When the air gap and installation tolerance is broader, such as the case of the TMR sensor, the requirement for assembly/installation can be reduced and overall reduction of manufacturing cost is achieved from a simplified assembly process.

**6. TMR sensor evaluation kit**

NTN-SNR and Sensitec created three types of evaluation kits for detection of rotation and position and are providing them to potential users for the broader use of the TMR sensor technology (Fig. 9 and 10). The configuration of the evaluation kits is shown as follows:

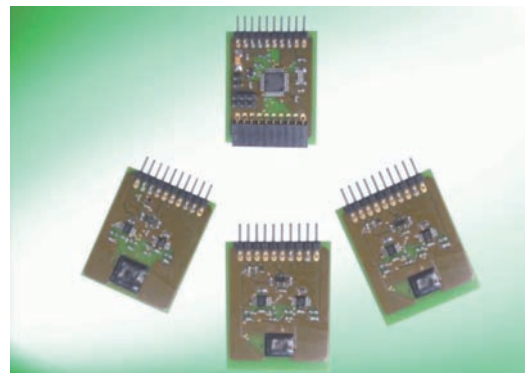


Fig. 9 TMR Evaluation PCB



Fig. 10 The three TMR Evaluation Kits

**Kit (1)****Low power consumption drive demo set**

- Sample board with TMR sensor for 360° angle detection to be placed at shaft end
- SPI communication by low-power consumption micro-computer
- Solar cell
- Magnet to be placed at shaft end

**Kit (2)****Active sensing <sup>\*5</sup> demo set**

- Sample board with TMR sensor
- High-resolution pulse output (phase A/B)
- Analog output
- Multi-pole magnet (linear and ring magnet)

**Kit (3)****Passive sensing <sup>\*6</sup> demo set**

- Sample board with TMR sensor and bias magnet
- High-resolution pulse output (phase A/B)
- Analog output
- Linear and ring gear

**7. Summary**

The TMR sensor has the following significantly superior properties and high potential as a next-generation magnetic sensor for automobile and industrial machine applications:

- **Basic performance (low power consumption/high output accuracy/high sensitivity)**
- **Operating range (high temperature/wide air gap/360° angle detection/detection of extremely low magnetic field)**
- **Freedom of design (smaller sensor size/larger installation tolerance)**
- **Robustness (ESD capability/high magnetic field tolerance)**
- **Low cost**

Taking advantage the TMR sensor and its use in many broader applications is expected, such as electronic compass, switches, non-destructive testing,

current sensors, speed sensors and position sensors, image processing equipment, and the medical field. NTN group including NTN-SNR will actively pursue further improvement and new market development of the TMR sensors.

**Reference**

- 1) P. Desbiolles, A. Friz: Development of High Resolution Sensor Element MPS40S and Dual Track Magnetic Encoder for Rotational Speed and Position Measurement, NTN TECHNICAL REVIEW, 75 (2007) 36-41.
- 2) [http://www.ntn-snr.com/industry/fr/en-en/file.cfm/MPS40S\\_datasheet\\_rev0.pdf?contentID=4826](http://www.ntn-snr.com/industry/fr/en-en/file.cfm/MPS40S_datasheet_rev0.pdf?contentID=4826)
- 3) H. Ito, T. Takahashi, P. Desbiolles, C. Peterschmitt, S. Ueno: High resolution sensor bearing with an index signal, NTN TECHNICAL REVIEW, 78 (2010)
- 4) [http://www.ntn.co.jp/english/news/news\\_files/new\\_products/news201000026.html](http://www.ntn.co.jp/english/news/news_files/new_products/news201000026.html)
- 5) C.P.O. Treutler: Magnetic sensors for automotive applications, Sensors and Actuators A91, 2-6 (2001)
- 6) M. Jullière: Tunneling between ferromagnetic films, Physics Letters, vol 54A, p225-226, 1975.
- 7) T. Miyazaki, N. Tezuka: Giant magnetic tunneling effect in Fe/Al<sub>2</sub>O<sub>3</sub>/Fe junction, Journal of Magnetism and Magnetic Materials 139, L231-L234 (1995)
- 8) J.S. Moodera, L.R. Kinder, T.M. Wong and R. Meservey: Large Magnetoresistance at Room Temperature in Ferromagnetic Thin Film Tunnel Junctions, Physical Review Letters, vol. 74, p. 3273-3276, 1995.
- 9) S. Ikeda, J. Hayakawa, Y. Ashizawa, Y. M. Lee, K. Miura, H. Hasegawa, M. Tsunoda, F. Matsukura, H. Ohno: Tunnel magnetoresistance of 604% at 300K by suppression of Ta diffusion in CoFeB/MgO/CoFeB pseudo-spin-valves annealed at high temperature, Applied Physics Letters, 93, 082508 (2008)
- 10) S. Yuasa, T. Nagahama, A. Fukushima, Y. Suzuki, K. Ando: Giant room-temperature magnetoresistance in single-crystal Fe/MgO/Fe magnetic tunnel junctions, Nature Materials, 3, p868-871, (2004)
- 11) S. S. P. Parkin, C. Kaiser, A. Panchula, P. M. Rice, B. Hughes, M. Samant, S-H Yang: Giant tunnelling magnetoresistance at room temperature with MgO (100) tunnel barriers, Nature Materials,3, p862-867 (2004)
- 12) B. N. Engel and al.: A4-Mb Toggle MRAM Based on a Novel Bit and Switching Method, IEEE Transactions on Magnetics, VOL. 41, NO. 1, p132-136, JANUARY 2005

\*5 Active sensing: A detection method with multi-pole magnet as the detection target

\*6 Passive sensing: A method, with a magnet placed behind the sensor, to detect change of magnetoresistance as a magnetic body passes through.

- 13) [www.nve.com/Downloads/AAT001.pdf](http://www.nve.com/Downloads/AAT001.pdf)
- 14) [http://cache.freescale.com/files/sensors/doc/data\\_sheet/MAG3110.pdf?pspll=1](http://cache.freescale.com/files/sensors/doc/data_sheet/MAG3110.pdf?pspll=1)
- 15) G. Malinowski, M. Hehn, S. Robert, O. Lenoble, and A. Schuhl: Magnetic origin of enhanced top exchange biasing in Py/IrMn/Py multilayers, *Phys. Rev. B* 68, 184404, 2003
- 16) G. Malinowski, M. Hehn, F. Montaigne, E. Jouguelet, and A. Schuhl: Intrinsic thermally compensated field sensor based on single magnetic tunnel junctions, *Applied Physics Letters*, 84, 1204, 2004
- 17) G. Malinowski, M. Hehn, F. Montaigne, A. Schuhl, C. Duret, R. Nantua, G. Chaumontet: Angular magnetic field sensor for automotive applications based on magnetic tunnel junctions using a current loop layout configuration, *Sensors and Actuators A*, 144, p263–266 (2008)
- 18) B. Negulescu, M. Hehn, A. Gerken, J. Paul, C. Duret: Magnetic tunnel junction linear field sensor for industrial applications, *Proc. of 10th MR Symposium*, Wetzlar, 2009
- 19) J. Paul, R. Lehndorff and C. Duret: Ressourceneffizienz am Beispiel magneto-resistiver Sensoren, *Proc. of MikroSystemTechnik Kongress*, 2011
- 20) R. Guerrero, M. Pannetier-Lecoeur, C. Fermon, S. Cardoso, R. Ferreira and P.P. Freitas: Low frequency noise in arrays of magnetic tunnel junctions connected in series and parallel, *Journal of Applied Physics*, 105, 113922 (2009)

#### Photo of authors

---



Christophe DURET  
NTN-SNR  
Research & Innovation  
Mechatronics



Shintaro UENO  
NTN-SNR  
Research & Innovation  
Mechatronics

# Long Life Technology of Grease for Journal Bearing

Takamasa TANAKA\*  
Hidenobu MIKAMI\*\*



Journal bearings are very important components of railway vehicles as they directly affect the vehicle's running stability. Sealed type double row tapered roller bearings with grease packed are traditionally used as journal bearings. The grease packed in the bearing has a tendency to move out from contact surface of raceways. Good oil providing capability of a grease to the raceways of a bearing is an important factor for the grease life.

NTN Engineering tested grease packed double row tapered roller bearings to investigate the relationship between oil separation of the grease and metal to metal contact of between bearing rollers and raceways. As a result, it was observed that bearings would be kept in good lubrication conditions by using the greases which had proper oil separation performance. This paper reports the effect of lubrication condition of rolling bearing due to oil separation of utilized the grease.

## 1. Introduction

There are typically three types of bearings used with railroad vehicles. These include bearings for the main motors used for driving the vehicles, bearings for the drive equipment used for transmission of driving power, and journal bearings to support the wheel axles. All of these bearings require a high reliability since they are directly related to the running of the vehicles. With the requirements for longer life come requirements for longer intervals between maintenance, making extending bearing life and maintaining reliability a difficult task <sup>1)</sup>.

Sealed-type double-row tapered roller bearings with grease lubrication are mainly used as journal bearings for use with railroad vehicles as longer grease life is required for longer maintenance intervals.

Improvements to such components as bearing seals and cages have helped to reduce the deterioration rate of grease in journal bearings. Since sealed-type double-row tapered roller bearings have line contact between the roller and the raceway, they require increased lubrication in comparison to ball bearings, which have point contact. Therefore, longer lubrication life through improvement of the grease itself is critical.

This paper investigates the effect of different greases' oil separation properties on journal bearing life of railroad vehicles with the intent of optimizing grease and bearing life.

## 2. Journal bearings

Under normal operation, journal bearings are installed in the journal box to support the wheel axle. While in operation, radial load from the vehicle weight, axial load from the vehicle movement, and vibration are applied to the journal bearings. While various bearing types were investigated, adopted, and used in the past, sealed-type rotating end cap tapered roller bearings (RCT), shown in Fig. 1, are the most prevalent design today.

Sealed-type rotating end cap tapered roller bearings consist of an inner ring, outer ring, rollers, cage, oil seal, slinger, back cover, etc. <sup>2)</sup> For a lubricant, a grease with a lithium soap as the thickener and mineral oil as a base oil is generally use. Grease is injected between the rollers and the cage but as the bearings rotate, grease is often pushed outward toward the (5) oil seal. Since sealed-type rotating end cap tapered roller bearings have a larger space between (3) the rollers and (5) the oil seal compared

\*Construction Machinery and Railway Engineering Department, Industrial Machinery Division

\*\*Advanced Technology R&D Center

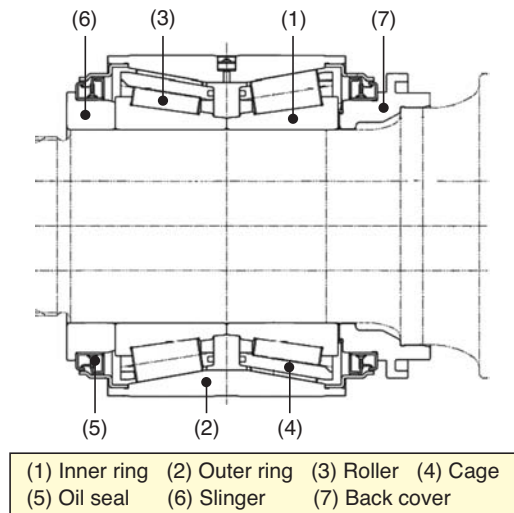


Fig. 1 RCT bearing for axleboxes

to other types of rolling bearings, it is necessary to pay attention to fluidity when selecting sealing grease. The rate of deterioration of grease in journal bearings is one important element for determining the maintenance intervals of the vehicles. The bearings are disassembled, inspected, and greased during the periodical maintenance.

So far, various measures have been taken to extend the maintenance intervals. Cages that in the past were made of steel were replaced with cages made of resin to reduce the metal abrasion powder, which can cause grease deterioration. In addition to this, low-heat generating seals were adopted to control degradation of grease due to temperature rise<sup>3)</sup>. Although these measures gradually extended the maintenance intervals, the requirement for further extension is still very high<sup>4)</sup>, requiring longer life of the grease itself.

### 3. Grease lubrication

The grease properties to be improved for long life vary depending on the use location and conditions.

Within the rolling bearings, grease itself penetrates in the rolling surface providing lubrication at the beginning of the operation; however, after some time in operation the base oil becomes the main vehicle for lubrication. Toward the end of lifecycle, seizure may be caused by shortage or deterioration of oil<sup>5)</sup>.

For cylindrical roller bearings, studies have already been conducted showing the relationship between lubrication life of bearings and oil separation property. It concluded that the optimum oil separation property would provide a longer bearing life<sup>6)</sup>.

In this paper, we investigated how the oil separation property of grease would affect lubrication of rotating end cap tapered roller bearings.

## 4. Oil separation property of grease

The oil separation property of grease varies depending on the type and amount of base oil and thickener, as well as the manufacturing method of the grease. For this test a total of 44 types of grease with various types and amounts of base oil and thickener were prepared to investigate the relationship between the grease composition and oil separation properties. For measuring oil separation properties, the following centrifugal oil separation testing method was used assuming that grease attached to the bearing cage would be separated from oil by centrifugal force.

### 4.1 Grease samples under test

Table 1 shows the composition of grease samples prepared for this test. For thickener, three types of urea compound and one type of lithium soap were selected and used with different blending amounts. For base oil, mineral oil and synthesized hydrocarbon oil were used.

Table 1 Composition of test grease

Group	M1	M2	M3	M4	S1	S2	S3	S4
Thickener	Aliphatic urea	Alicyclic urea	Aromatic urea	Li soap	Aliphatic urea	Alicyclic urea	Aromatic urea	Li soap
Amount of thickener wt%	7~13 6 combinations	7~10 4 combinations	18~30 6 combinations	9~13 6 combinations	11~24 6 combinations	17~28 6 combinations	22~41 6 combinations	16~34 4 combinations
Base oil	Mineral oil				Synthesized hydrocarbon oil			
Viscosity of base oil mm <sup>2</sup> /s (40°C)	100				46			

### 4.2 Centrifugal oil separation test

The oil separation property of the grease samples was investigated using the centrifugal separator. After rotating the centrifugal tube with 1.0 ± 0.1 g of grease sample under 3.9 × 10<sup>4</sup> G for 1 h, the weight of the separated oil within the centrifugal tube was measured, as shown in Fig.2. The centrifugal oil separation ratio was calculated as the ratio of the weight of separated oil against original grease using the following equation (1).

$$\text{Centrifugal oil separation ratio (\%)} = \frac{\text{Amount of separated oil in the test (g)}}{\text{Original amount of grease (g)}} \times 100 \dots \dots (1)$$

Fig. 3 and 4 show the measurement results as the centrifugal oil separation ratio. The centrifugal oil separation ratio decreases when the thickener is increased in any grease sample. When compared with the same amount of thickener, the centrifugal oil separation ratio varies depending on the type of thickener or base oil.

With mineral oil as base oil, as shown in Fig. 3, when aromatic urea (M3) is used as thickener, centrifugal oil separation ratio tended to be higher; however, no significant difference was observed among thickeners other than aromatic urea. When synthesized hydrocarbon oil was used as base oil, as shown in Fig. 4, the centrifugal oil separation ratio tended to be higher than when compared the cases where mineral oil was used as base oil. When aromatic urea was used as thickener, the centrifugal oil separation ratio tended to be higher too.

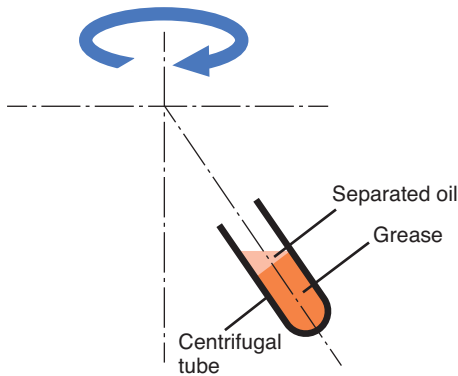


Fig. 2 Schematic diagram of centrifugal oil separation test

As a result, it is determined that the type and blending ratio of thickener as well as the type of base oil affect the centrifugal oil separation ratio.

## 5. Grease endurance test using rolling bearings

### 5.1 Test method

Five types of grease with different centrifugal oil separation ratio, M1-12% (expressed in group-amount of thickener), S2-17%, S3-22%, S4-16%, and S4-31% were sealed between the cage and inner ring of roller bearings. For this endurance test, 20g of grease was used in each bearing. Fig. 5 shows the overview of the test equipment and Table 2 shows the test

Table 2 Endurance test condition

Bearing	Tapered roller bearing ( $\phi 70 \times \phi 110 \times 31$ )
Number of bearings	Two (back to back)
Radial load (per 2 bearings)	10.78kN
Rotational speed	3000min <sup>-1</sup>
Temperature	Room temperature
Test duration	2000–10000 h

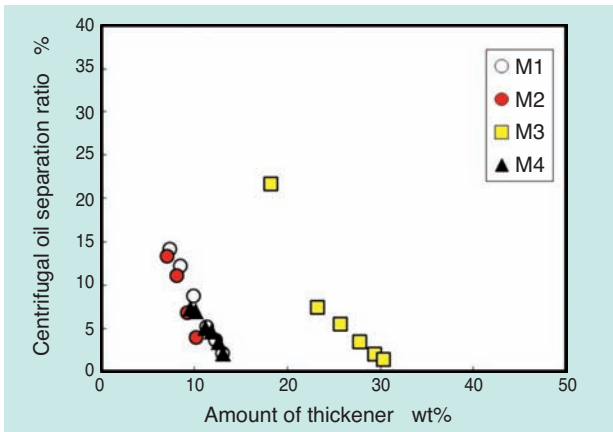


Fig. 3 Oil separation of test grease (M1 to M4)

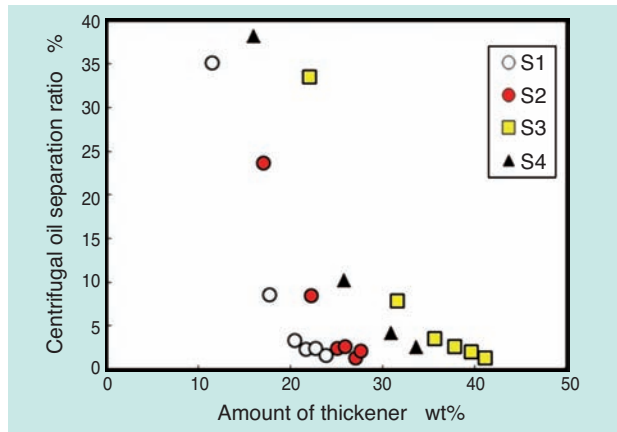


Fig. 4 Oil separation of test grease (S1 to S4)

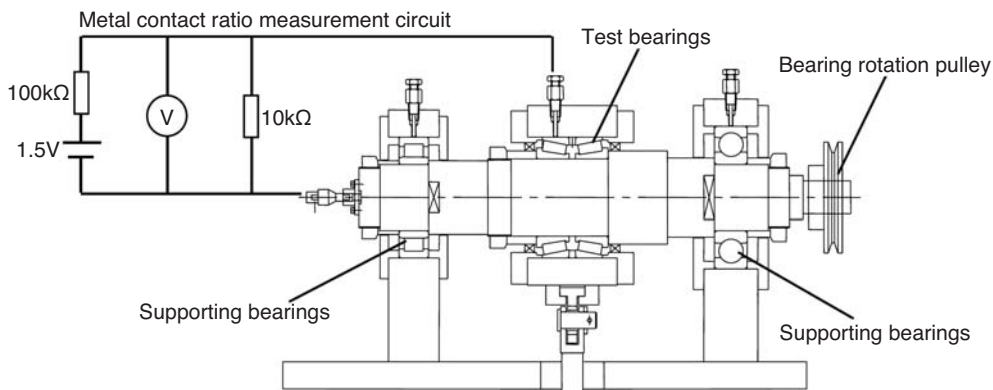


Fig. 5 Endurance test equipment

conditions. For bearings under test, two units of rotating end cap tapered roller bearings ( $\phi 70 \times \phi 110 \times 31$ ) were used. The bearings were rotated at a speed of  $3000 \text{ min}^{-1}$  with an applied radial load of 10.78 kN. During the test, the metal contact ratio between the inner and outer rings of the rolling bearings was measured using the electric resistance method. The test equipment was stopped after a predetermined duration and the oil reduction ratio of the grease measured. The calculation method of metal contact ratio and the oil reduction is shown in equations (2) and (3), respectively.

$$\text{Metal contact ratio (\%)} = \frac{\text{Voltage when insulated (V)} - \text{Voltage under operation (V)}}{\text{Voltage when insulated (V)}} \times 100 \dots (2)$$

$$\text{Oil reduction ratio (\%)} = \left( 1 - \frac{\text{Amount of thickener in the grease after operation (\%)}}{\text{Initial amount of thickener in grease (\%)}} \right) \times 100 \dots (3)$$

### 5.2 Status change of the grease after test

Fig. 6 shows the behavior of S4-16% grease during the endurance test. At the beginning of the operation, 100% of grease is inside the bearings. Some grease moves to the sealed area as the bearings start to operate (shown in Fig. 7). It was observed that the grease mostly remained after 2000 h of operation.

Fig. 8 shows the oil reduction ratio of the grease remaining inside the bearings and the grease attached to the sealed area. Since the oil reduction ratio of the grease remaining inside the bearings continues to increase after 2000 h, it is understood that the lubrication of the raceways is maintained using only the oil separated from the grease that remained inside the bearings.

Fig. 9 shows the relationship between the oil reduction ratio of the grease inside the bearings and the centrifugal oil separation ratio. There is an exponential correlation between the two. The oil separation of the grease inside the bearings in this test is assumed to be caused by the centrifugal force.

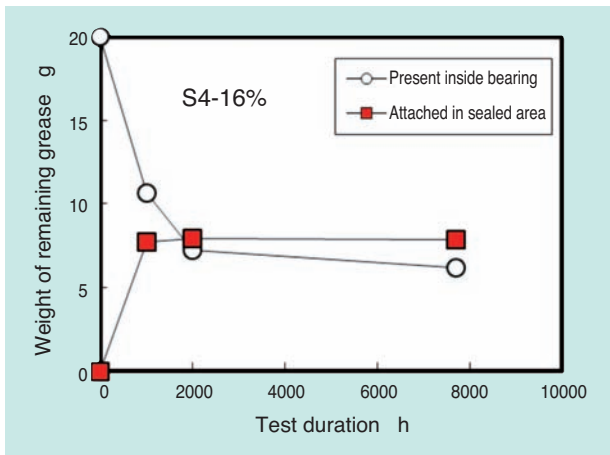


Fig. 6 Change of grease amount by test duration

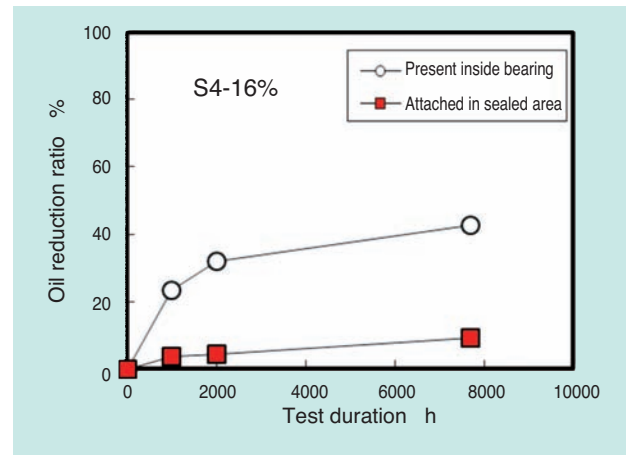


Fig. 8 Relationship between test duration and oil reduction

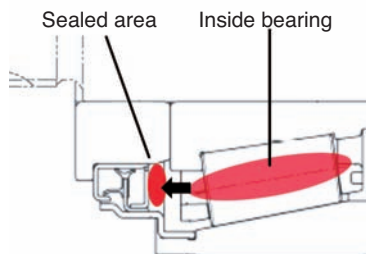


Fig. 7 Transfer state of grease in operation

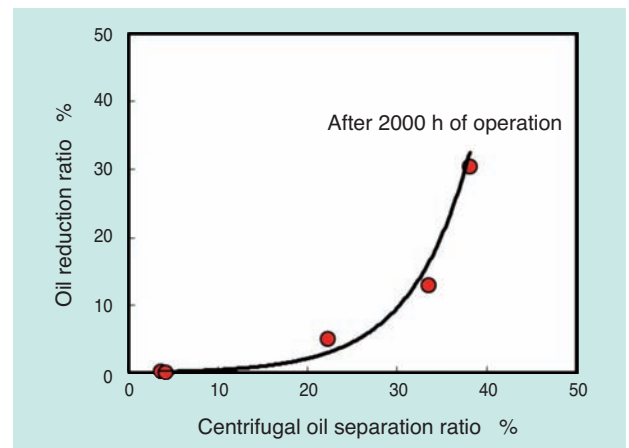
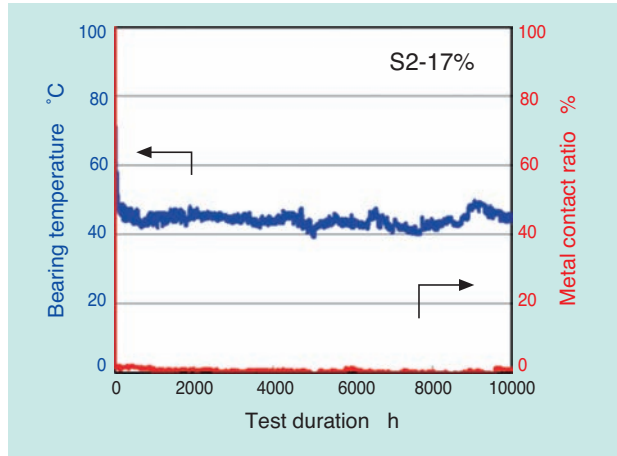


Fig. 9 Reduction rate of bearing inside grease after test

**5.3 Oil reduction ratio of the grease after test**

Fig. 10 to 14 show the temperature of the outer ring of the bearings and metal contact ratio between the inner/outer rings measured for the bearings with the five types of grease. S4-16% grease shown in Fig. 10 became unstable by both metal contact ratio and bearing temperature specifications after 3000 h of test. M1-12% grease in Fig. 11 and S4-31% grease in Fig. 14 had high metal contact ratio and bearing temperature from the beginning; therefore, the tests were terminated in 2000 h and 5000 h, respectively. In contrast, S2-17% grease in Fig. 12 and S3-22% grease in Fig. 13 were stable over 7500 h of operation.



**Fig. 12** Bearing temperature and metal contact ratio (S2-17%)

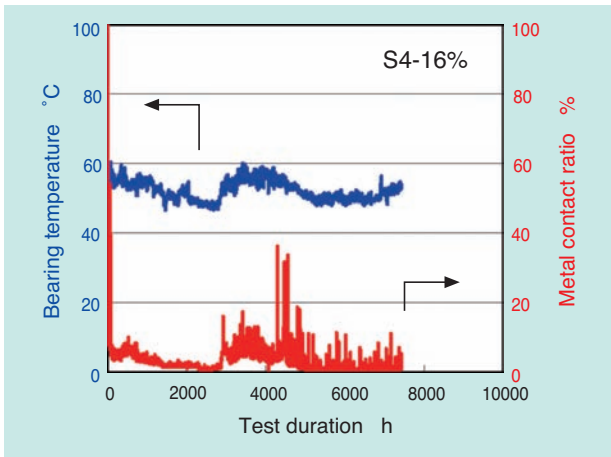


**Fig. 10** Bearing temperature and metal contact ratio (S4-16%)

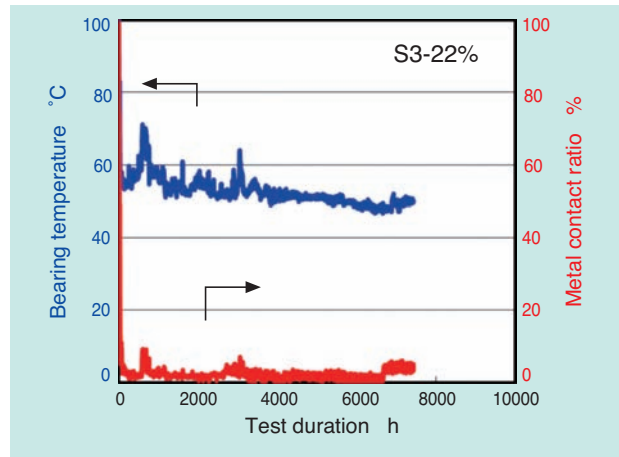


**Fig. 13** Bearing temperature and metal contact ratio (S3-22%)

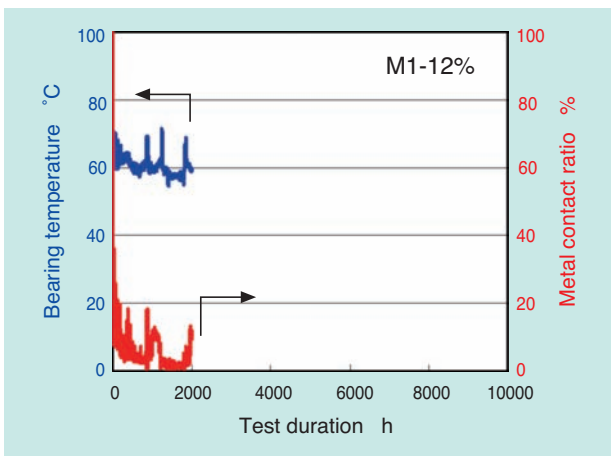


**Fig. 11** Bearing temperature and metal contact ratio (M1-12%)

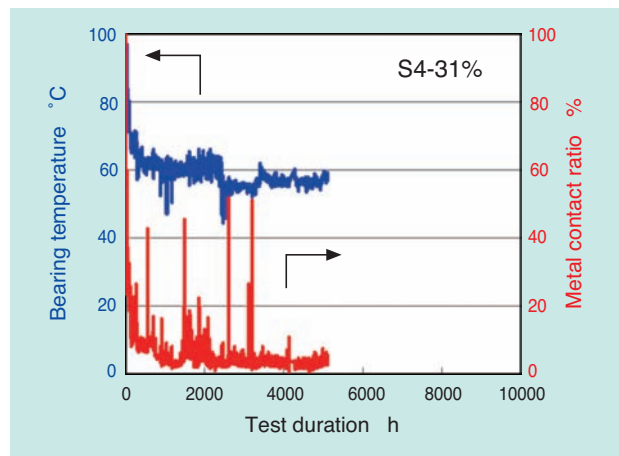


**Fig. 14** Bearing temperature and metal contact ratio (S4-31%)

**Table 3** summarizes the relationship between the centrifugal oil separation ratio and lubrication status measured as the metal contact ratio during the bearing endurance test. It was observed that the greases with a high or extremely low centrifugal oil separation ratio caused unstable bearing lubrication when used in tapered roller bearings under these operating conditions.

Grease with a high centrifugal oil separation ratio delivers a large amount of lubrication oil to the raceway early in terms of the life of the grease. It is assumed that this lubrication oil is depleted after some operation causing ill lubrication for longer term operating. Grease with an extremely low centrifugal oil separation ratio does not sufficiently deliver lubrication oil to the raceway; therefore, the lubrication is not good from the beginning of operation.

On the other hand, it is assumed that grease with the appropriate centrifugal oil separation ratio continues to deliver lubrication oil to the raceway throughout the operation, without depletion, maintaining a good lubrication state for a long time.

**Table 3** Centrifugal separation ratio and metal contact ratio of grease

Grease code	Centrifugal oil separation ratio wt%	Metal contact ratio during bearing operation
S4-16	38.0	△
S3-22	34.0	○
S2-17	22.0	◎
S4-31	4.2	×
M1-12	3.6	×

◎ ○ △ ×  
 Better ← → Worse  
 Judgment (metal contact ratio)

## 6. Conclusion

The impact that the oil separation property of grease on lubrication of bearings was investigated by testing and comparing the durability of tapered roller bearings with grease types of different oil separation properties. The study was completed with the purpose of pursuing grease with long life for journal bearings of railroad vehicles. The following findings were obtained:

- 1) Grease with a centrifugal oil separation ratio close to 40% shows good lubrication at the beginning; however, the lubrication performance degrades as the operation continues for a longer time.
- 2) Grease with an extremely low centrifugal oil separation ratio of 5% or less has low oil delivery capability; therefore, the state of lubrication is not good from the beginning.

- 3) Greases with centrifugal oil separation ratio of 20–35% show good lubrication for long periods time.
- 4) For improving the grease life of tapered roller bearings used in wheel axles, controlling the oil separation property of the utilized grease is one of the important factors.

We have studied the grease composition that contributes to extending life of journal bearings for railroad vehicles considering that the centrifugal oil separation property is one of the important factors for extending grease life for journal bearings. Based on the findings obtained in this study, we would like to conduct tests under closer operating conditions to the actual vehicles to verify the grease composition of appropriate oil separation properties in an effort to contribute to longer life and reliability improvement for journal bearings of railroad vehicles.

## Reference

- 1) Tsuyoshi Ichiki: Technology Standard and Maintenance Technology; New Vehicle Maintenance System for JR East Japan Railway, Rolling Stock and Technology No. 79 (2002) 6-11
- 2) Kosoku Sharyoyou Rinjiku Kennkyu Iinnkai: Tetsudo Rinjiku, Maruzen, 175-179
- 3) Ryutaro Oka: Development of New RCT Bearing for Axleboxes and Insulated Bearing with Shields, NTN TECHNICAL REVIEW No. 74 (2006) 80-85.
- 4) Japan Railway Engineers' Association: the Railway systems of Japan Coming after 20 Years, 213-221.
- 5) Japanese Society of Tribologists, Grease Technical Committee, "Lubrication Grease: Basics and Applications", Yokendo, 82-83.
- 6) Shigeki Komatsuzaki: 48th Tribology Advanced Course, Lubricant and Tribology, (1993).

## Photo of authors



Takamasa TANAKA  
 Railway Engineering  
 Department,  
 Industrial Machinery Division



Hidenobu MIKAMI  
 Advanced Technology  
 R&D Center

# Market Trend and High-Functionality of Wheel Bearings for Off-Highway Truck



Kenichiro NAITO\*  
Naota YAMAMOTO\*\*  
Katsunori SONE\*\*

Off-Highway Trucks are generally used in very severe mining conditions operating 24 hour duty cycles in natural environment with dust and contamination. In order to satisfy such market needs,

NTN developed high functionality of wheel bearing which is one of the major parts of the truck. In this paper, NTN new product features and specifications are introduced.

## 1. Introduction

Off-Highway Trucks in mines are generally used under very severe conditions of continuous operation for 24 hours per day., in dusty natural environment of sand and particles. In addition, “productivity/high efficiency,” is valued by the transported loads per hour; “durability/reliability” by supporting this productivity for a long period of time and “safety/comfort” for the workers is also required.

In order to address these market needs, NTN has developed new products shown in Fig. 1 with high-functionality for wheel bearings, which are the critical components of these trucks and is actively proposing them to the market. In this paper, we will discuss (1) Filter seal integrated large-sized bearings, (2) IC tag integrated bearing, and (3) Integrated rotation sensor large-sized bearing, which were developed by NTN.

## 2. Filter seal integrated large-sized bearing

Wheel bearings for off-highway trucks require special measures against severe operating environment and improved reliability in addition to long life and maintenance-free operation. However, damage due to denting on the bearing raceways caused by contamination from dust and particles into lubricant and metal abrasion powder from the gears around bearings is very common in only a short time of operation.

Filter seal integrated large-sized bearing developed by NTN (Fig. 2) does not allow foreign objects in the lubricant to enter into bearings, thus resulting in longer life; therefore, it is expected that the intervals for replacing the bearings will be extended. The following are the features and test results of these bearings.

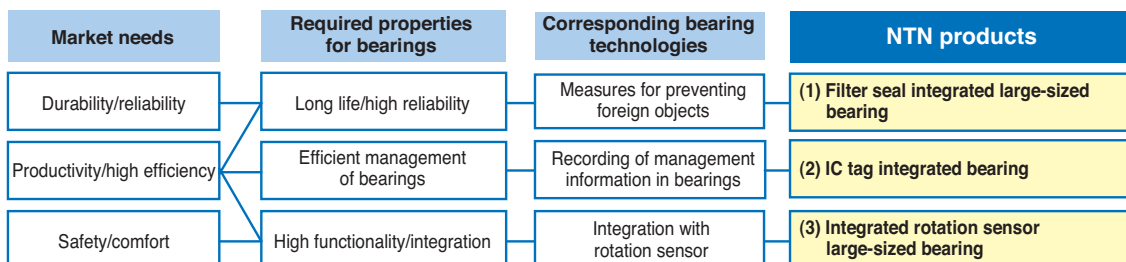


Fig. 1 Market needs for wheel bearings and NTN new products

\*Construction Machinery and Railway Engineering Department, Industrial Machinery Division

\*\*New Energy Engineering Department, Industrial Machinery Division

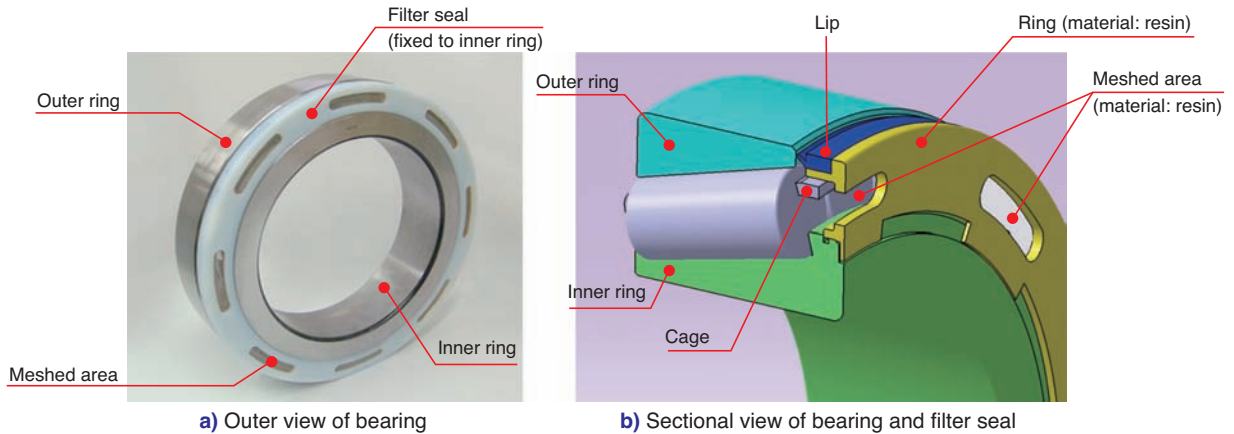


Fig. 2 Filter seal integrated large size bearing (Tapered roller bearing)

## 2.1 Features

### (1) Extending bearing replacing cycles

Denting on the bearing raceways can be prevented by the filter seal equipped with mesh that prevents foreign objects in the oil from entering into the bearings without blocking the flow of lubricant oil.

### (2) Compact design

Existing bearings can be replaced as the filter seal is attached without changing key dimensions (inner diameter/outer diameter/width) of the bearings.

### (3) Operable under vibration

They can be used with vibration acceleration of 10 G.

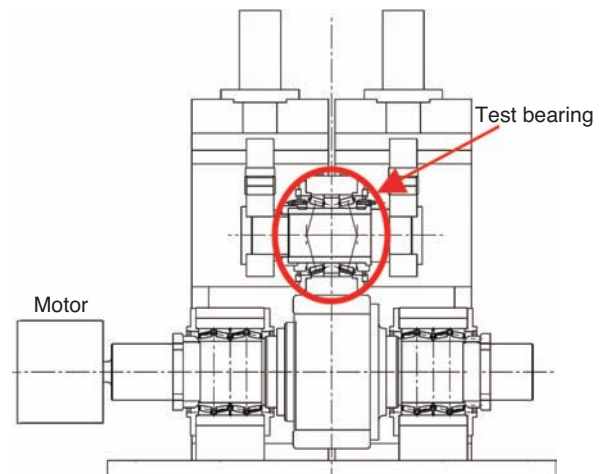


Fig. 3 NTN outer ring rotational test machine for large size bearings

## 2.2 Rotational test under the condition of foreign objects in the lubricant

### <Test condition>

Test machine: NTN outer ring rotational test machine for large-sized bearings (Fig. 3)

Bearings under test: Tapered roller inch bearings, back-to-back combination

Rotational speed: 50 min<sup>-1</sup>

Lubricant oil: Diesel engine oil ISO VG100

Foreign objects (Fig. 4): Size: max. 0.7 mm

Hardness: HRC 56 to 60

Amount: 2000 mg/L

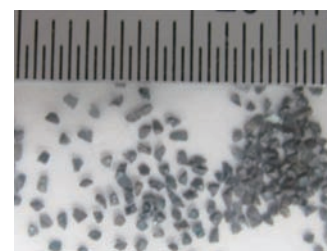


Fig. 4 Metal particle

### <Test results>

The control effect of denting by the filter seal was confirmed by observing dents on the inner ring raceway after the test, as shown in Fig. 5. As a result, no dents were observed on the inner ring raceway when the filter seal was attached. Thus, it was confirmed that the foreign objects were blocked.

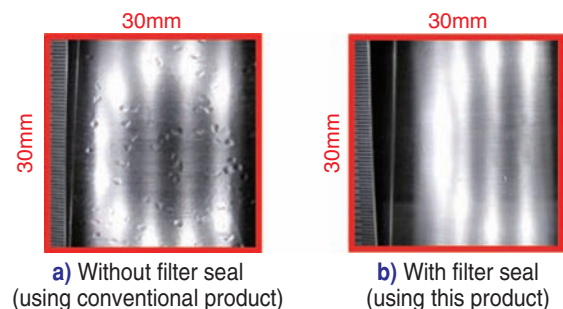


Fig. 5 Inner ring raceway after rotation test with metal particle

**2.3 Summary**

Filter seal integrated large-sized bearing blocks foreign objects in the lubricant oil entering into the bearing, and therefore, it is expected that the actual life of the bearing will be extended.

**3. IC tag integrated bearings**

Off-highway trucks are periodically inspected and repaired. For critical components such as bearings, maintenance records such as inspection date and operating hours are managed and kept. As bearings are used for a long time it is challenging to simplify the management and to secure inspection records against loss. Thus, management by IC tags (RFID: Radio Frequency Identification) was seen with high expectation. However, the existing IC tags do not allow reading or writing while embedded in metal and use of non-magnetic material for enabling read/write operation makes the tag size too large; therefore, IC tags have not been practical.

NTN has developed IC tag integrated bearings so that the quality information and operation history can be directly recorded on the bearings (Fig. 6). It is possible to read/write information on IC tag embedded directly in the bearings and to set management information for each user. In addition, bearing quality information including inspection records can be confirmed. The features, specifications, and the examples of usage are discussed in the following:



Fig. 6 IC Tag integrated bearing

**3.1 Features**

**(1) Quality information can be read directly from the actual bearings**

Quality information of the bearings at factory shipment such as accuracy of dimension for inner diameter, outer diameter and width, space information, and serial number can be read out.

**(2) Operating history of the bearings can be written and read out by the users**

The inspection information can be directly written/read from the bearings.

**(3) Management items can be freely set**

Management items can be set according to the users' needs.

**3.2 Specifications**

Tables 1 and 2 show the specifications of the IC tag and the reader/writer and Fig. 7 and 8 show their appearance.

Table 1 Specification of IC Tag

Item	Specification
Memory capacity	112 bytes
Carrier frequency	13.56 MHz
Compliance standard	ISO 15693
Transmission distance	Within 2 mm
Maximum operating temperature	120°C
Dimension	φ 4.5 × 4 mm

Table 2 Specification of reader and writer (PDA\*1 type)

Item	Specification
Carrier frequency	13.56 MHz
Compliance standard	ISO 15693
Operating temperature range	-10~50°C
Dimension	79 × 164 × 25 mm
Weight	320 g

\*1: PDA: Personal Digital Assistant

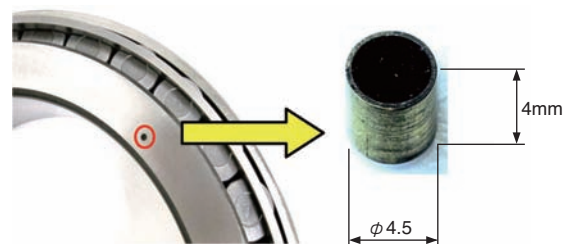


Fig. 7 IC Tag (Embed in bearing side face)

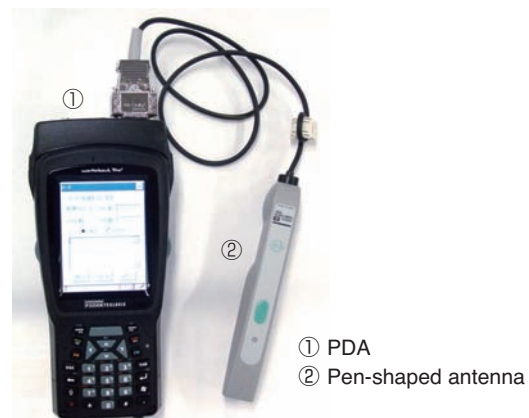


Fig. 8 Reader and Writer (PDA Type)

### 3.3 Examples of usage

- (1) Read the bearing data from the factory shipment and compare it with the user data at periodical inspections.
- (2) Periodically write the bearing management information and manage the change of the recorded data.
- (3) Store the bearing history data as electronic data on a PC and manage all the information related to the bearings of the entire machine.

#### ■ Examples of management items

1. Bearing quality information

**Fig. 9** shows an example of data that NTN records at the factory shipment.

2. User management information

**Fig. 10** shows an example of data that users can write, in addition, for the maintenance.

### 3.4 Summary

IC tag integrated bearings allow necessary information to be read/written directly from the bearings; therefore, the management of information can be simplified even in operating conditions where long-time reliability is required.

**Fig. 9** Example of input bearing quality information

**Fig. 10** Example of input user management information

## 4. Integrated rotation sensor large-sized bearing

As the off-highway trucks are driven on unpaved roads in the mines, slippage of wheels may cause accidents. As a countermeasure to avoid slippage trucks are equipped with , anti-lock brakes and traction control systems. These systems detect the rotation of the wheels to control them. The wheel rotation detection sensors are usually installed separately from the wheel bearings. In order to accurately detect the rotation speed, position adjustment is required for associated rotation sensor components.

NTN has developed an integrated rotation sensor large-sized bearing with a pulse detection sensor on the stationary inner ring, and a pulsar ring on the rotating outer ring, (**Fig. 11**).

By integrating the rotation sensor and bearings, sensor positioning adjustment is not required and the number of components is reduced. In addition, a disconnection prevention mechanism is adopted for sensor wiring so that even when slippage occurs between the axle and bearing inner ring(, called creep), rotational speed or direction can be detected without causing damage or errors to the sensor. The following are the features and specifications of an integrated rotation sensor large-sized bearing:

#### 4.1 Features

##### (1) Integration of rotational sensor and bearings

Reduced installation work, reduced number of components, and reduced size of peripherals.

##### (2) Mechanism of preventing disconnection of wiring even if creep (slippage) occurs between the axle and inner ring is adopted

Rotation speed can be detected even when the creep occurs at the inner ring.

##### (3) Operable in oil

No errors for rotational speed detection when immersed in the engine oil (oil temperature  $120^{\circ}\text{C} \times 2000 \text{ h}$ ) \*2

\*2: May be affected depending on the oil or additive types.

##### (4) Usable under vibration

No errors in rotational speed detection under vibration acceleration of 10 G.

#### 4.2 Structure

**Fig. 11** shows an example of the structure of tapered roller bearings used in rotational outer ring.

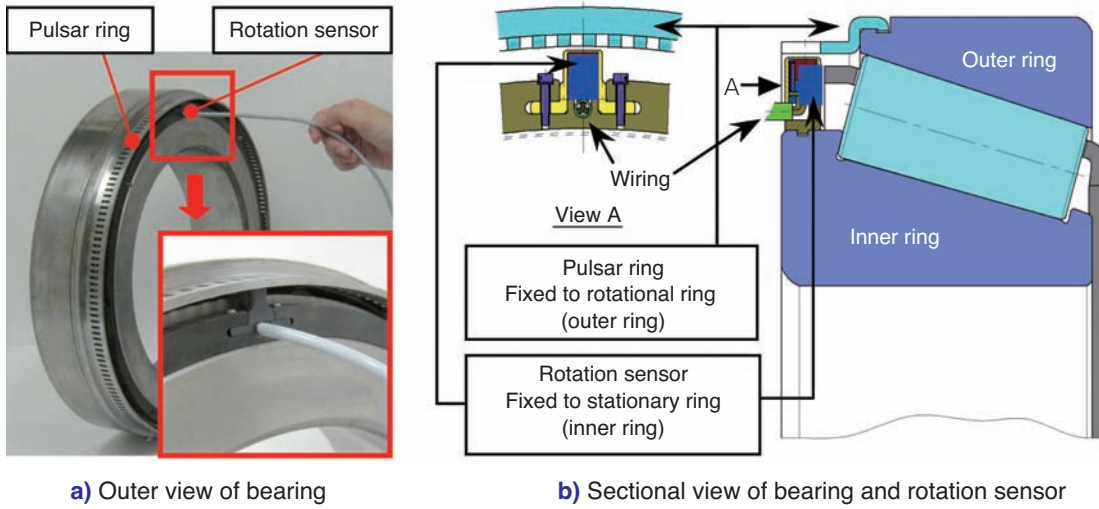


Fig. 11 Integrated rotation sensor large size bearing

### 4.3 Specification of a rotational sensor and an example of output

Table 3 shows the specification of a rotational sensor and Fig. 12 shows an example of output waveform.

Table 3 Specification of rotation sensor

Item	Specification
Sensor type	Back magnet type Hall IC
Resolution	192 pulses/rotation *3
Output phases	Single phase *4
Supply voltage	4~24V (DC)
Output waveform	Open collector (square wave)
Response frequency	12 kHz
Sink current	25 mA or less
Maximum operating temperature	120°C

\*3: Resolution when bearing outer diameter is  $\phi$  420

\*4: Two-phase output when detection specification is on the rotational direction

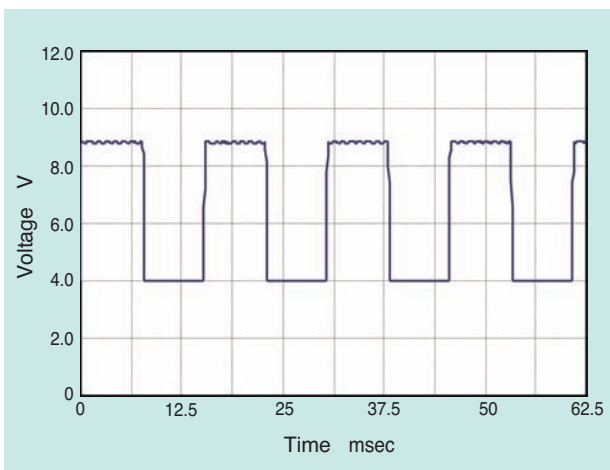


Fig. 12 Example of output style

### 4.4 Summary

Integrated rotation sensor large-sized bearing does not require position adjustment associated with assembly of sensor components, as the bearing and the sensor are integrated. This brings a reduced number of components and promises cost reduction.

## 5. Conclusion

In this paper, three new products that NTN developed are discussed as the high-functionality version of wheel bearings for off-highway trucks used in mines.

The demand for mineral resources continues to expand against a backdrop of population growth and urbanization in the emerging countries, and the mining development is expected to continue in the future.

NTN will continue developing products that respond to the requirements of productivity, reliability, and safety for mining machines such as off-highway trucks.

### Photo of authors



Kenichiro NAITO  
Railway Engineering  
Department,  
Industrial Machinery Division



Naota YAMAMOTO  
Railway Engineering  
Department,  
Industrial Machinery Division



Katsunori SONE  
New Energy Engineering  
Department,  
Industrial Machinery Division

## Multi Layer BEARPHITE



Yosuke SUGAI\*  
Toshihiko MOURI\*

Bearing for the joints of hydraulic excavator, are used under heavy load condition cases such as vibration and shock. Therefore it is necessary to ensure wear-resistance and endurance for the bearing. Generally bearings which are made from iron metal bush or are oil-impregnated and sintered are used, which have high cost.

NTN developed the “Multi-layer oil-impregnated sintered bearing (**Multi Layer BEARPHITE**)” by using a production method which consists of using different materials on the inner and outer side to maintain a balance between performance and cost.

### 1. Introduction

Oil-impregnated sintered bearings are usually used for light load application such as for small motors; however, for special purposes they can be used as heavy load slide bearings for the joints of hydraulic excavator as shown in **Fig. 1**. These bearings use a highly hardened and durable material, which is strengthened by carburized-hardening heat treatment process, etc., and then cut for precise dimension. They are more expensive than the bearings for light load applications, which are made by press forming, sintering, and sizing treatment.

In order to solve this problem for the two types of applications, NTN has developed the “two-color molding” method, which forms a single piece unit consisting of different materials for the inner layer and outer layer of the unit, and marketed as the “multi-layer oil-impregnated sintered bearings (Multi Layer BEARPHITE)” using a highly hardened and durable material for the inner layer of the bearings and regular high-strength structural material for the outer layer.

### 2. Conventional bearings

The conventional bearing material mixes 15% to 20% of Cu to prevent galling with the axle as well as Mo and Ni to obtain strength through heat treatment. As shown in the left column of **Fig. 2**, conventional

bearings secure surface strength by carburized hardening. Therefore, all the bearings become hard, which prevents from applying sizing work that is used by sintered bearings for correcting the dimension. Therefore, the precise dimension is secured by cutting after the heat treatment.

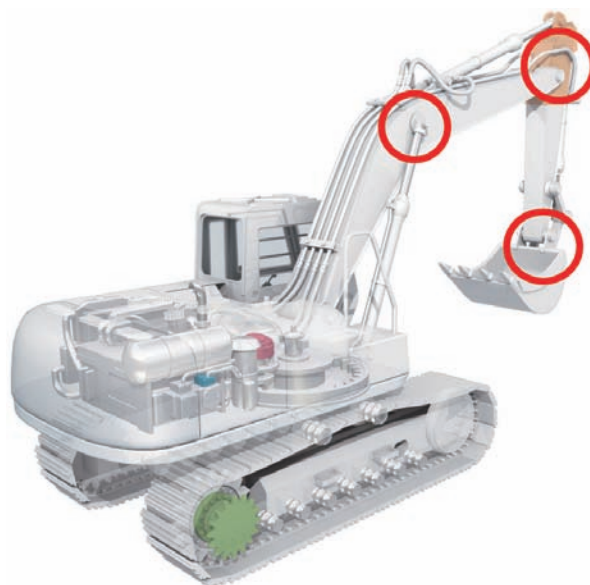


**Fig. 1** Oil-impregnated sintered bearing for hydraulic excavator

\*Engineering Department, NTN Powder Metal Corp.

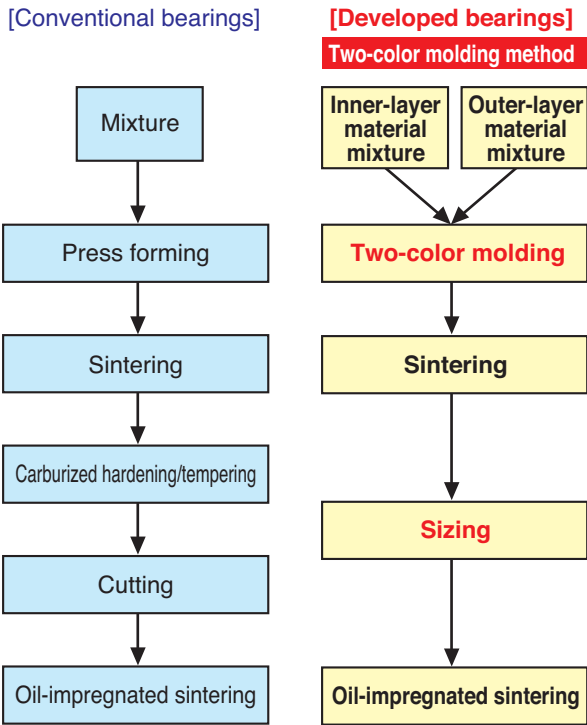


Fig. 2 Manufacturing process



Fig. 3 View of bearing

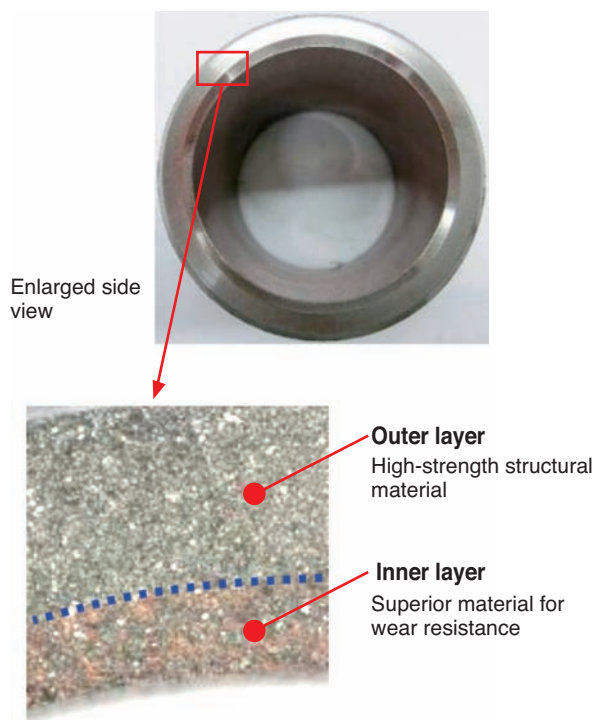


Fig. 4 View of multi-layer area

### 3. Developed bearings

#### 3.1 Structure and features

Fig. 3 shows the appearance of “multi-layer oil-impregnated sintered bearings,” Fig. 4 shows the enlarged view of the boundary between the inner layer and outer layer, and Table 1 shows the chemical composition. For inner-layer materials that compose the inner diameter surface, regular material is mixed with Cu, Mo, and Ni for strength, wear resistance and durability. In addition, for the outer layer, material equivalent to JIS-SMF4030 is used, which generally is used for machine structural components with high strength and is workable for sizing.

The right column in Fig. 2 shows the manufacturing process. Since high-strength structural material was adopted for the outer layer, no carburized hardening was required and the correction of dimension through sizing work was adopted.

The following displays the features:

#### [Features]

- Low hardness material was used for the outer layer enabling correction of dimension by sizing work
- Same material as the conventional bearings was used for the inner layer securing high sliding performance

Table 1 Chemical composition

	Composition	Mixed ratio wt%
Inner layer (inner cylindrical surface)	Cu	15~20
	Fe	Remainder
	C	0.3~0.8
	Ni	1.5~3.5
	Mo	0.5~1.5
Outer layer (outer cylindrical surface)	Cu	2~5
	Fe	Remainder
	C	0.2~0.8

### 3.2 Bonding status of inner/outer layer boundary

Fig. 5 and 6 show the concentration distribution of Fe and Ni at the inner/outer-layer boundary of the bearings made by the two-color molding method.

Fe is uniformly distributed in both inner and outer layers without segregation. Ni, which is only mixed in the inner layer, gradually changes the concentration from the boundary toward inside the outer layer, indicating that Ni is spread to the outer layer as a result of the bonding at the boundary.

### 3.3 Accuracy of dimension

In order to verify the correction effect of dimension of the developed bearings by sizing work, the dimension of the sintered product before and after sizing was measured. The results are shown in Tables 2 and 3.

The diameter variation after sizing is smaller than before sizing for both the inner and outer diameters indicating that the dimension accuracy has improved. On the other hand, no dimension correction was possible with the conventional bearings.

#### [Measurement condition]

Dimension of bearings: inner diameter 35 × outer diameter 45 × length 35

Measurement values: inner/outer diameter variation (max. – min. value of diameter)

### 3.4 Strength/hardness

Radial crushing strength and hardness of the

developed bearings are shown in Table 4. Both inner cylindrical surface and outer cylindrical surface of bearings were measured for hardness.

Radial crushing strength was equivalent to that of the conventional bearings, and hardness of inner cylindrical surface was equivalent to that of the conventional bearings. On the other hand, hardness of the outer cylindrical surface was lower and is appropriate for dimension correction by sizing work.

Table 2 Diameter difference of inner diameter

Test item	Diameter variation mm	
	Before sizing	After sizing
Developed bearings	0.025	0.015
Conventional bearings	0.200	Sizing not available

Table 3 Diameter difference of outer diameter

Test item	Diameter variation mm	
	Before sizing	After sizing
Developed bearings	0.060	0.030
Conventional bearings	0.200	Sizing not available

Table 4 Strength and hardness measurements

Test item	Measured item	Radial crushing strength MPa	Hardness HRA
Developed bearings		540	Inner layer 54 Outer layer 46
Conventional bearings		550	54

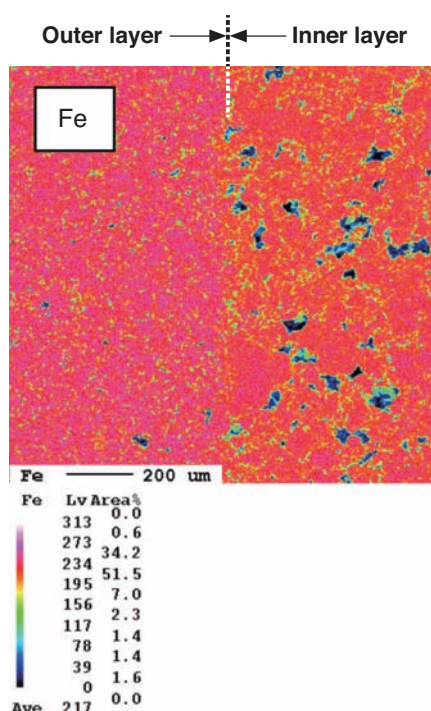


Fig. 5 Fe concentration distribution of surfactant

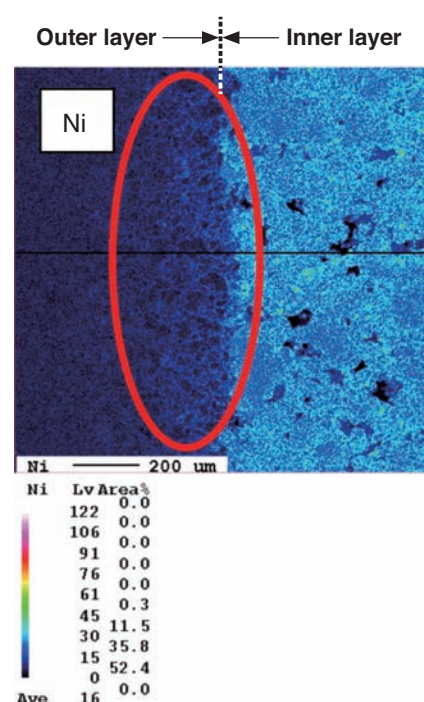


Fig. 6 Ni concentration distribution of surfactant

**[Measurement condition]**

Dimension of bearings: inner diameter 35 × outer diameter 45 × length 35  
 Measurement of radial crushing strength: ring compression rate 10 mm/min.  
 Measurement of hardness: inner/outer cylindrical surface of bearings HRA

**3.5 Friction property**

The friction coefficient of the developed bearings was equivalent to that of the conventional bearings (Fig. 7).

**[Measurement condition]**

Pressure on friction surface: 100 MPa  
 Atmosphere temperature: 70°C  
 Slide velocity: 0.014 m/s  
 Dimension of bearings: inner diameter 6 × outer diameter 12 × length 4  
 Mating cylinder material: S45C induction hardened material

**4. Summary**

“Multi-layer oil-impregnated sintered bearings” using “two-color molding” method, which forms different materials into one piece, is discussed.

Since it exhibits different properties in one bearing unit, this forming technology is expected to contribute to high functionality and low cost of not only joints of hydraulic excavators but also many bearings and machine components in different sectors of industrial machines and automobiles.

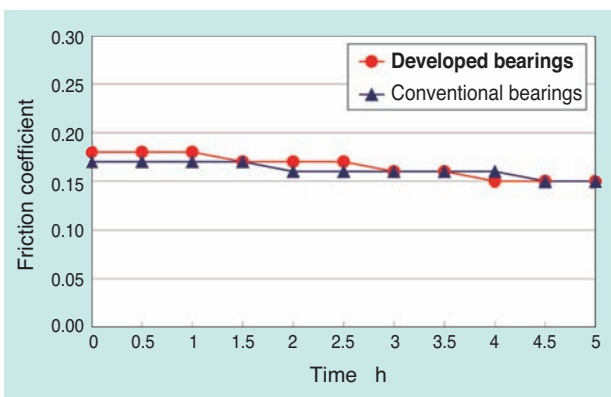


**Fig. 7** Friction coefficient measurements

Photo of authors



Yosuke SUGAI  
 Engineering Department,  
 NTN Powder Metal Corp.



Toshihiko MOURI  
 Engineering Department,  
 NTN Powder Metal Corp.

## Introduction of Magnetic Material Products



Takuji HARANO\*  
Shinji MIYAZAKI\*  
Hajime KATSUURA\*

**Nippon Kagaku Yakin Co., Ltd.**, as one of the NTN group companies, develops various types of magnetic material products that meet customer demand for characteristics.

The major product is the Amorphous core which has characteristics of high saturated magnetic flux-density, low core loss and superior frequency characteristics.

This article introduces the features and applications of these products.

### 1. Introduction

In recent years, requirements for reactors installed in electric vehicles (EVs) and hybrid electric vehicles (HEVs) include high current and frequency, as well as high reliability in severe conditions, to which the conventional ferrite core technology may not be able to respond.

Nippon Kagaku Yakin Co., Ltd., one of the NTN Group companies, develops various types of magnetic material products. In this paper, magnetic material products that present high saturated flux density with low core loss and good frequency response are discussed together with their application examples.

### 2. Classification of magnetic material products of Nippon Kagaku Yakin

Magnetic material products are mainly divided into soft magnetic material and hard magnetic material.

Soft magnetic material is characterized by low coercive force and high permeability and used in various magnetic material products using amorphous magnetic material with low core loss and good frequency response. Particularly, an injection core made by injection molding of this material has a high degree of freedom for the shape and superior DC bias characteristic.

Hard magnetic material has high coercive force and is used as a permanent magnet. Magnetic material for magnetic recording is classified for this category.

### 3. Soft magnetic materials

#### (1) High property injection core

##### 1) Material property

Amorphous injection material (AS10) is a complex material made of iron-based amorphous particles that do not have crystalline structure and resin material.

**Table 1** shows the material property of AS10.

**Table 1** Material properties of AS10

Material	Density g/cm <sup>3</sup>	Radial crushing strength MPa
AS10	4.65	80

##### 2) Features

**Fig. 1** shows the inductance deviation rate (DC bias characteristic), which serves as a measure of the magnetic field generation capability when applied current is swept for AS10 and the conventional ferrite/iron-silicon (Fe-6.5Si) magnetic material.

In addition, **Fig. 2** shows the frequency response of the inductance when weak current is applied. From these properties, the following features are derived:

\*Engineering Department, Nippon Kagaku Yakin Co., Ltd.

- Inductance deviation rate is small even when high current is applied compared to the conventional magnetic material ferrite and Fe-6.5Si.
- Inductance deviation rate in high frequency range is small compared to ferrite with stable properties.

From the above, AS10 is suitable for applications requiring high current and stable high-frequency response characteristics.

### 3) Application examples

#### ● Choke coil

Since high current can be applied and high-frequency response is stable, it is applied to choke coils. Specifically, choke coils are applied to power supply for medical MRI and industrial machines (Fig. 3 to 6). In this application, reduction of volume and weight of about 1/8 was achieved compared to the conventional ferrite products.

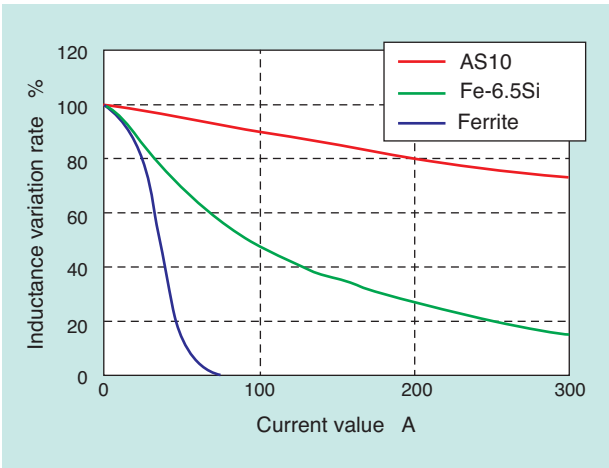


Fig. 1 DC bias characteristics

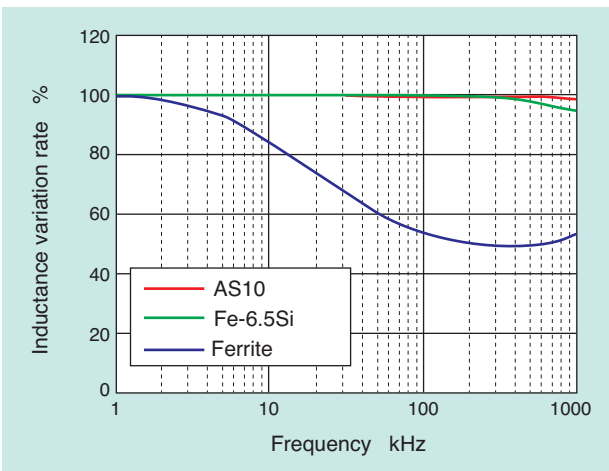


Fig. 2 Frequency characteristics



Fig. 3 Medical magnetic resonance imaging

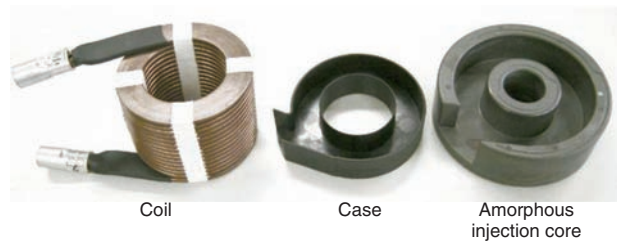


Fig. 4 Parts of choke coil



Fig. 5 Choke coil for MRI power supply



Choke coil



Amorphous core (a component of choke coil)

Fig. 6 Power supply circuit of industrial equipment

(2) Amorphous-based dust core

1) Material property

Amorphous-based dust core material (AL60) is a complex material made of iron-based amorphous particles that do not have crystalline structure with 1–2 vol% of additives.

Table 2 shows the material property of AL60 and Table 3 shows relative permeability of AL60 and AS10.

Since AL60 contains only a little additive including resin, i.e., 1/40 to 1/20 of AS10, injection molding is not possible. In addition, AL60 needs special mold and high forming pressure since iron-based amorphous particles are hard.

2) Features

Fig. 7 shows the DC bias characteristic and Fig 8 shows frequency response of AL60 and ferrite. From these properties and Tables 2 and 3, the following features are derived:

- Relative permeability of amorphous-based dust core material (AL60) is 6 times that of amorphous injection material (AS10) (Table 3).
- On the other hand, inductance variation rate of AL60 is higher than AS10. This is caused by

Table 2 Material properties of AL60

Material	Density g/cm <sup>3</sup>	Radial crushing strength MPa
AL60	5.5	40

Table 3 Relative permeability of AL60 and AS10

Material	AL60	AS10
Relative permeability	60	10

increased mutual contact of metal particles since it contains more iron-based amorphous particles.

- Inductance deviation rate of frequency response with AL60 in high frequency range is smaller compared to ferrite, providing stable properties.

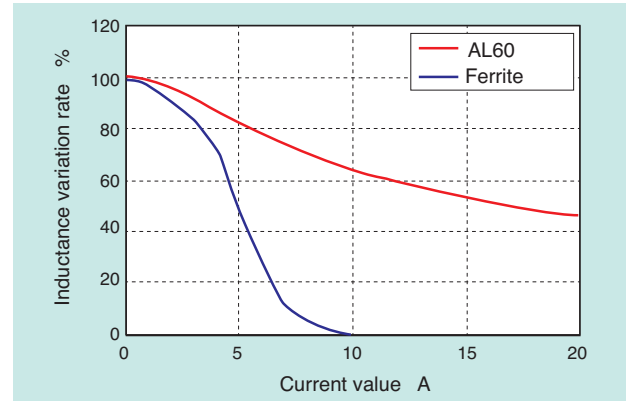


Fig. 7 DC bias characteristics

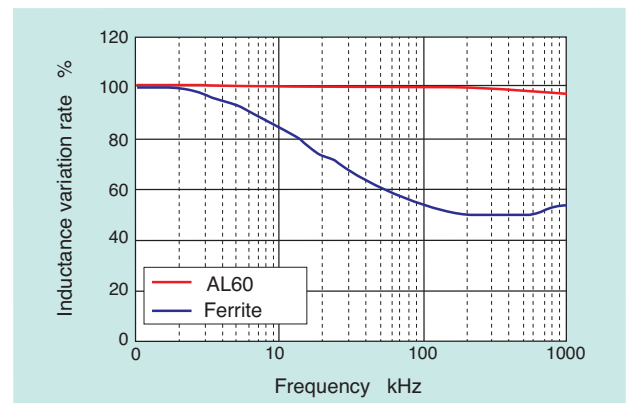


Fig. 8 Frequency characteristics

3) Application examples

• Reactive core material for voltage booster of HEV

A reactor is included in the voltage boosting circuit for increasing motor torque by increasing the battery voltage. In this case, AL60, which has high relative permeability and low core loss, is applied as the reactive core material shown in Fig. 9.

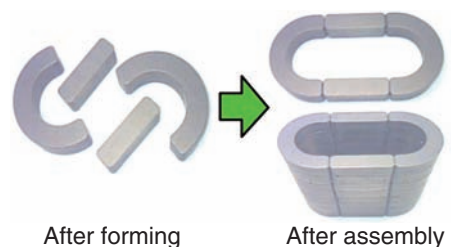


Fig. 9 Reactive coil core for HEV

## 4. Hard magnetic materials

Fig. 10 shows a map of hard magnetic materials. Nippon Kagaku Yakin has a line-up of bonded magnetic products from compression molding to injection molding of hard magnetic materials.

### (1) Compression bonded magnet

#### 1) Material property

Compression bonded magnet is a complex material, which is made by compression molding, mixing magnetic particles such as ferrite magnet and resin materials. Table 4 shows the material properties of isotropic compression bonded magnet (ME12M), which uses either granulated or Nd-Fe-B-based magnetic particles.

Table 4 Material properties of ME12M

Material	Density g/cm <sup>3</sup>	Radial crushing strength MPa
ME12M	6.4	110

#### 2) Features

- Maximum energy product: 8 to 12 MGOe
- Good squareness that allows a wide range of magnetic circuit designs

### (2) Injection bonded magnet

#### 1) Material property

Table 5 shows the material properties of isotropic injection bonded magnet (AS4M), which uses Nd-Fe-B-based magnetic particles.

Table 5 Material properties of AS4M

Material	Density g/cm <sup>3</sup>	Radial crushing strength MPa
AS4M	4.6	80

#### 2) Features

- Maximum energy product: 4 to 6 MGOe
- Injection bonded magnet surface is covered by resin skin layer providing good anti-corrosion property
- No anti-corrosion paint is required
- High design degree of freedom even for complicated shapes due to injection molding

#### 3) Application examples

Fig. 11 shows application examples of compression bonded magnet and injection bonded magnet, which are hard magnetic materials, to an automobile.

- **Compression bonded magnet**  
Rudder angle sensor, exhaust sensor
- **Injection bonded magnet**  
Sensor for key-less entry  
Position, angle, and rotational speed of the target object are detected using change of magnetic flux density and switching of magnetic poles.

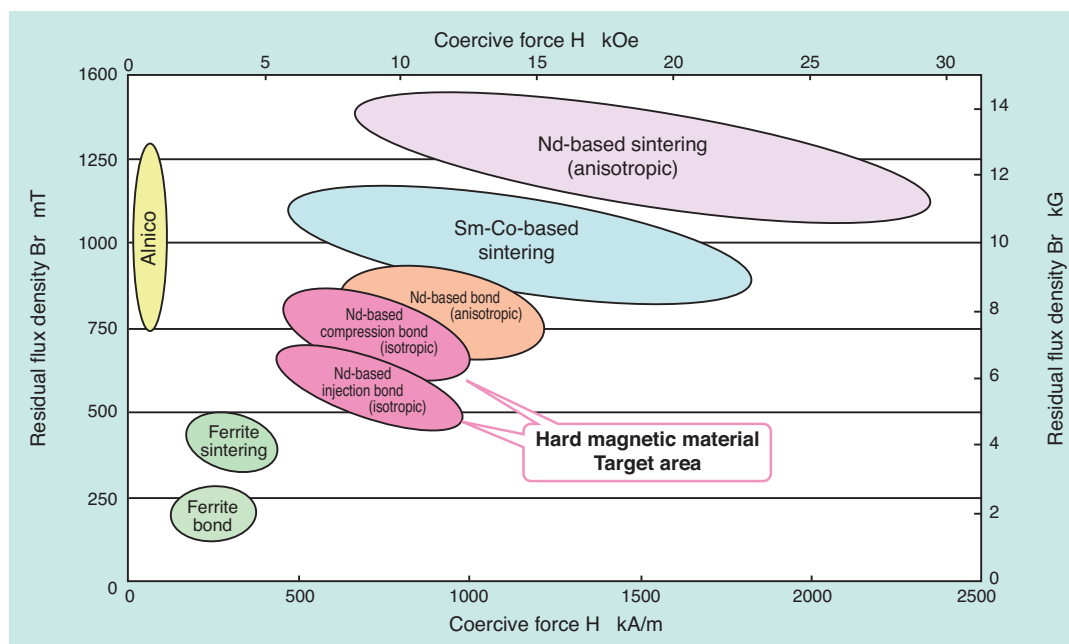
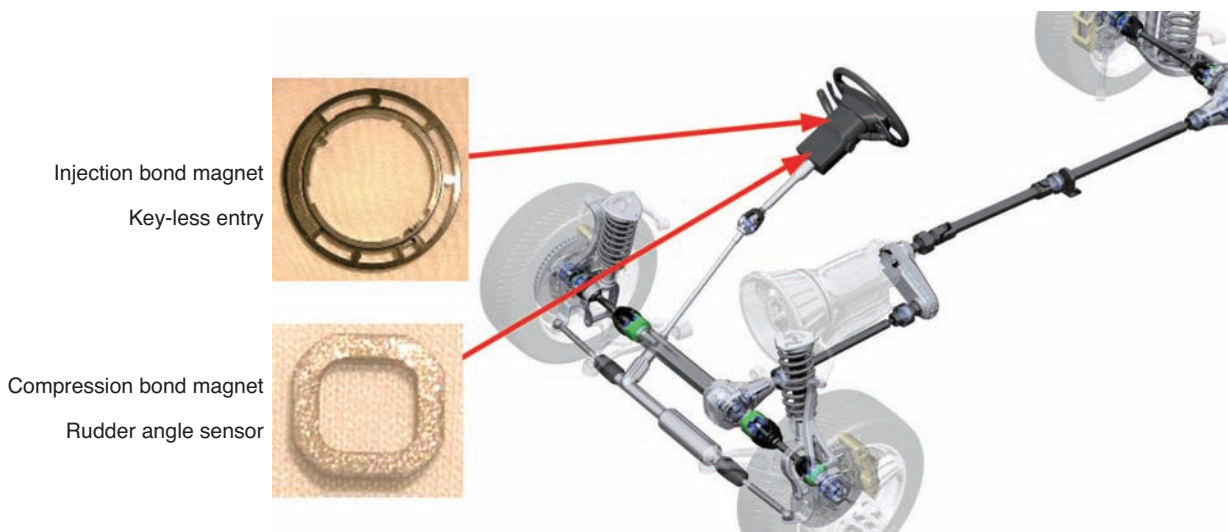


Fig. 10 Map of hard magnetic materials



<p><b>Key-less entry</b></p>		<p>Key-less entry magnet flux density distribution</p>	<p>Switch ON/OFF based on change of flux density</p>
<p><b>Rudder angle sensor</b></p>		<p>The magnet rotates proportionally to the steering angle</p>	<p>Rotational angle is determined by the number of switchovers of the magnetic poles</p>

Fig. 11 Application for automobile

## 5. Summary

We believe that the magnetic material products discussed in this paper will be applied to the electronic circuit components of electric vehicles, and contribute to downsizing of industrial machines and reduction of energy loss. We are poised to continue our development of magnetic material products that respond to the market needs as new energy proliferates.

Photo of authors



Takuji HARANO  
Engineering Department,  
Nippon Kagaku Yakin Co., Ltd.



Shinji MIYAZAKI  
Engineering Department,  
Nippon Kagaku Yakin Co., Ltd.

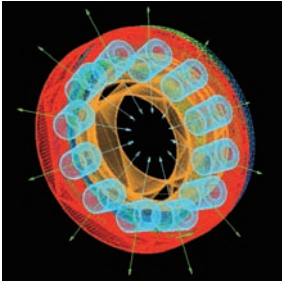


Hajime KATSUURA  
Engineering Department,  
Nippon Kagaku Yakin Co., Ltd.

Awarded: "The Japanese Society of Tribologists 2011" Technology Award

# Advancement of Cage Stress Analysis of Rolling Bearings

Tomoya SAKAGUCHI, Kazuyoshi HARADA, Sadatsune KAZAMA



## 1. Overview

Common methods in which to increase the capacity of a bearing are to increase the size and/or quantity of rolling elements. As such, cage design becomes more difficult due to the reduction of remaining volume within the bearing. In many cases an appropriate design can be made, but in certain applications excessive cage stress may be seen. Therefore, a cage must be analyzed to ensure proper strength. We have been developing the technology to obtain cage stress by analyzing it within its application<sup>1) to 4)</sup>. This technology received the "2011 Japanese Society of Tribologists Technology Award," which is given to excellent new technologies in tribology. This article will provide an overview of this analytical method.

## 2. Characteristics of the analytical system

This technology is built as a CAE system<sup>3)</sup> for analyzing common bearing types in complex operating conditions such as planetary motion and crank rotation (Fig. 1). This system enables calculation of cage stress during operation, by coupled analysis of the motion of the rolling elements and cage as well as the elastic deformation of the cage. Rolling element to raceway contact analysis is performed by precise modeling of the contact geometry, effects of a dynamic oil film, and including the elastic deformation of the cage using the mode synthesis method<sup>5)</sup>, a method which is superior in calculation speed compared to the finite element method. Accuracy of the stress calculation has also been improved by the way in which the cage mode synthesis method is applied. The analysis is typically used for three-dimensional models, however two-dimensional analysis is also possible; another advantage in the speed of calculation<sup>3)</sup>.

## 3. An examples of analysis

Fig. 2 shows cage stress results of a two-dimensional, needle roller bearing analysis which uses 10 or 11 rollers

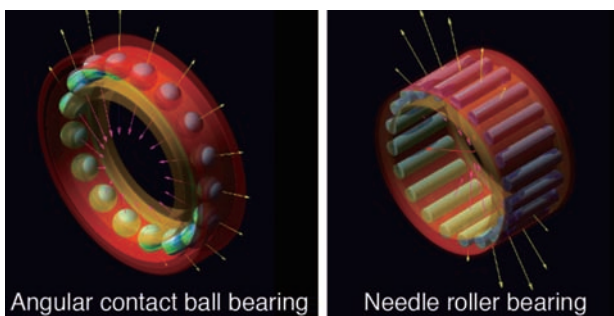


Fig. 1 Analyzed rolling bearings

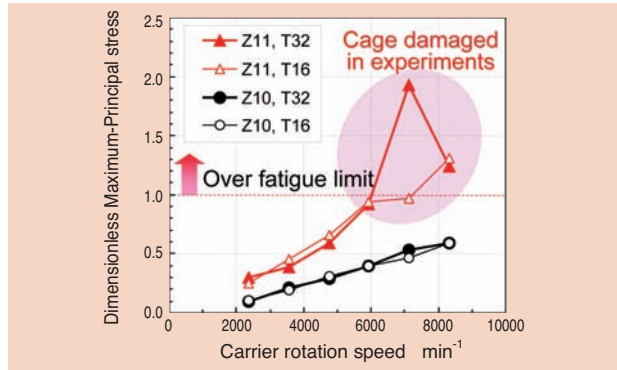


Fig. 2 Cage stress vs. carrier rotation speed<sup>1)</sup>

(Z) and is used in a planetary reduction gear. The maximum principle stress of the cage has been normalized to the fatigue limit of the cage material and based on the rotational speed of the carrier. In the cases where rotational speed is 6000 rpm or more and Z is 11, the stress calculated exceeded the fatigue limit. Likewise, experiments show that under these conditions, cages frequently failed. The cause of failure was assumed to be fatigue breakdown. The results indicate that this analysis is effective.

This journal bearing model is being displayed in the first-floor lobby of our Industrial Technical Center in Kuwana-shi, Mie.

## References

- 1) T. Sakaguchi, et al.: Dynamic Analysis of Cage Stress in Needle Roller Bearings Under Planetary Motions, IJTC2007, 44189.
- 2) T. Sakaguchi, et al.: Dynamic Analysis of Cage Stress in Tapered Roller Bearings Using Component-Mode- Synthesis Method, ASME J. Tribol., 131(2009)011102.
- 3) Sekiya: Integrated Bearing Dynamic Analysis System (IBDAS), NTN TECHNICAL REVIEW, 79 (2011) 119.
- 4) Sakaguchi, et al.: Advancement of Cage Stress Analysis of Rolling Bearings, Tribology Conference, Spring 2012, Tokyo (2012) 233.

Photo of authors (Affiliations are at the time of presentation at a conference)



Tomoya SAKAGUCHI

Advanced Technology R&D Center

Kazuyoshi HARADA

Advanced Technology R&D Center

Sadatsune KAZAMA

Needle Roller Bearing Engineering Department, Automotive Business HQ

## 2011 “CHO” MONODZUKURI Innovative Parts and Components Awards” Machinery Component Award

## Desktop Type Microscopic Coating Applicator

Motohiro UCHIYAMA

### 1. Introduction

The “Desktop-Type Microscopic Coating Applicator” is a specifically designed tool to repair LCD panel color filters. Its ability to apply a microscopic coating of a few pico liters of liquid was recognized for its compact size, ease of operation, and high coating performance. For these features, it was given the 2011 “CHO” MONODZUKURI Innovative Parts and Components Awards” Machinery Component Award.

This device has also received many inquiries including some from advanced research institutions. These organizations studied its application to micro-coating in the area of:

- material coating process for special sensors
- application of adhesive on small optical components
- application of material on electronic devices, and
- dividing specimens into small quantities in bio-related areas

All these processes conventionally depended on manual procedures or processes.

### 2. Background

NTN is the leading producer of mechanical devices that repair missing or mixed color defects in LCD panel color filters. Due to the recent trend towards larger LCD panels, the size of current repair devices used in the production lines has increased to over 4 meters. The smaller desktop size of this product allows use in small preproduction applications or research and development work, in addition to LCD panel manufacturing.

### 3. Features

For applying a predetermined amount of liquid, the dispenser method and ink jet method are well known. However, with these methods, liquid is delivered through a very thin tube or hole. With this technique, clogging has always been a problem. This device adopts a unique application method using an applicator needle with a small amount of liquid on the tip. Light contact, transfers the liquid to the target object. Therefore, it can handle a wide variety of liquids of different viscosity without the problem of clogging of nozzles, etc.

Also, for ease of operation, setup uses a mouse to accurately position the application to specified points.

We hope this product helps advance research in electronics and medical/bio sciences, and contributes to the further development of new technologies and new materials.



Fig. 1 Desktop type microscopic coating applicator

### References

- 1) Akihiro Yamanaka, Desktop Type Microscopic Coating Applicator, its Technology and Features, Monthly JETI, Vol. 58, No. 11, 101-102, 2010.
- 2) Katsuyoshi Suzuki, Development and Application of Desktop Type Microscopic Coating Applicator, Monthly Tribology, No. 294, 34-36, 2012

### Photo of author



Motohiro UCHIYAMA

Product Engineering Department,  
Precision Equipment Division

## Electric Braking System with Parking Capability

**A lightweight and compact design with enhanced convenience and safety is achieved by integrating an electric braking system with parking brake functionality!**



### Features

#### [1] Enhanced convenience and safety

- Parking operation is simplified by electronic control of parking brake (Auto-parking feature, release reminder feature)

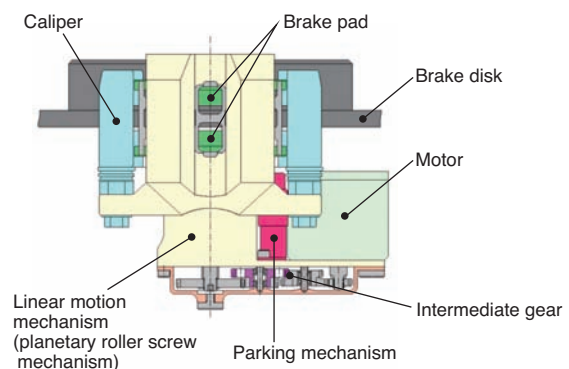
#### [2] Lightweight, compact

- Parking brake unit (solenoid) is placed in the space between linear motion mechanism and motor

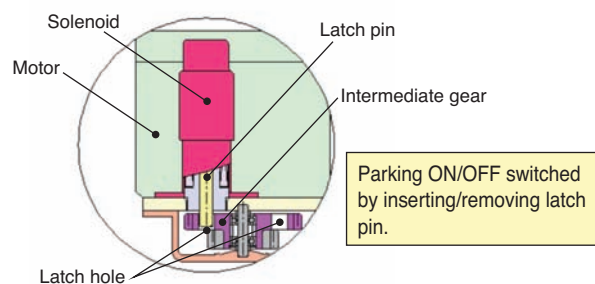
### Applications

- Electric vehicle, hybrid vehicle (electric parking brake)

### Structure

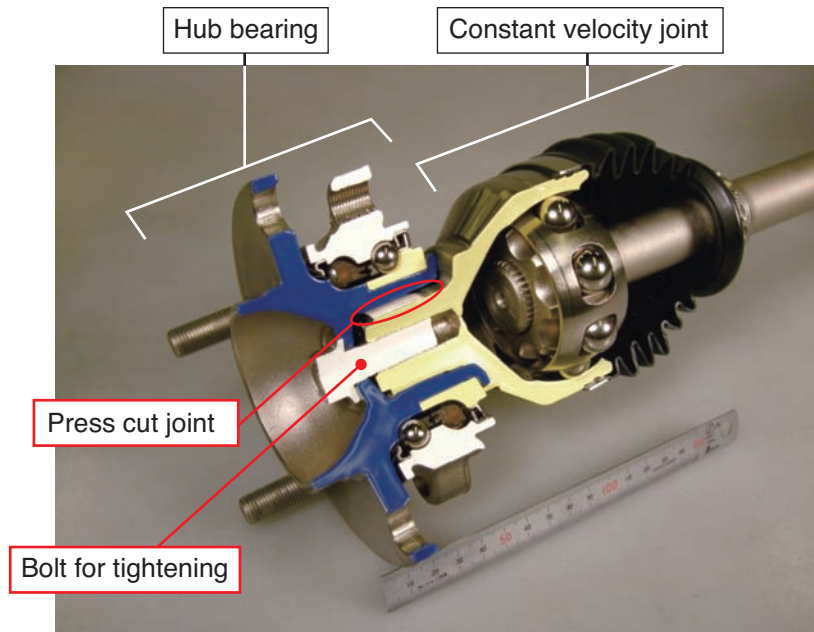


#### Detailed view of parking mechanism



## Press Cut Spline Hub Joint “PCS-H/J”

**Achievement of significantly lighter weight and higher performance is obtained by the unique joint mechanism of hub bearing and constant velocity joint!**



### Features

#### [1] Lightweight

- 12% lighter than the current third-generation hub bearing + constant velocity joint

#### [2] High performance

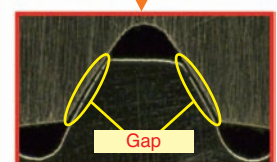
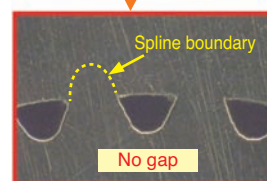
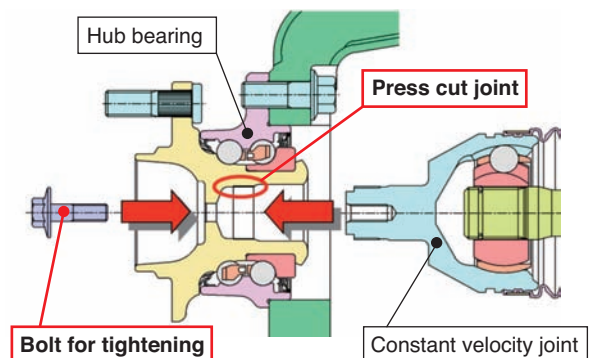
- By our unique press cut joint technology with small spline inside hub ring “Zero” clearance between hub bearing and constant velocity joint
- Reduction of stick slip noise

### Applications

- Axles for passenger cars



### Structure



Press cut spline (section)

Ordinary spline fit (section)

# Next-generation high-efficiency fixed constant velocity joint “CFJ”

CFJ : Cross groove Fixed Joint

**Contributing to vehicle fuel economy with the world’s top-level transmission efficiency is the adoption of spherical cross groove technology!**



## Features

- [1] **World’s top-level transmission efficiency**
  - Torque loss rate: 50% reduction compared to the conventional product, EBJ
- [2] **Low heat dissipation**
  - Temperature rise: 50% reduction compared to the conventional product, EBJ
- [3] **Maximum operating angle**
  - 47°

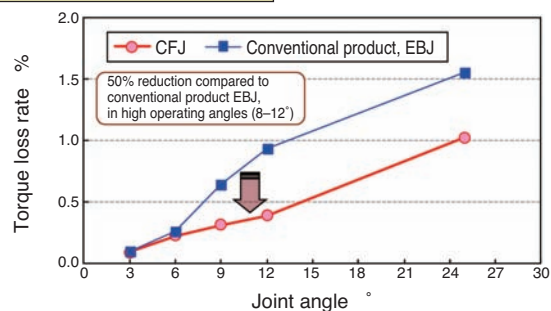
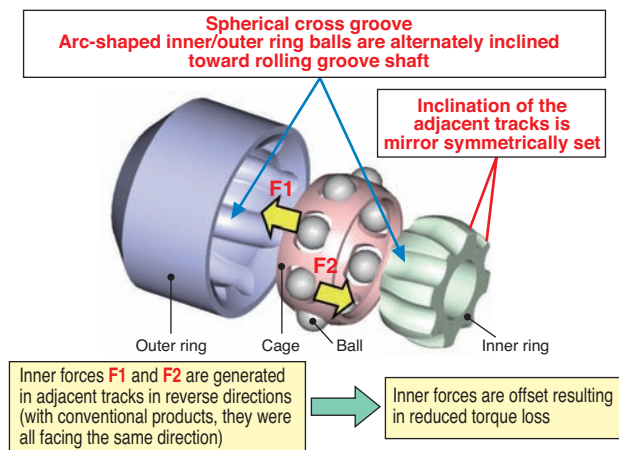
## Applications

- Drive shaft and propeller shaft for SUV, ECO car, etc.



- Drive shaft
- Propeller shaft

## Structure



# High speed/low torque deep groove ball bearing for EV and HEV

High-speed rotation and over 50% in reduction of running torque are achieved by adopting new type of resin for cages!



## Features

### [1] High speed rotation

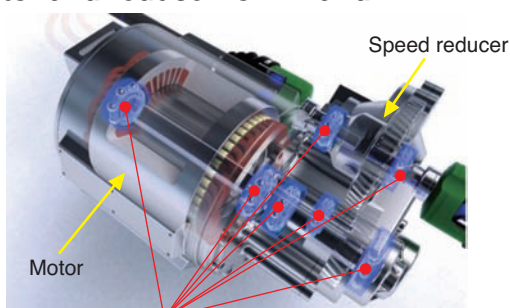
- dn value: 1.2 million  
In the case that the bearing inner diameter is 40 mm, rotational speed: 30000 min<sup>-1</sup>

### [2] Low torque

- Over 50% reduction when compared to our standard deep groove ball bearing with oil lubrication.

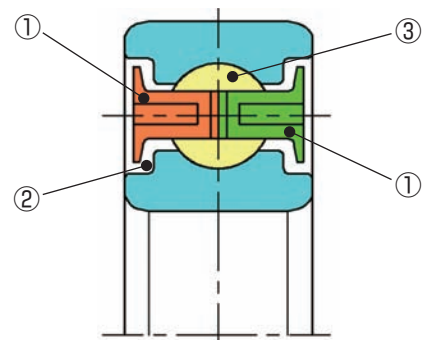
## Applications

- Motor and reducer for EV and HEV

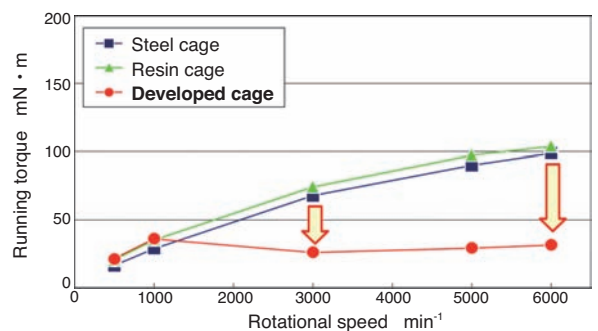


Developed product (applied to oil lubrication)

## Structure

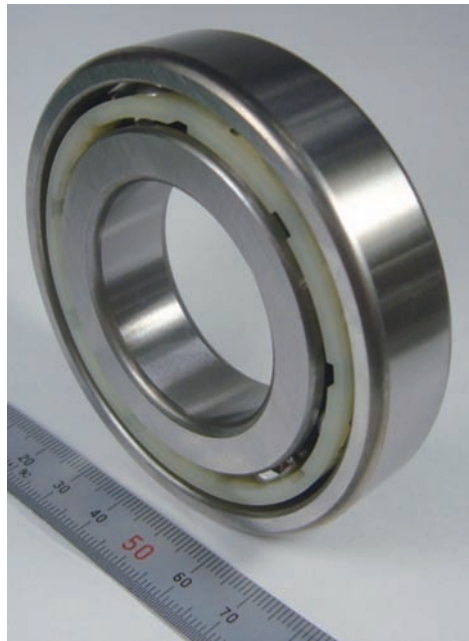


- ① Two new resin cages of the same type are adopted
- ② Controls in-flow of oil inside bearings
- ③ Optimized internal bearing specification



## Deep groove ball bearing for high thrust load

Significant improvement of thrust load capability for deep groove ball bearing!  
**Tapered roller bearing can be replaced by this new technology!**



### Features

#### [1] Thrust load capacity

- Three times the conventional standard deep groove ball bearing

#### [2] Bearing running torque

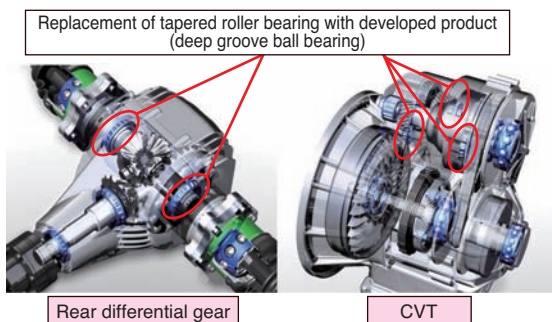
- 60% reduction compared to tapered roller bearing

#### [3] Reduction of assembly work time

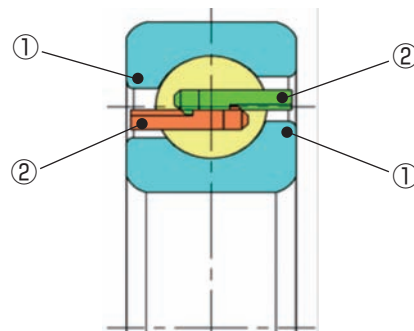
- No pre-load adjustment required for incorporating bearings

### Applications

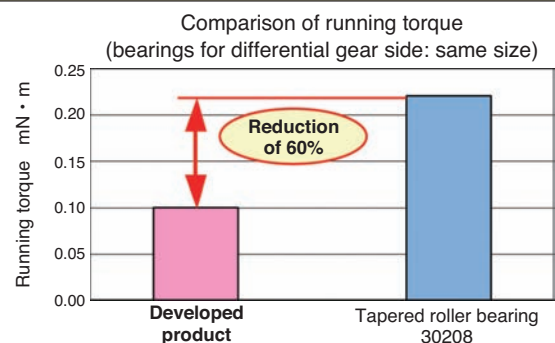
#### • Transmission for vehicles



### Structure

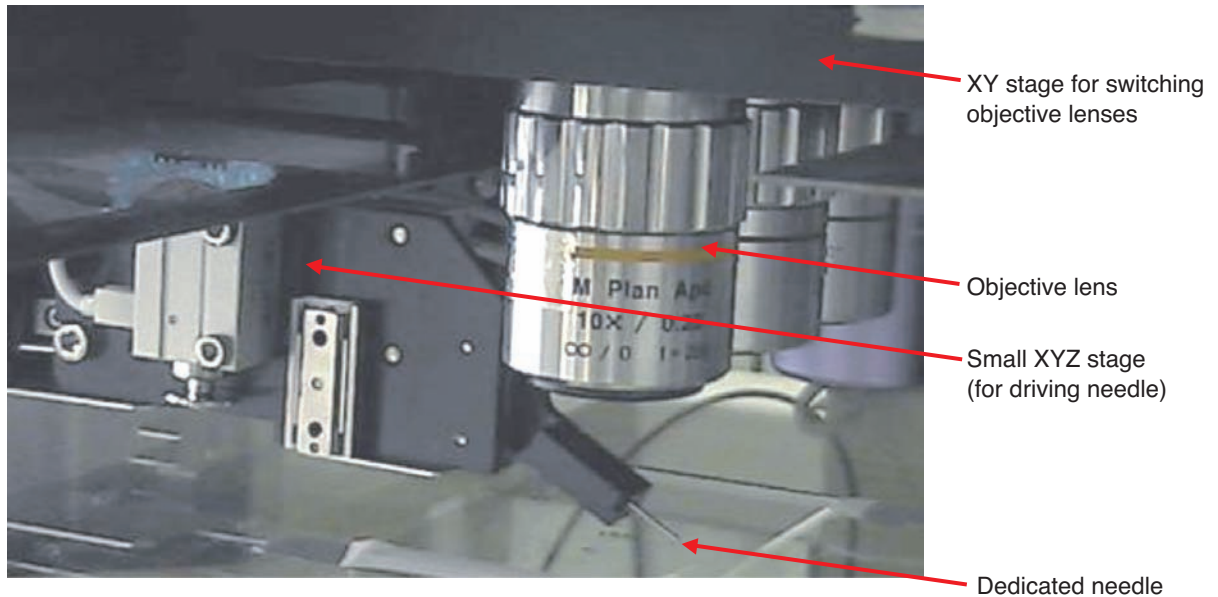


- ① Thrust load side profile is added based on the standard deep groove ball bearing
- ② Adopted new resin cage combining small diameter and large diameter



# Removal Device of Microscopic Foreign Object

New Repair technology **contributes to the increased productivity** of FPD board manufacturing process!



## Features

- [1] **Removal of foreign objects using a special needle with slotted screwdriver-shaped tip**  
 ⇒ Allows the removal of micron-scale foreign objects that was difficult using conventional removal methods such as laser cutting, grinding, etc.
- [2] **Specify foreign objects repair areas using a mouse on the monitor**  
 ⇒ Allows the removal of foreign objects while minimizing damage to surrounding components
- [3] **Reliable collection of removed foreign objects or residue from foreign objects adhered to the needle using suction or adhesive rollers**  
 ⇒ Cleaning process can be simplified or eliminated after repairs

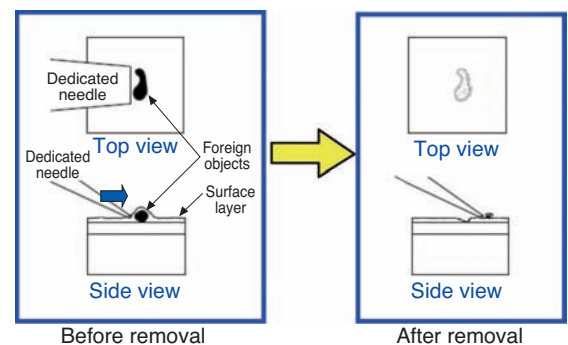
## Applications

- Removal of foreign objects from flat panel display (FPD) substrate
- Removal of foreign objects from photo-mask substrate for exposure

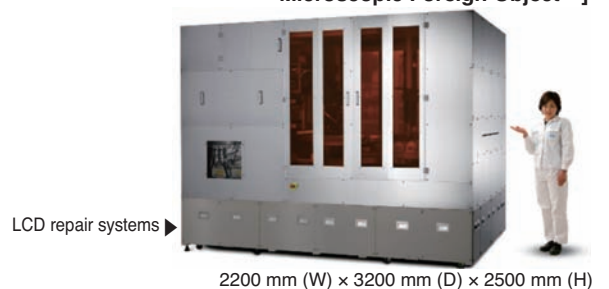
## Structure

Removal of foreign objects by dedicated needle

Foreign objects are removed by being pushed by the needle tip (needle is installed on the stage with mobility to XYZ directions)

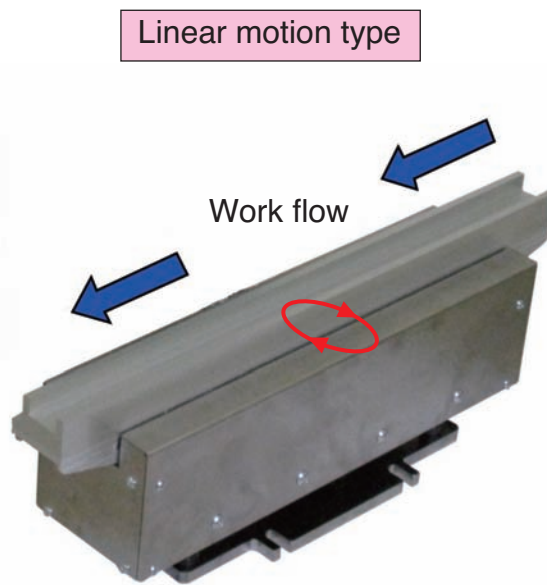


[Application example of "Removal Device of Microscopic Foreign Object" ]



# Elliptic Vibratory Parts Feeder

**High-speed transfer and low noise are achieved by horizontal elliptical vibration!**



## Features

### [1] Improved feeding capacity by high-speed transfer

- Bowl type: 12 m/min. (150% compared to conventional products)
- Linear motion type: 10 m/min. (160% compared to conventional products)

### [2] Achieve low noise of alignment feeding

- Improved quietness with smooth motion by elliptical vibration  
(Noise reduced 10% compared to conventional products)

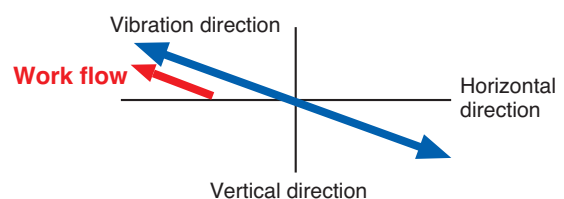
### [3] Pitching problem inherent in linear motion type part feeders is resolved

## Applications

- Alignment feeding of low-profile/light-weight components for automobiles, electronics, and medical equipment

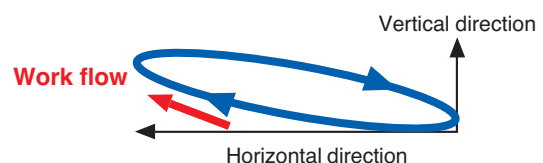
## Structure

### Conventional product



Work is thrown up by diagonal vibration generated by the combination of horizontal magnetic attractive force and reaction force of a slantedly installed leaf spring (simple to-and-fro motion)

### Developed product (elliptical vibration)



Elliptical vibration is generated by two independently installed electromagnets in horizontal and vertical directions. Transfer suitable to work property can be achieved by flexible control of driving force in two directions.